CLEARINGHOUSE FOR FEDERAL SCIENTIFIC AND TECHNICAL INFORMATION CFSTI
DOCUMENT MANAGEMENT BRANCH 410.11

LIMITATIONS IN REPRODUCTION QUALITY

ACCESSION # AD [illegible] 160

☒ 1. WE REGRET THAT LEGIBILITY OF THIS DOCUMENT IS IN PART UNSATISFACTORY. REPRODUCTION HAS BEEN MADE FROM BEST AVAILABLE COPY.

☒ 2. A PORTION OF THE ORIGINAL DOCUMENT CONTAINS FINE DETAIL WHICH MAY MAKE READING OF PHOTOCOPY DIFFICULT.

☐ 3. THE ORIGINAL DOCUMENT CONTAINS COLOR, BUT DISTRIBUTION COPIES ARE AVAILABLE IN BLACK-AND-WHITE REPRODUCTION ONLY.

☐ 4. THE INITIAL DISTRIBUTION COPIES CONTAIN COLOR WHICH WILL BE SHOWN IN BLACK-AND-WHITE WHEN IT IS NECESSARY TO REPRINT.

☐ 5. LIMITED SUPPLY ON HAND: WHEN EXHAUSTED, DOCUMENT WILL BE AVAILABLE IN MICROFICHE ONLY.

☐ 6. LIMITED SUPPLY ON HAND: WHEN EXHAUSTED DOCUMENT WILL NOT BE AVAILABLE.

☐ 7. DOCUMENT IS AVAILABLE IN MICROFICHE ONLY.

☐ 8. DOCUMENT AVAILABLE ON LOAN FROM CFSTI (TT DOCUMENTS ONLY).

☐ 9.

PROCESSOR: [illegible]

TS[illegible]-107-10 64

DISCLAIMER NOTICE

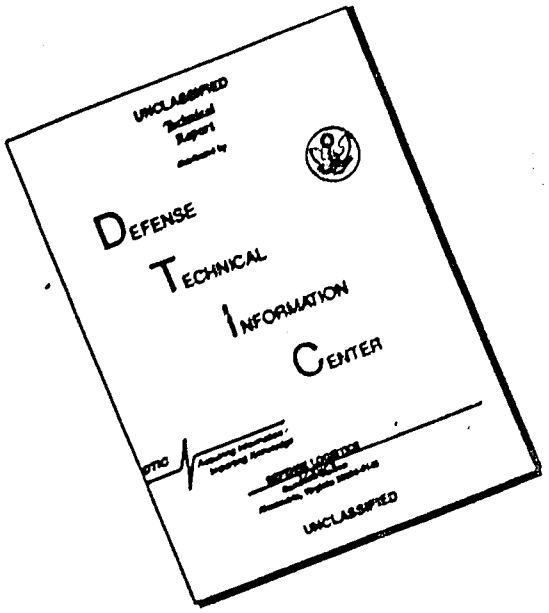

THIS DOCUMENT IS BEST QUALITY AVAILABLE. THE COPY FURNISHED TO DTIC CONTAINED A SIGNIFICANT NUMBER OF PAGES WHICH DO NOT REPRODUCE LEGIBLY.

Study of Helicopter Gear Lubrication

for

Bureau of Naval Weapons

Washington 25, D. C.

Contract No. NOw 63-0557-c

Final Report

June 1, 1963 - May 31, 1964

SHELL DEVELOPMENT COMPANY

A DIVISION OF SHELL OIL COMPANY

Emeryville, California

S-13926

STUDY OF HELICOPTER GEAR LUBRICATION

for

Bureau of Naval Weapons
Washington, D.C.

Contract NOw 63-0557-c

Final Report
June 1, 1963 - May 31, 1964

Reported and Reviewed: S. J. Beaubien
L. Lichtman

Participants: C. A. Converse
R. L. Jensen

Approved: C. G. Clear

SHELL DEVELOPMENT COMPANY
A Division of Shell Oil Company
Emeryville, California

S-13926

CONTENTS

STUDY OF HELICOPTER GEAR LUBRICATION

Introduction

This is a report of work done at Shell Development Company under a contract with the U. S. Navy, relating to the study of helicopter gear lubrication. It is a final report of the work done at the Emeryville laboratories.

The approach used in this project to the study of helicopter gear lubrication consists in a study of the types of failure that have occurred in helicopter transmissions in the field, and an attempt to learn the causes of such failures on a theoretical and experimental basis. The overall objectives of the work, however, are not limited to solutions of gear lubrication problems of existing helicopter transmissions, but also aim at developing information useful to future transmission designs and, in part, applicable to other gear systems.

From discussions with Navy personnel, and as a result of a visit to Navy helicopter overhaul facilities, it was concluded that the principal mode of helicopter transmission gear failure was pitting. Accordingly, appreciable effort was made to learn something about the gear tooth contact conditions and mechanisms that lead to this type of failure.

The lubrication of helicopter gears is not different, in principle, from the lubrication of other geared systems, and it is possible to apply the technology which has been previously developed to the problem. At the same time, it is important to consider the particular values of the variables which are present in helicopter gears, so that the research can be applied specifically to the problems at hand. For this reason, the work in this report includes not only analysis of involute gears in general, but includes in particular, a study of 8/10 pitch stub tooth gears of 22-1/2° pressure angle, and a comparison of these gears with full depth gears. This is because the stub tooth gears have been specified in the gear boxes of helicopters used by the contracting agency, and are therefore of special interest. Similarly, the lubricants used in all the experimental work reported here have been chosen because they are the lubricants which are used in helicopters.

Instead of attempting to study the problem in the full scale equipment, the approach was to study laboratory test gears in a gear test machine with which we already had gained a good deal of experience. Concurrently with this study, a new Rotary Contact Simulator, using steel disk specimens was applied to the problem. Conditions of a gear tooth vary from point to point along the tooth surface, so that a gear represents a composite of a large number of adjacent contact conditions. In one sense, this is an advantage for study, because in a single test a gear can produce a range of phenomena for interpretation. It is not necessary to explore the range of conditions on a gear tooth point by point to discover important or interesting phenomena; by the mechanism of failure, the important areas call attention to themselves. In another sense, however, the succession of adjacent conditions along the gear tooth makes study difficult, because no large area of homogeneous damage

can be studied. Conditions existing at a single line of contact are not the same as conditions on the neighboring lines, so it is difficult to assess the character of the damage in many cases, or trace its origin. In this important respect the Rotary Contact Simulator adds to the power of observation of anyone studying gear contacts. A pair of metal disks is brought into contact at the same rpm as the gears being simulated, with the appropriate radii of curvature and load, so that all important parameters existing at a contact point on a pair of gear teeth are duplicated continuously around the entire circumference of the disks. A more complete discussion of this matter is presented in a later section, but it is important to appreciate, at this point, the fact that the disks in the Rotary Contact Simulator actually recreate the conditions at the point of interest in the gears, and do this in such a way that an appreciable area of surface is produced which shows the effects of the contact conditions, free of interference from, or influence by, the adjoining conditions.

The portion of the work under the general heading of theoretical calculations covers a number of subjects, which will be reviewed briefly here. It is useful, in the study of gears, to keep track of the stresses produced in the metal by the applied loads. The stress in a contacting pair of gear teeth is essentially a Hertz stress, produced by the flattening of two curved surfaces in contact. The Hertz equation is strictly applicable for the contact of two cylinders, but can be regarded as a close approximation for two involutes. In this report a method is presented for calculating the Hertz stress in gears, based on the Hertz equation, but so arranged that the stress distribution is easily seen. This is based on the development of a simple parameter, X, which represents the travel of the contact point along the line of action. In order to calculate Hertz stress, it is necessary to know the force between two gear teeth, and this depends, not only on the total force being transmitted from one gear to the other, but also on the number of teeth sharing in the load transmission, and on the manner in which they share the load. In order to facilitate these considerations on a general level, curves were developed by means of which the load sharing regions can be found with respect to the parameter X. By means of these curves, together with the curves for calculating Hertz stress, it is possible to obtain a clear picture of the Hertz stress distribution on gear teeth, and to estimate the effect of each variable on the stress. For full depth teeth it is possible to construct these curves independently of diametral pitch, so that they can be applied to all gears at the chosen pressure angle (20° in this case). Since the helicopter gear box data are taken from a system in which stub tooth gears are used, with a 22-1/2° pressure angle, a separate set of curves had to be calculated. Unfortunately, in the Fellows Stub tooth system, it was not possible to make the curves independent of diametral pitch, so the curves apply only to 8/10 pitch gears.

The method of visualizing and calculating Hertz stresses for gears suggests a stress criterion for gear design which is also presented in this report. Briefly, this criterion is based on the concept of "balanced" stresses. The region of the gear tooth affected by loads carried in single-tooth contact is stressed more highly than the regions immediately adjacent to it. However, due to the geometry of an involute, the stresses may reach very high values in the regions near the beginning and end of double tooth contact, if the loads

are carried at either very low or very high values of X. Since the region of single-tooth contact establishes a stress level not readily subject to modification, it is good engineering practice to avoid stresses on other parts of the tooth which are excessive with respect to this level. The stress calculation method developed, as described above, is readily applicable to this problem, and it has been used to show that for any gear ratio there is a minimum number of teeth which must be present in the gears to avoid overstress. This differs for full depth teeth and stub teeth, so calculations have been made for both systems, and comparisons are presented.

A comparison is also presented of the stresses present in a full depth gear tooth and a stub tooth, with respect to the location and magnitude of maximum stress. Stub teeth, while offering several advantages, suffer from the fact that the maximum stress arises at a point of higher sliding velocity than in full depth gears. This fact, although its importance is not assessed, should be considered in any study of gear tooth damage.

Much effort has been given to the analysis of gears because it is important that details of stress and energy input at the contact be known if one is to establish a cause-and-effect relationship between contact severity and surface damage. Thus, a consideration of the magnitude and cyclic nature of the contact stresses, along with observations of surface failure, led to the formulation of a fatigue-scoring hypothesis. This hypothesis has been confirmed in laboratory tests, and it has been extended to include the mechanism of pitting. The hypothesis has also been useful in clarifying the complex phenomenon of break-in, and in guiding the design of laboratory experiments. In the following work, fatigue, scoring, pitting, and break-in are all discussed, along with their interactions, and with relation to the contact conditions that bring them into effect.

Analysis of Gears

The geometry of a particular pair of gears has an effect on the load carried by the individual teeth, on the variation in load as the contact moves along the tooth face, and on the stress experienced by the gear tooth surface as the load passes over it. In this section an analysis will be presented showing how the surface stress varies at a known tooth load for various spur gear pairs, and how the tooth load is affected by load sharing. The analysis has been applied to full depth gears of 20° pressure angle, and to stub tooth gears of 8/10 diametral pitch and 22-1/2° pressure angle. This information is needed for rational comparison of gear distress for different systems. Some details of gear action will be presented first to establish a basis for the analysis.

Gear Geometry

Figure 1 shows the essential mathematical elements in a mating pair of spur gears. The line of centers is vertical in the figure. About two points, O and O', on this line are drawn the base circles of two gears. A common tangent to these base circles is the line of action, AB, drawn with a 20° pressure angle, α. Later in this section, gears with a 22-1/2 degree

pressure angle are considered. The intersection of the line of centers and the line of action is the pitch point P, and one can imagine a tangent pair of pitch circles running through this point. They have not been drawn because they would add very little to the present discussion, and their inclusion would only crowd the diagram. The addendum circles, which establish the height of the teeth, are shown.

For clarity a pair of involutes in contact is shown in contact at an arbitrary point C along the line of action. This represents the contact of a pair of teeth. The driver in this diagram has been drawn smaller than the driven member of the pair, but the discussion to follow does not rely on this fact, and indeed, the identities of driver and driven, rather than pinion and gear are to be maintained. Contact begins at point D on the line of action where the addendum circle of the driven gear crosses the line of action. Contact ends at point E, where the addendum circle of the driving gear crosses the line of action.

Contact points can be visualized as entering the line of action at A and travelling toward B with uniform velocity and spacing. The spacing between contact points is equal to the circumference of either base circle divided by the corresponding number of teeth. This parameter must obviously be the same for each of the mating gears of a pair, and is given by the expression

$$\Delta S = \frac{\pi \times PD \times \cos \alpha}{N} . \qquad (1)$$

When this expression is written in the form

$$\Delta S = \frac{\pi \cos \alpha}{DP} \qquad (2)$$

where

ΔS = the distance along the line of action between contact points
PD = pitch diameter
PD x cos α = base circle diameter
α = pressure angle
N = number of teeth
DP = diametral pitch = N/PD

it is evident that ΔS is the same for all gears of a single-diametral pitch and pressure angle.

The distance between the start of the line of action and the contact point can be divided by the length of the line of action to obtain the non-dimensional parameter X.

$$X = \frac{\overline{AC}}{\overline{AB}} . \qquad (3)$$

This parameter is useful in the development of curves for Hertz stress and for the presentation of information on load sharing, and will therefore be used throughout this work.

The fractional distance between two adjacent points of contact is

$$\Delta X = \frac{\Delta S}{\overline{AB}} \tag{4}$$

where $\overline{AB}$ is defined in Figure 1 and equals $\overline{AP} + \overline{PB}$.

$$\overline{AP} = \frac{PD_1}{2} \sin \alpha \tag{5}$$

$$\overline{PB} = \frac{PD_2}{2} \sin \alpha \tag{6}$$

so that

$$\Delta X = \frac{2\Delta S}{(PD_1 + PD_2) \sin \alpha} \tag{7}$$

or from (2)

$$\Delta X = \frac{2\pi \cos \alpha}{DP(PD_1 + PD_2) \sin \alpha} \tag{8}$$

or

$$\Delta X = \frac{2\pi \cot \alpha}{N_1 + N_2} . \tag{9}$$

A graph of ΔX for 20° full depth gears is presented in Figure 2. A similar graph for 22-1/2° stub tooth gears is presented in Figure 3.

Load Sharing

The design of a set of gears that will run smoothly requires that each pair of teeth approaching mesh accept a portion of the load before the preceding teeth in the mesh release the entire load. This "overlap" comes about automatically for most reasonable gear ratios and numbers of teeth, and it results in load sharing among the teeth for a portion of the mesh cycle. In the usual case the load is carried alternately in single and double-tooth contact, but under some conditions the number of contacts can get higher. This fact is important in the calculation of Hertz stresses on the gear teeth. In order to calculate the stress, one must know the load on the pair of teeth being examined. This may be the total load being transmitted by one gear to the other, or it may be a fraction of this load, in the neighborhood of 50%. For the test gears used in this research program (to be described in greater detail in the section on gear tests,) the load sharing schedule is shown in Figure 4. This curve shows the percentage of the total transmitted load carried by a tooth as a function of X. Between X = 0 and X = .1, the tooth has not entered contact, so the load is zero. At X = .1, the tooth enters contact, and the load on it increases abruptly to 40% of the total transmitted load. From

this point to X = .3555 the load increases uniformly to 60% of the transmitted load. It then jumps to 100% as the tooth goes into single-tooth contact. The load remains 100% until double-tooth contact is reestablished at X = .5817, and then the load drops back to 60%. The load then decreases uniformly to 40% at X = .8351 and then drops to zero as the tooth goes out of contact. This curve is obtained by calculating the values of X at which the transitions take place, and plotting the percent loads as measured by strain gages on a actual gear. These curves are idealized, and apply for speeds up to a few thousand rpm; at higher speeds dynamic effects such as tooth vibration begin to complicate the picture.

A general set of curves like that in Figure 4 cannot be presented, but at least the points where contact starts and stops, and where single-tooth contact starts and stops can be calculated. Figures 5 through 11 represent the calculated values of X where these events take place over a range of gear ratios from 1:3 to 3:1, for full depth gears having up to 50 teeth. The test gears have nearly a 1:1 ratio, so we can compare the curves in Figure 4 with that in Figure 8 to see the correspondence. According to Figure 8, a 1:1 gear set with 18 teeth on each member (the test gears have 17 and 19, respectively) starts contact at X = .13. Single-tooth contact begins at X = .39 and ends at X = .61. Contact ends at X = .87. These values are comparable to the values listed above for the transition points of the 17:19 system. When the curves are presented in this form the diametral pitch is not specified, so the curves apply to gears of all diametral pitches.

Contact begins in a spur gear at the point where the addendum of the driven member first crosses the line of action. At a point ΔX ahead of this on the line of action, a contact point is already in existence, where the full transmitted load is being carried. At the same moment as contact is beginning for one tooth, then double-tooth contact is beginning for the preceding tooth, at a position along the line of action $X + \Delta X$. Similarly, contact ends where the addendum circle of the driver crosses the line of action, and double-tooth contact ends at a value ΔX ahead of the end of contact. When this method of calculation is used, all the correct contacts are predicted, but some additional contacts are predicted which are only of mathematical interest, but which cannot exist in the actual gears. No contact can occur on the line of action for negative values of X, even though mathematically it is possible to predict such contacts. For clarity of presentation the curves are shown extending into the negative area, but they are shown dashed, to indicate that such values are not real. At the point where the calculated curve goes below zero or over one, the actual curve has a discontinuity of slope, and continues along the zero or one axis. At this point the corresponding curve for start or end of single-tooth contact has a sudden change of slope also. It is impossible for the limits of single-tooth contact to lie beyond the start or end of contact, but it is possible to calculate values for the curves which make them lie outside. Such curves are shown dotted, to indicate that they are of purely mathematical interest.

The areas of real contact have been shaded, to distinguish them from areas where no contact can take place. The areas of single-tooth contact are shaded differently from those of double-tooth contact. Figures 12 through 19

are similarly developed for stub tooth gears of 8/10 diametral pitch and 22-1/2° pressure angle. Unfortunately, it is not possible to develop a single set of curves for all pitches, so it was chosen to present a single set which apply to the helicopter design being considered specifically in this study.

It should be pointed out that Figures 5 through 11 apply to all full depth gears of 20° pressure angle, regardless of diametral pitch. Figures 12 through 19 are specific to stub-tooth gears of 8/10 pitch and 22-1/2° pressure angle.

Hertz Stress

The stress at the point of contact is related to the transmitted force per unit width of tooth, the radii of curvature of the teeth at the contact point, and the properties of the gear material. The actual stress can be closely approximated by calculating the stress between two contacting parallel cylinders having radii equal to the radii of curvature of the teeth at the point in question. The Hertz equation is used for this:

$$\sigma = .418\sqrt{\frac{EF}{w}\left[\frac{1}{r_1} + \frac{1}{r_2}\right]}^{\frac{1}{2}} \tag{10}$$

where

σ = Hertz stress
E = modulus of elasticity
F = normal force
w = width of teeth or cylinders over which force acts
r = radius of curvature .

It should be noted that AC is the radius of curvature of the driver tooth at C, while BC is the radius of curvature of the driven tooth.

$$AC + BC = r_1 + r_2 = \frac{PD_1 + PD_2}{2} \sin \alpha \tag{11}$$

where PD = pitch diameter.

With this equation we can now derive an expression for the Hertz stress at the middle of the line of action (X = .5). Note that this is not the pitch point except for a 1:1 gear ratio. The Hertz equation applies:

$$\sigma_{.5} = .418\sqrt{\frac{EF}{w}\left[\frac{1}{r_1} + \frac{1}{r_2}\right]}^{\frac{1}{2}} . \tag{12}$$

But at X = .5

$$r_1 = r_2 = \frac{r_1 + r_2}{2} \tag{13}$$

and applying equation (11)

$$r_1 = r_2 = \frac{PD_1 + PD_2}{4} \sin \alpha \ . \tag{14}$$

Substituting (14) into (12) we obtain

$$\sigma_{.5} = .418 \sqrt{\frac{EF}{w}} \left[\frac{8}{(PD_1 + PD_2) \sin \alpha} \right]^{\frac{1}{2}} \ . \tag{15}$$

If we now take the gear ratio as

$$n = \frac{PD_2}{PD_1} \tag{16}$$

we obtain

$$\sigma_{.5} = .418 \sqrt{\frac{EF}{w}} \left[\frac{8}{PD_1(1 + n) \sin \alpha} \right]^{\frac{1}{2}} \ . \tag{17}$$

If we introduce the value

$E = 29 \times 10^6$ psi for steel and $\alpha = 20°$, and reduce the expression, we obtain

$$\sigma_{.5} = \frac{10.887 \times 10^3}{\sqrt{PD_1(1 + n)}} \sqrt{\frac{F}{w}} \text{ psi} \tag{18}$$

which can be written as

$$\sigma_{.5} = K_1 \sqrt{\frac{F}{w}} \tag{19}$$

where

$$K_1 = \frac{10.887 \times 10^3}{\sqrt{PD_1(1 + n)}} \ . \tag{20}$$

Figure 20 is a family of curves for K_1 for a range of gear ratios and pinion diameters. One can see from the curves that for a given pinion size the stresses become lower as the gear becomes larger. Also, smaller pinions at constant gear ratio result in higher stresses.

The Hertz stresses just calculated exist at the middle of the line of action. A single curve can be developed to relate stresses at all other points on the line of action to those at the middle. The development is presented here. If we designate the stress at some arbitrary value of X as σ_X, then from (10), (14) and (15),

$$\frac{\sigma_X}{\sigma_{.5}} = \frac{.418 \sqrt{\frac{EF}{w}} \left[\frac{1}{r_1} + \frac{1}{r_2} \right]^{\frac{1}{2}}}{.418 \sqrt{\frac{EF}{w}} \left[\frac{2}{r_1 + r_2} + \frac{2}{r_1 + r_2} \right]^{\frac{1}{2}}} \tag{21}$$

which simplifies to

$$\frac{\sigma_X}{\sigma_{.5}} = \left[\frac{(r_1 + r_2)^2}{4r_1r_2}\right]^{\frac{1}{2}} . \tag{22}$$

Upon substitution of $X = \frac{r_1}{r_1 + r_2}$ (23)

where r_1 refers to driver, regardless of whether it is pinion or gear, and

$$1 - X = \frac{r_2}{r_1 + r_2} \tag{24}$$

which can be obtained from the defining equation (3) one obtains

$$\frac{\sigma_X}{\sigma_{.5}} = \frac{1}{2\sqrt{x(1 - x)}} . \tag{25}$$

For convenience this ratio is defined as F_X.

A plot of this relation appears in Figure 21. This curve is symmetrical, passing through unity at X = .5, and reaching very high values at values of X approaching zero or one. This curve applies to all diametral pitches and all pressure angles for full depth and steel-tooth gears.

The following important observations should be noted. The minimum stress level for a given force occurs at X = .5. The stress at other points is simply related to the X = .5 value. The curves in Figure 20 indicate how stresses generally vary from one gear system to another. Figure 21 shows how the stress varies along any tooth for a given tooth load. The product of these two relations allows the actual stress at any point to be determined. However, not every point along the line of action receives the same load. The total transmitted load of the gearset must be multiplied by a function varying between zero and one to find the actual tooth load. Contact generally does not begin at X = 0, so the load function is zero up to a certain value of X. Similarly, since contact generally ends before X = 1, the load function drops to zero above certain values of X. While the minimum value of F_X occurs at X = .5, the point X = .5 may not come within the range of X where load is carried.

As shown in equation (15), the Hertz stress is related to the pressure angle. For the helicopter gears this angle is 22-1/2°, so Figure 20 does not apply. If we introduce the value α = 22-1/2 we obtain

$$\sigma_{.5} = .418\sqrt{\frac{EF}{w}}\left[\frac{8}{PD_1(1 + n)\sin\alpha}\right]^{\frac{1}{2}} \tag{26}$$

$$\sigma_{.5} = \frac{10.290 \times 10^3}{\sqrt{PD_1(1 + n)}}\sqrt{\frac{F}{w}} \tag{27}$$

which can be written as $\sigma_{.5} = K_2\sqrt{\frac{F}{w}}$. Figure 22 can be used to aid in the calculation of $\sigma_{.5}$ from this equation.

"Balanced Stress" Criterion

From the Hertz stress and load sharing calculation techniques developed in the two preceding sections it is possible to make a further development which may be of value in understanding of gear design and distress. The load which appears on a gear tooth in the neighborhood of the pitch line is produced by single-tooth contact. The resultant Hertz stress is higher than that in the adjacent double-tooth contact regions, for the same transmitted load. This is illustrated in Figure 24. From the shape of the F_x vs X curve, it can be seen that for values of X below a certain limit, or above a certain limit, the Hertz stress will rise to a level equal to the maximum which exists in the single-tooth contact zone. Stresses in excess of this level may be expected to produce damage before the pitch-line area is damaged, particularly since the sliding velocity at points removed from the vicinity of the pitch line is higher than near the pitch line. Because of the nature of the curve, it is possible for very high values of stress to develop if extreme values of X come into the load carrying region.

Based on this line of reasoning, it is possible to establish a criterion, that a gear is well designed only if the Hertz stresses in addendum and dedendum regions are limited to "reasonable" values with respect to the stresses in the single-tooth contact zone. What constitutes a reasonable value cannot be established on the basis of available evidence, but an arbitrary criterion may be established, and explored in relation to gear failure data to see whether any similarity between the criterion and failure results exists. The criterion which has been chosen here, for simplicity, is

$$\Sigma_s \geq m \, \Sigma_d \tag{29}$$

where

Σ_s = maximum Hertz stress in single-tooth contact
Σ_d = maximum Hertz stress in double-tooth contact
m = constant of proportionality.

That is, the Hertz stress in double tooth contact should never be permitted to exceed m times the maximum single-tooth contact Hertz stress. In this study m has been allowed to vary over a range, but for simplicity in the development, we shall fix the value at $m = 1$. In later paragraphs we shall show the consequences of varying m. The ratio of Hertz stress at a given transmitted load with and without load sharing is $\sqrt{2}$, if one adopts the assumption that load is shared equally by the two contacts. Figure 23 shows a curve of

$$F_x \text{ and } \frac{F_x}{\sqrt{2}} .$$

The point representing the first contact must occur on the lower curve. As the gears rotate, the point moves to the right, and then jumps abruptly to the upper curve when single tooth contact begins. The value of X where the maximum stress occurs in double-tooth contact is designated X_d, and the point where the maximum stress occurs in single-tooth contact is designated X_s. Our criterion is that

$$\frac{F_{x_d}}{\sqrt{2}} \leq F_{x_s} \tag{30}$$

where F_{x_d} is the value of F_x at $X = X_d$. Since

$$F_{x_d} = \frac{1}{2\sqrt{X_d(1 - X_d)}} \tag{31}$$

and

$$F_{x_s} = \frac{1}{2\sqrt{X_s(1 - X_s)}} \tag{32}$$

we can obtain by substitution,

$$\frac{1}{2\sqrt{2}\ \sqrt{X_d(1 - X_d}} \leq \frac{1}{2\sqrt{X_s(1 - X_s)}} \tag{33}$$

or

$$2X_d(1 - X_d) \geq X_s(1 - X_s). \tag{34}$$

If we write this as an equality, we define a curve separating the acceptable values of X_d and X_s from the unacceptable or "forbidden" values under the criterion.

$$2X_d(1 - X_d) = X_s(1 - X_s). \tag{35}$$

Solving this equation for X_d we obtain

$$X_d = \frac{1 \pm \sqrt{1 - 2X_s(1 - X_s)}}{2}. \tag{36}$$

A plot of this equation on an X_d vs X_s plane is shown in Figure 25. Any point lying on or between the curves satisfies the inequality in (34). Thos values lying outside this region are "forbidden".

We must now determine which gears produce contacts lying in these two regions. This depends on load sharing information obtainable from the curves in Figures 5 through 19. If we are dealing with full depth gears, the curves in Figures 5 through 11 are used, and the resulting information is applicable to gears of all diametral pitches, and 20° pressure angle. For 8/10 pitch 22-1/2° pressure angle stub tooth gears, Figures 12 through 19 are used, and the information applies to this gear geometry only. Values of X_d are obtained from the "Start of Contact" curves (double tooth), and X_s from the curves indicating the start of single-tooth contact, for each gear ratio and each number of teeth. Thus, a point on the X_d vs X_s plane represents a certain gear ratio with a certain number of teeth in the gear. If we plot such curves for the 20° full depth gears, at constant gear ratio we obtain Figure 26. The portions of these curves lying between the two limit curves represent "permissible gearsets, and those lying outside this region are "forbidden" by the

criterion. The intersection of each of these curves with the limit of the forbidden region establishes the limiting number of teeth at that gear ratio which will satisfy the balanced stress criterion. Another set of curves can be drawn through the curves for various gear ratios, in which the number of teeth in the gear remains constant for each curve. This is also shown in Figure 26. From this figure one can obtain the limiting number of teeth required for a permissible gear, and construct a curve of number of teeth vs gear ratio. This is shown in Figure 27. This curve goes through a minimum for a 1:1 gear ratio, and is symmetrical for step-up and step-down gearing. This curve shows that for a 1:1 gearset the minimum number of teeth required to keep the maximum stress down to the level existing during single-tooth contact is 18 teeth. For gears having 1:2 or 2:1 ratios, the minimum number of teeth rises to 34. The number of teeth required for 3:1 and 1:3 was not obtained because the curves were difficult to interpret in that region, due to crowding. However, by extrapolation, one can estimate that approximately 50 teeth are required.

Figure 28 is a plot of X_s vs X_d for the 8/10 pitch stub tooth helicopter gears, with a 22-1/2° pressure angle, constructed from Figures12 through 19. For moderate sized teeth, such as are being considered here, the second number in the diametral pitch designation is two higher than the first. The fact that there is a constant difference, rather than a constant ratio, means that the teeth of differing diametral pitches have not only differing size, but also differing shape. Therefore, it is not possible to represent all the different diametral pitches by one set of curves. The 8/10 pitch gears are presented in these calculations, because this is the pitch used in a particular helicopter transmission of interest, and because it serves as an illustration of the difference from full depth gearing. Figure 28 is analogous to Figure 26, except that the curves are more crowded so it is not practical to draw in the curves of constant numbers of teeth, which were shown in red in Figure 26.

It can be seen from Figure 28 that the curves cross into the "forbidden region" over a very narrow range of X_d from about .06 to about .08. The technique for finding the limiting number of teeth for these gears was therefore different from that used with the full depth gears. A family of curves for the start of contact was plotted, as shown in Figure 29. On this curve, a line was drawn through the values of X where the curves in Figure 28 enter the "forbidden region". This line is labelled m = 1. (The meaning of the line labelled m = .8 will be explained presently.) The points where this line crosses the curves establishes the minimum number of teeth at each gear ratio required to avoid the forbidden region. When these points are plotted against gear ratio, one obtains the left half of Figure 30. The right half is drawn from considerations of symmetry. The actual construction would entail drawing the curves similar to those in Figure 29 for the end contact, and drawing a line across in the region of $X_d = .93$.

As mentioned earlier, the condition that the maximum stress at the start or end of contact shall not exceed the maximum in the region of single-tooth contact is arbitrary. It is likely that comparisons of these curves with gear failure data, if they do reveal that this approach is valid, may indicate that some other ratio of stresses is a more appropriate limit. The criterion of equal stresses was taken for simplicity in the development, by setting m = 1 in the expression

$$Z_s \geq m Z_d \, . \qquad (37)$$

This led to the equation

$$X_d = \frac{1 \pm \sqrt{1 - 2X_s(1 - X_s)}}{2} \tag{38}$$

which is plotted in Figure 25. If we solve the problem while allowing m to remain general, we obtain the equation

$$X_d = \frac{1 \pm \sqrt{1 - 2m^2X_s(1 - X_s)}}{2} \tag{39}$$

which forms a family of curves with m as a parameter, as shown in Figure 31. These curves are symmetrical in X_d and X_s, with large values of m making the curves approach the X_s axis, and small values making them approach the X_d axis.

The curves are separated into two groups by a degenerate set of curves for the value m = .707, which form two intersecting straight lines. It is obvious that X_d can never exceed X_s for a real pair of gears, and therefore none of the curves for values of $m < .707$ can have any real significance. This means that in any set of gears which will operate, the stress at the start or end of contact must always equal at least .707 times the maximum stress in the region of single-tooth contact. Any effort to decrease it further would prevent load sharing, which is essential to the smooth transfer of the load from one contacting tooth pair to the next.

We can omit from the figure those portions which do not permit load sharing, and if we also realize the symmetry of the system, we can omit half the remainder, to obtain Figure 32. We may now superimpose the curves of X_s vs X_d from Figures 26 and 28 on Figure 32 to obtain the limiting number of teeth for various values of m, in the full depth gears, and in the stub tooth system.

It is not necessary for our purposes here to go through the actual mechanics of this process. Figures 33, 34 and 35 give the results, with which we can make several valuable comparisons. Figure 33 shows, for m = 1, the difference in the number of teeth required for full depth gears and for 8/10 pitch gears at various ratios The fact that full depth gears require more teeth to meet the balanced stress criterion is obvious. Figure 34 shows the effect, for full depth gears, of varying the value of m. The range from m = .8 to 2 is covered. The difference between the curve for m = .8 and m = 1 is substantial. At a 1:1.5 ratio, the m = .8 curve requires that the gears have about twice as many teeth. In this region, in other words, reductions in the stress at start or end of contact are obtained at fairly high cost, in number of teeth. On the other hand, permitting the value of m to go to 2 does not permit much saving in the number of teeth required, but it does permit high stresses to develop. It thus appears that values of m in the neighborhood of 1 may be the most practical to adopt. Figure 35 shows the variation in the same curves for the 8/10 pitch gears. For these gears the effect of going from m = 1 to m = .8 is small in the neighborhood of 1:1 gear ratio, but becomes larger as other ratios are considered. The difference between m = 1 and m = 2 is not great. It appears here, as in the consideration of full depth gears, that a value of m = 1 cannot be far from the best practical value.

Analysis of Helicopter Gear Mechanics

Speed

Laboratory gear tests have been conducted at 1000, 1600, 3200, 6400, and 12,800 rpm, in order to reveal any speed dependent variations of important phenomena. The speeds of various components in the transmission of a typical helicopter gear box are known, and a comparison with test gear speeds is therefore possible. Since there are differences in gear geometry, a direct correspondence over the entire tooth profile of sliding and rolling velocities between the two systems does not exist; but it is still important to make comparisons as well as is reasonably possible.

The helicopter transmission we are concerned with includes two series-coupled planetary stages, in which the sun of the first stage is normally driven at 1690 rpm. The planet cage of the first stage drives the sun of the second stage at 599 rpm. The ring gears in both stages are fixed. Since the geometry of a planetary transmission is somewhat more complex than that of a spur gear pair, these figures cannot be compared directly with the speeds which would exist if the sun and planet gear of the same number of teeth were in mesh as spur gears. A relationship which makes such a comparison possible may be derived as follows:

The peripheral speed of the pitch circle of the sun gear is given by

$$\frac{\omega_S PD_S}{2} . \tag{37}$$

Since the planet gears are rolling with the same surface velocity where they mesh with the sun gear, and zero surface velocity where they mesh the stationary ring gear, their center line speed is

$$\frac{\omega_S PD_S}{4} . \tag{38}$$

The angular velocity of a planet gear can be obtained from

$$\omega_P = \frac{\omega_S PD_S}{4} \div \frac{PD_P}{2} = \frac{\omega_S}{2} \frac{PD_S}{PD_P} . \tag{39}$$

The angular velocity with which the cage rotates is given by

$$\omega_c = \frac{\omega_S PD_S}{4} \div \frac{PD_S + PD_P}{2} . \tag{40}$$

If an observer turns with the planetary cage, he sees the sun gear rotating at a speed equal to the difference between the actual sun speed and the cage speed. He regards the center of each planet gear as stationary in his frame of reference, so he can consider the sun and any planet to be a pair of spur gears in mesh. The effective speed of the sun gear, then, is

$$\omega_{s_{eff}} = \omega_s - \omega_c = \omega_s - \frac{\omega_s}{2} \frac{PD_s}{PD_s + PD_p} = \omega_s \left[1 - \frac{PD_s}{2(PD_s + PD_p)} \right] \qquad (41)$$

or

$$\frac{\omega_{s_{eff}}}{\omega_s} = 1 - \frac{1}{2(1 + PD_p/PD_s)} \quad . \qquad (42)$$

In other words, the effective speed of the sun gear, considered as a member of a spur gear pair is less than its actual speed by the ratio above. In order to simulate the relations between the sun and any planet, a test gear rig should be operated at correspondingly reduced speed. Since this "speed factor" depends only on the ratio of pitch diameters, and therefore on the gear ratio, it is useful to calculate it for a range of gear ratios for future reference. Figure 36 is a plot of the Effective Sun Speed Factor as a function of gear ratio over a range of gear ratios from 0.1 to 10. The curve approaches 0.5 for very small ratios and 1 for very large ones.

For the transmission under consideration here, the ratio of planet gear diameter to sun gear diameter is .4118. This corresponds to an effective sun speed factor of .6458. Therefore, the first stage sun effective speed is

1690 rpm x 0.6458 = 1091 rpm.

The sun gear is in mesh with planet gears with a gear ratio of

$$\frac{6.375}{2.625} = 2.429 \ ,$$

so the effective speed of the planet gears is

2.429 x 1091 = 2650 rpm.

The speed of the sun gear in the second stage is 599 rpm, or .3544 x the speed in the first stage. Thus the effective speeds in the second stage are

Sun: 1091 x .3544 = 386.6 rpm

Planet: 2650 x .3544 = 939.2 rpm.

Thus, we find that the speed range involved in the helicopter transmission gears that are pitting is from a speed well below the laboratory test speeds to a speed which comes into the lower portion of the test range.

Load and Stress

In an earlier section of this report a method was presented for calculation of Hertz stresses in gears, and by which the influence of various parameters can be easily visualized. This method will now be applied to the appropriate gears in the helicopter transmission being examined in this study, and to our test gears. The helicopter gears can be analyzed by means of the load sharing and Hertz stress curves calculated for 8/10 diametral pitch

stub-tooth gears with 22-1/2° pressure angle. The test gears can be analyzed by the use of the curves for standard depth gears of 20° pressure angle.

Figure 37 shows the power profile for the helicopter in terms of the percent of operating time spent at each power level. The calculations which follow will be based on the maximum power of 705 hp, which is developed 10% of the time. The highest stress developed is much more influential than any lower stress on the failure. The helicopter develops 625 hp 40% of the time, and this operating point is also of interest because operation at lower stresses than the maximum may be beneficial, rather than harmful, under some conditions, as will be shown in a later section.

The sun gear in the first stage operates at 1690 rpm. This corresponds to a torque of 2,190 lb-ft, at 705 hp. The sun gear pitch radius is 3.1875 inches. At this radius the tangetial force summation transmitted to the planet gears is

$$\frac{2190 \times 12}{3.1875} = 8230 \text{ lb.}$$

There are four planet gears in the first stage, so the force per planet is

$$\frac{8230}{4} = 2050 \text{ lb.}$$

The calculations for the second stage must take into account the torque multiplication of the first stage and the larger number of planet gears. This will be considered later.

The gears have a pressure angle of 22-1/2° so the transmitted force along the line of action corresponding to the above tangetial force summation is

$$\frac{2050}{\cos 22\text{-}1/2^\circ} = 2230 \text{ lb.}$$

The gears have a face width of 1-1/2 inches. Therefore, the force per unit width (F/W) is

$$\frac{F}{W} = \frac{2230}{1.5} = 1488 \text{ lb/inch.}$$

Figure 22 provides a means of finding the Hertz stress at the middle of the line of action for these gears. This stress is

$$\sigma_{.s} = K_2 \sqrt{\frac{F}{W}}$$

where $K_2 = \dfrac{10.293 \times 10^3}{\sqrt{PD_1(1 + n)}}$

and can either be calculated or taken from the graph. Since the planet gear has a pitch diameter of $PD_1 = 2.625$, and the sun gear has a pitch diameter of $PD_2 = 6.375$, one can calculate

$$n = \frac{PD_2}{PD_1} = \frac{6.375}{2.625} = 2.4286 .$$

From these figures one obtains

$$K_2 = \frac{10.293 \times 10^3}{\sqrt{2.625\ (1 + 2.4286)}} = 3431.$$

Therefore,

$$\sigma_{.5} = K_2 \sqrt{\frac{F}{W}} = 3431 \sqrt{1488} = 132{,}300 \text{ psi} .$$

From the above figure the Hertz stress at any point on the line of action can be calculated by use of Figure 21, and with a knowledge of the values of X at which loads are picked up and shared by the teeth. This latter information is contained in Figure 18, which gives the following information:

Contact begins	.5457
Single-tooth contact begins	.6574
Pitch line[a)]	.7083
Single-tooth contact ends	.7564

If these points are applied to Figure 23 we obtain Figure 38. The values of abscissa in Figure 38 can now be multiplied by the value of Hertz stress at the middle of the line of action, calculated above, to obtain the solid curve in Figure 40. The dashed curve, which represents the Hertz stress distribution for the second stage, was obtained from the first curve. The torque multiplication through the first stage is

$$\frac{\text{1st Stage Sun rpm}}{\text{2nd Stage Sun rpm}} = \frac{1690 \text{ rpm}}{599 \text{ rpm}} = 2.66995 .$$

The transmitted load per planet gear in the second stage is increased in this ratio, and decreased in the ratio of 4/9, which is the ratio of the number of planet gears in the first stage to the number in the second stage. The net increase in transmitted load per gear in the second stage is therefore

$$2.66995 \times 4/9 = 1.1864 .$$

The Hertz stress is therefore increased in the ratio of

$$\sqrt{1.1864} = 1.0893 .$$

---

a) Listed for completeness only, this information is not pertinent to the present discussion.

The load sharing among gear teeth occurs in what is referred to by stress analysists as a statically indeterminate system. This means that from ordinary calculations it is not possible to calculate the percentage of load carried by each tooth. The division depends on the relative flexibility of the teeth and gear hub, regarded as a mechanical structure. Measurements on the test gears indicate that the load is not shared equally by the contact, as shown in Figure 4, and it is reasonable to expect that in the helicopter gears the load sharing is likewise not equal. However, since no exact load sharing information is available for the helicopter gears, it has been assumed that the sharing is 50% to each contact. In order to keep all calculations on the same basis, the approximation will be introduced in the consideration of test gears, that the load sharing is also on an equal basis.

One other approximation must be mentioned here, briefly, although the degree of error introduced by it cannot presently be assessed. In the above calculations it has been assumed that all planet gears share the load equally. While this is certainly true on the average, it must be realized that the same conditions of static indeterminacy apply to the load sharing among gears, as to load sharing among teeth. In a statically indeterminate system the load carrying member which is most rigid carries the largest load. Whether a gear is stiffer when in single-tooth contact or in double-tooth contact has not been determined in this study, and the answer is not immediately obvious. However, it is known that the stiffness of any gear set goes through maxima and minima during rotation. If it should happen that all the planet gears are phased in such a way that one gear is passing through its maximum stiffness while all the others are passing through their minima, then this gear would be more heavily loaded than our calculations show, during that portion of the revolution for which that condition continued to exist. While this is an extreme condition, admittedly, the phasing of the gears to provide that they all pass through their maximum and minimum stiffness together is also an extreme condition, which is probably never realized in practice. This fact would probably tend to make the loads on the teeth in their stiffest position statistically higher than those calculated by taking an average over the number of gears, and the loads in their most compliant position statistically lower.

Test gears are operated over a wide range of loads, and it is not appropriate to put forth a "power spectrum curve" as for the helicopter gears. Loads in the testing program are governed by the requirements of certain standard tests and the reaction of the lubricants to various load conditions. The load level may vary from practically zero to the full capacity of the test rig. Loads are applied by adjusting a scale load, called the "beam load". The corresponding transmitted load on the gears is 17.7 x beam load. Hertz stress curves for 10-lb beam load and 20-lb beam load are presented in Figure 41. The development of these curves follows a procedure similar to that for the helicopter gears.

The Hertz stress at the middle of the line of action is obtained with the aid of Figure 20. At 10-lb beam load the transmitted load is 177 lb. This is applied to 0.1-inch face width of the gear tooth, so that F/W = 1770 lb/in. Since the gears do not fall exactly on one of the curves, it is convenient to calculate the value of K_1 from the expression

$$K_1 = \frac{10.887 \times 10^3}{\sqrt{PD_1(1 + n)}}$$

where

$$n = \frac{19}{17} = 1.1177$$

and

$$PD_1 = 2.8333 \text{ in}$$

so

$$K_1 = \frac{10.887 \times 10^3}{\sqrt{2.8333 \times 2.1177}} = 4444.6 .$$

The ratio of Hertz stress at any point along the line of action to that at the midpoint is obtained from Figure 23, modified by the load sharing information obtainable approximately from Figure 8, which applies exactly for 1:1 gears. Since our gears are not exactly 1:1, we shall use information calculated specifically for this case.

	X
Contact begins	.1021
Single-tooth contact beings	.3556
Pitch line[a)]	.4722
Single-tooth contact ends	.5817
Contact ends	.8352

When these figures are applied to Figure 23, one obtains Figure 39. Multiplying the values in Figure 39 by

$$K_1\sqrt{F/W} ,$$

where

$$\sqrt{F/W} = 42.1 ,$$

produces the solid curve in Figure 41. The dashed curve is produced by multiplying by the value of

$$\sqrt{F/W} = 59.5 ,$$

which corresponds to 20-lb beam load.

This calculation assumes that during load sharing the load is taken equally by the two contacts. Figure 4, based on experimental data obtained prior to this project, shows that the actual load on the gear teeth ranges

a) Listed for completeness only.

from 40 to 60%. However, since it is desired to compare the data for the test gears with that for helicopter gears, for which no such comparable data are available, it was decided to place all calculations on a common basis by introducing the approximation for the test gears which was necessary for the helicopter gears. The actual load division is not seriously different from that which has been assumed.

Comparison of Stub-tooth Characteristics With Full Depth Teeth

Figure 42 shows the significant points along the line of action on a curve of F_x vs X for the helicopter sun-planet pair. Figure 43 shows the same information, together with the same information for a similar gear pair having 8 DP full depth teeth instead of stub teeth. In addition, information is presented showing the relation of stress during load sharing to that in single-tooth contact. All labels which are drawn below the curves pertain to 8/10 teeth, while all those above the curves are for 8 DP gears. The location of the arrowheads indicates the shifting of operating stress from the lower curve to the upper, and back again.

In the 8/10 DP gears, contact begins later at X = .5680. Single-tooth contact begins earlier at X = .6266, and ends later at X = .7787. Contact ends earlier at X = .8373. It is evident from this that the maximum Hertz stress reached on the tooth is slightly higher for the 8/10 gears. Further, since sliding velocity is proportional to $(X - X_{\text{pitch line}})$, it is clear that the sliding velocity in the 8/10 gears is appreciably higher at their point of maximum stress than the velocity in the 8 DP gears at their point of maximum stress. Thus, although the stub tooth operates with reduced sliding velocity at the tip of the addendum (end of contact) and provides increased tooth strength and rigidity, it results in increased sliding velocity at the point of maximum stress. This increase in contact severity occurs near the middle of the tooth profile, which is, of course, the region in which pitting damage has often occurred in the field. It may be that the use of stub teeth postpones addendum scoring, but it must impose an increased pitting burden upon the middle region of the tooth face.

Spur Gear Tests - Equipment and Procedure

All spur gear tests were carried out in this program by the use of a high speed spur gear machine, which uses sets of standardized test gears as specimens. A pair of these gears in mesh is shown in Figure 44. Figure 45 is a photograph of this machine. The machine uses the usual four-square principle to introduce torque into a closed loop, so that large power levels can be transmitted by the test gears without the need for expending large amounts of power in operating the machine. This spur gear machine, however, uses a somewhat unusual method of introducing the torque (load), which it will be worthwhile to describe.

The gearing system is shown diagramatically in Figure 46. Power input takes place through the shaft at the back of the machine, through a timing belt. The test gears are mounted on the two shafts which emerge through the front of the assembly into the test chamber. The 17-tooth gear is mounted on a shaft which is colinear with the power input shaft, and the

19-tooth gear shaft is gear driven from the power input shaft. The power flow between the 17-tooth gear shaft and the power input shaft takes place through a stub-shaft which is supported in a roller-bearing mounted carriage. This stub shaft is coupled into the loop by two gears of unequal diameter. When the machine is in the unloaded position these gears are simply in mesh with their mating gears. Loading of the gears is accomplished by rotating the carriage about the axis of the input shaft and 17-tooth gear shaft. This causes the stub shaft and its gears to roll on their mating gears. Since the stub shaft with its gears are assembled into a rigid system, they try to rotate as a unit. However, the fact that the two gears on the stub shaft are of different size causes them to try to rotate by different amounts. This results in the introduction of deflections into all the shafts in the loop, and the development of torsion in the shafts. The carriage is deflected by a cable, which can be seen in Figure 45, having a spring scale in it. The load can be applied or changed while the machine is in operation, and can be observed at all times on the spring scale. Any changes in load which are caused by wear in the gear teeth can be noted and compensated for. The provision of a means of load adjustment during running of the machine is an advantage which many four-square rigs do not have.

Lubricant is pumped at the rate of 10 cc per second through an inlet line at the top of the test chamber, and it flows into the gear mesh from above. The effect of varying the lubricant flow rate and inlet position has been studied previously, and this configuration and flow rate have been selected as standard conditions for tests. The effectiveness of lubrication is a function of flow rate, and for low flow rates, increases in lubricant flow improve the performance of the gear/lubricant system. At some flow rates below 10 cc per second, the curve flattens so that further increases in flow rate produce little additional benefit. The rate of 10 cc per second was chosen because it is high enough to make the tests insensitive to minor variations in flow rate.

This machine can be operated at test pinion speeds from 800 rpm to 30,000 rpm. The speed range is selected by installation of appropriate drive pulley ratios between the drive motor and the input power shaft. With any one pulley set installed, the speed can then be adjusted by controlling the DC drive motor.

Test gears are 6 DP, having 17 and 19 teeth, respectively, (17 = pinion, 19 = gear). Face width is 1/4-inch. The use of an odd, non-integral tooth ratio results in "hunting tooth" action. This means that each tooth of the pinion contacts each tooth of the gear in the course of a test, and the results tend to be "averaged out". The effects of minor errors in the teeth are thus distributed, so that each tooth presents essentially the same picture as the others. This is in contrast to the other machines, in which there is no hunting tooth action, and where all the teeth have to be inspected for an assessment to be made of the damage. The presence of hunting tooth action may have ramifications in the interpretation of the data which will be referred to later.

In all the tests conducted in this program, the gears were run with an axial offset in the mounting, so that only a portion of the face width was used in each test. This is accomplished by insertion of precision made spacers on the shafts along with the gears, so that either the pinion or the gear is moved axially 0.150" with respect to its mate. This results in an effective face width of only 0.1". This practice has three advantages in this program:

1. The strength of the teeth remains the same, but the force required to produce a certain force per unit width decreases. Thus, tests at high stress can be conducted without danger of tooth breakage or machine overload.

2. The number of tests which can be run on each gear is doubled.

3. A band of metal remains down the middle of each tooth which has not been effected by the tests, so it is possible to compare the damaged or worn surfaces with fresh surfaces on the same teeth.

By using the offset gear mounting, and by using the front and back of each tooth, it is possible to conduct four separate tests on each gear pair.

After passing over the gears, the oil is returned to a sump by gravity. Oil from the sump is circulated by a gear pump through a heater and a cooler, which are adjusted to bring the test oil temperature to the desired point. In all of these tests, the temperature was 100°F.

Load-Carrying Capacity Tests

A Load Carrying Capacity (LCC) test is designed to determine how much load a pair of standard gears can sustain at a given speed without damage from scoring. In the conduct of such a test, the gears are mounted in the machine and run for five minutes at no load with lubrication by the test lubricant as described above. The load is then increased to a reading of - lb on the scale (+ lb "beam load"), corresponding to 71.7 lb transmitted load, and the gears are run again for five minutes.[a] Loads are increased in --lb load steps and run for five minutes at each load step. At the end of each five minute running period the gears are unloaded by releasing the tension in the loading cable, and the machine is stopped. An inspection of the teeth of both pinion and gear is made at each step with the use of a microscope having a magnification adjustable over the range from 3.5 to 15. The LCC test schedule is plotted for a typical case in Figures 53 and 5-. During the inspection, the gear and pinion are rated with respect to the following kinds of damage, using a rating scale from zero to five:

abrasion
pitting
scoring

a) The term "transmitted load", as used in this report denotes the sum of all forces acting along the line of action by the teeth of the driver upon the teeth of the driven gear.

Addendum and dedendum are rated separately, essentially by the rule that a zero rating indicates that no damage of the type indicated has occurred, and for each unit of rating increase, 20% of the area is affected. Thus, a rating of five indicates that the entire area is covered by the type of damage listed. The severity of damage can vary, and some recognition of this is made in the ratings by increasing the numbers slightly if the damage is heavy, or decreasing them if the damage is light. This must necessarily be done in a qualitative manner and one must regard the ratings as descriptive, rather than quantitative. In this research program, all the gear ratings were done by the same person, so there is little likelihood of personal variations affecting the results.

The load carrying capacity tests are generally continued until the first evidence of scoring of the addendum of the pinion teeth is observed. The load carrying capacity value assigned to the oil is the load just prior to that at which the first scoring was observed.

Constant Load Tests

Tests were conducted on some of the lubricants in which the stepwise increasing loading schedule was not used, but instead, a certain constant load was applied to the gears after they were brought up to speed. The time required at constant load for either scoring or pitting damage to occur is recorded.

While the load carrying capacity test is based on the assumption that a lubricant has a certain "breaking strength" or score load, the constant load test is based on the assumption that the load carrying capacity of the oil depends on the load-time history through which the system has passed. This test standardizes this history at a constant load, and the test is continued at this load until the gears fail, or until it is clear that failure is not going to occur. Tests may last from 1 minute to many hours.

In actual preparation for a test, the steps are identical to those followed in an LCC test. Gears are mounted in the same way, and the lubricant is brought to the test temperature. The gear machine is then brought up to the test speed and held constant during any one test. The load is then applied by means of the loading scale, but instead of the stepwise increasing loading schedule, a single load is applied, and this is held until a failure is observed. In order to detect failure, the test is interrupted after five minutes, after twenty-five minutes, and every half-hour thereafter. In each inspection, the same procedure and rating system is used as in the LCC test.

Figure 53 shows the schedule of the Constant load test in comparison with the LCC test. Inspections are indicated for both tests by the small plusses. The circles indicate scoring. On some of the tests, scoring did not occur within the limits of the test period, and this was indicated by an arrow.

Break-In Tests

It was found, with some of the lubricants, that higher loads could be sustained after a break-in period. Several exploratory tests were conducted in an effort to determine how the break-in could best be measured. These efforts included running LCC type tests with longer times at each step, and various ways of bringing the load up in steps to the level at which constant load tests could then be run. By the latter part of the program a particular type of break-in test was found which proved to give useful and interesting information. In this procedure, the loading steps from an LCC test were duplicated, but at a load one or two steps below the score load, the test was continued at constant load for a period of time from a few minutes to several hours. Following this period of running, the load was then raised one step, and the test was continued until the gears scored. The load program for this type of test is shown in Figure 54 together with an LCC test, which is shown for comparison. At each speed, several break-in tests were conducted in which the time spent at the "break-in" load was varied, and the time to failure at the "failure load" was measured. The results of these tests are presented in Figures 61 through 71.

Spur Gear Results

Gear tests were run on several oils and over a range of speeds, as shown in the following chart. The oils were selected primarily because of their applicability to helicopter gearbox lubrication. The lubricants will be designated by their Mil Spec. numbers only:

	1000 rpm	1600 rpm	3200 rpm	6400 rpm	12,800 rpm
MIL-L-7808 C			LCC[a] CL[b]	LCC	
MIL-L-7808 D		LCC		LCC CL	LCC
MIL-L-7808 E		LCC CL	LCC CL BI[c]	LCC BI CL	LCC CL
MIL-L-21260 Grade (2)	LCC BI	LCC CL BI	LCC CL BI	LCC CL BI	

a) LCC = Load Carrying Capacity Test.
b) CL = Constant Load Test.
c) BI = Break-in Test.

The notations in the boxes indicate that tests of the type indicated were conducted for that lubricant at the speed indicated. The first tests were conducted on a MIL-L-7808 C lubricant but the program was shifted to a 7808 D lubricant as soon as it was obtained, since this was considered to be of greater interest. During the second half of the program, a MIL-L-7808 E lubricant was fully explored, and finally the MIL-L-21260 was investigated as fully as time permitted. A modification of the gear machine was required to permit running at speeds below 1600 rpm, and this was made late in the program, so that only the MIL-L-2160 was studied at 1000 rpm. It would have been useful to study the 7808 D and E lubricants at lower speeds also, but the information relating to the speed ranges of the helicopter transmissions was not received early enough to permit this.

Load Carrying Capacity Tests

Figure 47 is a typical load carrying capacity curve for a mineral oil. It has been included here to illustrate the nature of such a curve, and to show what might be expected of the curves developed in this program if the speed range were extended. In the low speed range scoring becomes difficult or impossible, because, with low sliding velocities, the contact temperatures cannot approach the melting temperature of the metal. The curve therefore goes up very steeply in this range. The data in this program essentially cover the medium speed range, which is characterized by a decreasing load carrying capacity with increasing speed. The high speed range is characterized by an upturn in the curve; this was not reached for the oils studied in this program, for which the data are presented in Figures 48 through 52. The load carrying capacity of the MIL-L-7808 C oil was measured at only two speeds before the testing of this oil was discontinued. The data are shown in Figure 48, where it can be seen that it is approximately 530 ± 35 at 3200 rpm, and 460 ± 35 at 6400 rpm. The spread in the data represents a difference of one load step which is at the level of reproducibility of the test equipment. The slope of the straight line representing these data is such that a reduction of one load step, 70.7 lb transmitted load, occurs for a doubling of the speed. Figure 49 shows the data for load carrying capacity vs speed for a MIL-L-7808 D oil, for a range of speed from 1600 rpm to 12,800 rpm. The load carrying capacity varies from approximately 600 lb transmitted load at 1600 rpm to approximately 150 lb transmitted load at 12,800 rpm. The slope of the line corresponds to 140 lb transmitted load per doubling of the speed. Figure 50 shows the data for a MIL-L-7808E oil. The scatter in the data here is greater than with the other oils, and in fact, it is so great that one could reasonably draw a line through the data parallel to the speed axis, as though the load carrying capacity were independent of speed, with a value of 360 lb transmitted load. However, the measurement at 1600 rpm was duplicated, and all other data indicate that the load carrying capacity must drop with increasing speed in this range. The line representing the data has been drawn with a slope corresponding to 110 lb transmitted load per speed doubling. The data for MIL-L-21260 (Grade 2) are shown in Figure 51. The load carrying capacity at 1000 rpm is 780 lb transmitted load, and this drops to approximately 210 lb at 6400 rpm. The slope of this curve corresponds to 220 lb per speed doubling. These curves are shown together in Figure 52, where it can be seen that MIL-L-7808 C has the highest load carrying capacity and the least drop-off with speed of the lubricants tested. MIL-L-21260 (Grade 2) has the lowest load carrying capacity over most of the speed range, and the highest slope. Therefore, this lubricant exceeds the others in load carrying capacity at speeds below 1600 rpm, which is the range of interest in the helicopter gears. This fact is important; oils should not be judged for service in one speed range on the basis of experience in another speed range.

Constant Load Tests

Data for Constant Load tests for MIL-L-7808 C oil with gears running at 3200 rpm are shown in Figure 55. Scoring of the pinion addendum is represented by circular data points, while gear adderdum scoring is represented by diamonds. The gear addendum generally scores earlier, a fact which is evident in this graph, and which is observable in most of the data obtained.

A straight line has been drawn through the data points with a slope corresponding to a decrease of about 24.7 lb transmitted load per doubling of life. This slope is not great, and it is difficult to determine accurately, because of the fact that the changes in score load are of the order of the reproducibility of the equipment. The load carrying capacity from the previously described tests is shown on this graph as a dashed line.

Figures 56 through 58 show the data obtained for MIL-L-7808 D oil at 1600 rpm through 12,800 rpm. The curve at 6400 rpm is based on the largest number of tests, and it is considered reliable. At 12,800 rpm, only one test was conducted, and the curve was drawn with the same slope as at 6400 rpm. The data at 1600 rpm are not sufficient in themselves to justify the curve which has been drawn through them, but in connection with the other data, it is considered reasonable to draw such a curve. Again, the slope has been matched to that obtained for 6400 rpm. No data were obtained at 3200 rpm for this oil. and therefore, a curve for this oil at this speed must be obtained by estimation from the other oils. The family of curves for this oil is shown in Figure 59. The curve for 6400 rpm has been drawn as a solid line, to indicate its greater reliability than the others. The other curves have been drawn as dashed lines, to indicate their dependence on the former.

Break-In Tests

Figure 60 shows the effects of eight different tests on MIL-L-7808 E oil at 1600 rpm, including three LCC tests, and five constant load tests. The load schedule is shown here, on a load vs time plane. The load carrying capacity test appears as a staircase, with the failure point at its end. In this case, one test produced a failure at 350 lb transmitted load, and two tests indicated a score load of 640 lb transmitted load. Constant load tests at 490 lb and 530 lb both produced immediate scoring. Further constant load tests at 350 lb and 420 lb did not produce scoring in a period of 360 minutes. This behavior tends to discredit the single score load determination at 350 lb and add additional confidence in the duplicate points at 640 lb. This fact is specifically mentioned, because the curve in Figure 50 of score load vs speed has been drawn to favor the 640 lb value.

These data are not wholly consistent with the constant load vs life concept, since constant loads above about 450 lb produced immediate failure, while those below did not produce failure in six hours of running. Thus, one cannot easily construct a relationship between life and load. On the other hand, one can see that the standard LCC value is repeatably higher than the constant load the gears can sustain. Inasmuch as the LCC test inherently provides a break-in schedule, by virtue of the stepwise running at increasing loads, it appears logical to look into the effect of break-in on the gear-oil performance in a more general way.

Figure 61 presents data obtained with the same oil at 3200 rpm. The LCC test "staircase" can be seen at the left, ending at 350 lb transmitted load. A constant load test at this level produced immediate scoring. One constant load test one step lower, at 320 lb also produced immediate scoring, while another did not produce scoring after 240 hours. A constant load test at 280 lb did not produce scoring after 360 hours. This indicates that the

limit of load carrying capacity for constant loads lies at about 320 lb. Below this level the gears appear to be able to run indefinitely without damage. This information, in itself, does not particularly suggest much break-in sensitivity, since the limit for constant load lies at approximately the same level as the standard LCC value. However, as an exploratory test, a load of 180 lb transmitted load was applied for 65 minutes, followed by stepwise increasing loads in increments of half the value used in the LCC test, or 35 lb transmitted load per step. The initial load was selected because it was well below that which in constant load tests had not produced damage. This loading program is shown in the figure, and it can be seen that it resulted in an increase in score load to 630 lb which is almost double the standard LCC value.

At 6400 rpm, as shown in Figure 62 various efforts were made to discover the interrelation between the LCC test, the behavior at constant load, and the effect of break-in. A standard LCC test resulted in a value of 350 lb. Constant load tests indicated that a limit exists at about 180 lb, as shown by the fact that at this level the transition occurs between immediate scoring and indefinite life (tests out to 6 hours). Only one constant load test, at about 145 lb resulted in a measureable life, thirty-five minutes. These data, again, do not support the construction of constant load vs life curves. Two tests were conducted starting at 70.7 lb transmitted load, and increasing in five-minute steps equal to half the standard LCC value, or 35 lb per step. These resulted in failures at 320 lb and 390 lb, which bracket the standard LCC value. A test which started at 35 lb, and increased in 17-1/2 lb steps resulted in a failure load of 480 lb, which is the highest load carried by this oil at this speed. A test in which constant loads of 110 lb and 140 lb for one hour each, followed by increasing loads in 35-lb steps of five minutes each resulted in a failure at 425 lb. Thus, certain kinds of break-in procedure definitely have the effect of increasing the load at which the gears score. However, one test also indicated that there is a fatigue sensitivity involved in these effects. In this test, the load was increased along a "staircase" with steps of 35 lb, starting at 70.7 lb, with five minutes at each step. At 280 lb the load was sustained for 210 minutes. At 320 lb the load was sustained for 150 minutes. The load was then increased to 350 lb, and failure resulted after thirty minutes. The fact that failure occurred after a delay indicates that there is a time dependence of scoring, even in the presence of break-in. This is probably a fatigue effect, as discussed elsewhere in this report.

Figure 63 shows LCC and break-in test data for a MIL-L-21260 (Grade 2) oil at 1000 rpm. The LCC test program is shown, ending in scoring failure at 850 lb transmitted load. The other data show the effect of break-in at a load two steps below the score load. The load was increased along the normal LCC "staircase" up to 707 lb transmitted load, and then held at this level for various lengths of time, after which it was increased one load step, to 771 lb. The tests were continued to failure at this level. It can be seen that running at the "break-in" load for 120 minutes resulted in survival of the gears at the "failure" level for 30 minutes.[a] Increasing the time at the "break-in" level

a) "Break-in level" shall be defined as that constant load one step below the test to failure. "Failure level" shall be defined as that constant load at which the gears are operated after break-in, until they fail.

to just under 200 minutes resulted in very large increases in life at the next load step. These results are plotted in Figure 67 where it is shown that there appears to be a maximum in the beneficial effect of running at the break-in load. However, since no data were obtained at this speed for the decreasing side of the curve, this has been shown as a dashed curve, merely to suggest its presence. Data for other speeds will be shown presently to support this.

Figure 64 shows the data for a MIL-L-21260 (Grade 2) oil at 1600 rpm. Three LCC tests are shown in which score loads of 630 lb, 705, and 780 lb were obtained. Constant load tests at 620 and 705 lb resulted in failure as soon as the load was applied. The gears were not run for even one five-minute period. No constant load tests were conducted at lighter loads as with the previous oils; instead the effect of break in was investigated. In each test, the schedule of the load carrying capacity test was followed up to 570 lb. This load was sustained for various lengths of time, as shown in the graph, and then raised to 630 lb. In four of the tests, failure occurred at this level after delays which ranged from five minutes to over 300 minutes. Figure 68 shows the relation of time spent running at 566 lb to time survived at 630 lb. The first point on the curve is obtained from one of the LCC tests, in which the normal schedule provides 5 minutes at 566 lb, and in which failure resulted during the next load step. The last point on the curve was obtained by running the test at 566 lb until failure occurred, which corresponds to zero minutes at the next load level. It can be seen that a very high maximum exists in the curve. In the neighborhood of 75 to 100 minutes at 566 lb, the time to failure at 630 lb goes to a very high maximum.

In some of the tests, the load was raised to a level still higher than 630 lb before failure resulted, Figure 64. These tests cannot be plotted exactly on Figure 68 since the time to failure was not reached at the failure load. However, one can see that these tests represent points arrived at by the gears without failure. The data are consistent with the curve drawn in Figure 68 and are shown on the graph as arrows, pointing in the direction where the points must lie.

Figure 65 shows the break-in data for MIL-L-21260 (Grade 2) at 3200 rpm, and an LCC test. The score load obtained from the LCC test was 430 lb transmitted load. A constant load test at 350 lb resulted in scoring during the first five minutes. Several, somewhat random loading schedules were also tried, resulting in a range of loads from 320 to 425 lb. Since there is always some scatter in gear data of this type, it is difficult to be certain that the differences are due to the variables. However, certain notable differences should be pointed out. Point C was reached by doubling the time spent at each load step of an otherwise normal LCC test. This resulted in a reduction in score load of one step. However, when the time spent at the preceding step, 280 lb was extended to thirty minutes, it became possible to run for 210 minutes at 350 lb, without damage, and even to go up to point E before scoring occurred. In one test, the initial load of 175 lb was held for thirty minutes, and then the load was increased in small steps until 320 lb was reached. At this level the test was continued until scoring occurred at point D. Point F was reached by following the same schedule up to 280 lb, and holding this level for 180 minutes. The schedule shown after that was followed up to point F, which lies

off the graph to the right, at 690 minutes. Thus, in the tests terminating in points E and F, the gears were able to operate for long periods at 350 lb without failure, while in other tests failures occurred at lower levels or at this level in short times.

Figure 66 shows the break-in data and an LCC test for the same oil at 6400 rpm. In this series the tests were organized around the idea of measuring the effect of operation at one load, somewhat below the level of an LCC score load, on the survival at the next higher load step. Two LCC tests were conducted, as shown, resulting in score loads of 280 lb and 355 lb. A single constant load test at 280 lb showed that some break-in was necessary for survival at this load. The gears scored within the first five minutes. Loads were raised along a "staircase" schedule to 210 lb and held at this level for various lengths of time before being raised to the next level of 280 lb. The survival times at 280 lb go through a maximum in the neighborhood of 100 minutes break-in, but this maximum is not as high as those noted at 1000 rpm and 1600 rpm. The curve in Figure 69 shows the relation between break-in time at 212 lb and survival time at 283 lb. In one test the load was not raised to 283 lb and the gears were run until failure at the break-in load. This took 540 minutes at that load. This point is plotted as having zero survival time at 283 lb.

If the curves of survival time vs break-in time are grouped together, Figure 70 is obtained. It appears from these data that the peak shifts to the left and drops as the speed increases. The number of revolutions in a given time is proportional to the speed, so this may be a factor which may tend to combine these curves into one. If one plots the data in terms of number of revolutions of break-in vs number of revolutions survived at the next higher load step, one obtains Figure 71. It can be seen that the data for 1000 rpm and 1600 rpm can be reasonably well represented by one curve, which has a very high peak at about 200,000 revolutions. The data for 6400 rpm definitely fall on a different curve, whose peak falls at about 600,000 revolutions and is much lower. This may mean that the data divide into two groups: the low-speed range, represented by the 1000-1600 rpm curve, and a high-speed range, represented by the 6400 rpm curve. However, the speed separation between 1000 rpm and 1600 rpm is not great, and the natural scatter in the data may mask the difference between two curves for these two speeds. If this is the case, then a family of curves with speed as a correlating parameter most likely is necessary to represent this effect. It is unfortunate that data in this form at 3200 rpm were not obtained, because this would probably resolve this question.

Rotary Contact Simulator Tests

This machine makes it possible to simulate with mathematical precision the contact conditions existing at any selected point in a pair of gears. It does this by revolving against each other a pair of disks having the same radii of curvature as the radii of curvature of the gear teeth at the point in question. A pair of such simulator specimens is shown in Figure 72 in the same relation to each other as they would have if mounted in the machine. Each of these specimens would be gripped along its hub by a collet, and

revolved about its axis at a predetermined speed. This produces a combination of rolling and sliding at the contact point which duplicates that existing at the point between gear teeth being simulated. Lubricant is pumped in a stream over the disks.

Before going further into the mechanical construction details of this machine, let us explore the basis for simulation so that the validity of this approach will be clear, and so some differentiation between this and other rigs can be pointed out. In the contact point between two gear teeth the conditions can be thought of as falling into two categories: imposed and dependent. The imposed conditions are those which are determined from without either by the person operating the gears or by the designer of the gears. Imposed conditions include environment temperature, load, speed, radius of curvature, surface finish, etc. Dependent conditions are those which arise as a result of the action or interaction of the imposed conditions. These would include lubricant film thickness, surface temperature, wear rate, and so on.

It can be seen that if all the imposed conditions of a set of gears were duplicated exactly, then all the dependent conditions would naturally arrange themselves to duplicate those of the gears. This is true, even though the experimenter does not understand the mechanisms fully which lead to the dependent conditions, and it includes even those dependent conditions the experimenter may be unaware of. This is an essential point to be appreciated in the study of any system which is not fully understood. This makes it possible to discover facts about the system from observation of the simulating system without having to question what mysterious parameters may have been upset in the process of creating the simulation.

At this point one may ask why one bothers to simulate gears at all, when the actual gears are available for study, and can be examined for the same effects which have been so carefully reproduced in the disks. There are several answers to this. The contact conditions along the surface of a gear tooth are different at all points. Sliding goes from a high positive value at one end of the tooth to a high negative value at the other, passing through zero at the pitch line. The Hertz stress goes through a minimum at the middle of the line of action, with respect to a fixed tooth load, but the tooth load is not constant over the whole tooth, since it is affected by load sharing. Thus, each element of the tooth surface exists in a complex gradient of several variables. In order to understand how the running of the gear has affected the tooth surface, the experimenter should have a large enough sample of homogeneous surface to examine with confidence. In a gearset, rigorously speaking, he has none. If one neglects the gradients, and examines a small region, one is still forced to draw conclusions about a very small region and generalize from them. Some effects, such as pitting and cracking, are statistical in nature. If one subjects a large area to identical conditions, one sees that bits of damage occur here and there. But if one has a very tiny section out of the area to examine, one may or may not look at a bit of damage in any given case. It would be very difficult for even a trained observer to state, for example, that certain conditions generally lead to cracking, if he had to reach this conclusion by observing small pieces of surface, which occasionally contained cracks. The Contact Simulator creates a homogeneous sample of surface entirely around the disk which exhibits the characteristics

of the point on the gear tooth under study. It is easy to recognize effects when they are produced in this way.

A second factor is the ease of observation. Gear teeth are difficult to observe with a microscope, especially when the gears are still mounted in the test rig, because of problems of controlling the lighting, and because the surfaces are curved at a disadvantageous angle and somewhat masked by other teeth. The fact that disk specimens can be observed normally, or at any desired angle, and can be illuminated with relative ease makes the accurate classification of surface effects much easier. Under the category of observation, one might include photography. As will be shown later, a method of photography of the disks is available which reveals surface irregularities very plainly. This technique has been valuable in determining the type of damage on the disks. This method is inapplicable to gears.

A third advantage of the use of the contact simulator is the elimination of the effects of gear geometry errors. In any gear, there are errors such as eccentricity, involute profile error and tooth spacing error. These errors have been reduced to a practical minimum in our test gears, but they can never be wholly eliminated. In addition, elastic tooth deflections under load cause changes in the relation of the surfaces entering contact, so that interference may result. It is easier to make a pair of disks accurately than a pair of gears, because the surface is a simple cylinder. Eccentricity is more serious if it occurs in the Rotary Contact Simulator than in the Gear machine, because it changes the shaft-to-shaft distance during each revolution. This requires the acceleration of the mass of the carriage through which the loading is applied, and this could result in fairly high forces being superimposed on the load. The advantage of the Contact Simulator is that these errors can be reduced to negligible proportions with care, while the production of gears without errors is practically impossible, and the elimination of tooth deflections is actually impossible.

Mathematical Basis of Simulation

As mentioned earlier, if all the imposed conditions existing in gears are matched, the dependent conditions must also be matched. The matching of some of the imposed conditions is intuitively obvious; the lubricant composition and bulk temperature must be the same in the two systems, and the metallurgy of the specimens must be the same. It is fairly obvious that if the radii of curvature and load are matched, the Hertz stress and contact width will also match. But what conditions must be met in order that sliding velocity, rolling velocity, time of contact, time out of contact, contact frequency, are matched?

The movement of surfaces of two gear teeth can be analyzed in terms of the diagram in Figure 1, with certain modifications. Figure 73 has been derived from Figure 1 to facilitate the discussion which follows. Since we are now interested in the details of movement of the surfaces in the neighborhood of the contact point, the base circles and addendum circles have been eliminated from the figure. The same arbitrary contact point, C, has been retained and attention is directed to the movement of the driven gear. The line OC is revolving with the angular velocity of the driven gear, so the velocity of the end of the line, C, is given by

$$U_2 = \overline{OC}\omega_2 .$$

This velocity vector is at right angles to the line OC, and can be resolved into components along the line of action, and normal to it, as shown. Angle DCE can easily be shown to be equal to α, and triangle DCE is similar to triangle BOC. One can therefore write

$$\frac{U_2}{\overline{OC}} = \frac{\overline{DE}}{\overline{BC}} = \frac{\overline{CD}}{\overline{OB}} \qquad (a)$$

or

$$\frac{U_2}{\overline{OC}} = \frac{\overline{DE}}{r_2} = \frac{\overline{CD}}{\overline{OB}} . \qquad (b)$$

But $\overline{CD}$ is the velocity of a contact point along the line of action, which is the same as the tangential velocity of a point on the base circle, which is given by

$$\overline{CD} = \omega_2\overline{OB} \qquad (c)$$

so we can substitute in (b) above to obtain

$$\frac{U_2}{\overline{OC}} = \frac{\overline{DE}}{r_2} = \frac{\overline{OB}\omega_2}{\overline{OB}} = \omega_2 . \qquad (d)$$

Therefore,

$$\overline{DE} = \omega_2 r_2 . \qquad (e)$$

By similar logic one can show that the component of velocity on the driver normal to the line of action is

$$\omega_1 r_1 . \qquad (f)$$

The component of velocity of the driver along the line of action must be identically equal to $\overline{CD}$ in order that the two involutes remain in contact.

At this point we make a critically important observation:

The components of velocity normal to the line of action of the surfaces in contact are identical to the surface speeds of disks having the same angular velocities as the gears, and having the same radii of curvature, respectively, as the teeth have at the point of contact.

From this point on, it is simple to demonstrate simulation of gears by disks. The sliding velocity at point C is equal to the difference in velocity normal to the line of action between the two surfaces, and this is given by

$$V_s = \omega_2 r_2 - \omega_1 r_1 .$$

If we now picture a pair of disks in contact, having radii r_1 and r_2, and revolving with angular velocities ω_1 and ω_2, we can see that the same sliding velocity is produced. The rolling velocity of each disk is similarly equal to the rolling velocity of the corresponding point on the gear tooth.

In achieving simulation the forces must also be matched; it follows that with identical radii of curvature arising from the above arguement, the Hertz stresses and contact width are also simulated. With equal contact width and equal velocities the times of contact must also be equal. Since the time required for a full revolution of a disk is identical to that required for the revolution of the corresponding gear, the time out of contact for corresponding points in the two systems is also identical. This consideration could be important in the study of EP film formation and destruction, since such films depend upon reaction rates and times.

Mechanical System

The Rotary Contact System can best be described as consisting of several interrelated sub-systems:

Basic machine
Hydraulic drive system
Speed control system
Friction measuring system
Test lubricant circulation system

The basic machine consists of a pair of hydraulic motors, driving through a pair of 10/1 ratio gearboxes to a pair of shafts which are arranged to hold a pair of specimens in the relation shown in Figure 72. Of this pair of drive trains, one is designated the "Driving Side" and the other the "Driven Side". The motors, gearboxes and shafts are identical on the two sides, but there are important differences in the mounting of these units to the base of the machine. The driving side assembly is attached to the foundation of the machine by bearings directly below the specimen axis, so that rotation of the entire carriage is possible, advancing the specimen toward the axis of the other specimen. A piston, advanced by air pressure, operates on the carriage to produce the rotation just described so that controlled loads between the specimens can be produced.

The driven side assembly is mounted to the base of the machine through bearings which are coaxial with the axis of the specimen. The friction torque produced as the specimens are brought together and rotated causes the driven side carriage to deflect against a spring, so that the friction measuring system is actuated. The rotation of the driven side carriage operates a linear differential transformer, whose output is amplified and recorded.

The hydraulic drive system consists of an electric motor driving a pair of variable volume positive displacement pumps. One pump delivers flow to the driving side hydraulic motor, from which it is returned at low pressure to a sump. The other pump delivers flow to the driven side hydraulic motor, after which it flows through a manually controlled back-pressure valve, through a large diameter coil of steel tubing to a water-cooled heat exchanger and to the sump. The same sump feeds both systems. The volume rate of the pumps is

individually controlled by operation of a pneumatic motor valve topworks, which strokes a control rod in the top of the pump. It is desired that the hydraulic connections to the driving and driven carriages not interfere with the accuracy of loading or of friction measurement, so special arrangements of the tubing were necessary. On the driving side, the hydraulic fluid is delivered to the motor through long runs of slender steel tubing, with loops added at every turn to increase flexibility. The fluid return from the motor to the sump was made through flexible plastic impregnated cloth tubing. On the driven side, the hydraulic fluid was delivered to the motor through coils of tubing which were designed to produce part of the spring force against which friction is measured. Two coils of opposite rotation were used, to cancel Bourdon effects, which would otherwise introduce errors into the friction measurement with changes in pressure. The low pressure return line, described above as a large diameter coil of steel tubing, acts as a spring in conjunction with the delivery lines to facilitate the torque measurement. No precautions were taken to cancel Bourdon effects because the pressure is low in this line, and the error from this is considered negligible.

The speed control system operates from two magnetic pulse counters mounted at the ends of the driving and driven shafts. Each shaft carries with it a non-magnetic disk with six steel pins, so that six pulses per revolution are produced. These pulses are counted and displayed on a pair of electronic pulse counters. The counting interval used is one second. The speed is given by

$$\text{rpm} = \frac{\text{revolutions}}{\text{second}} \times \frac{60 \text{ sec/min}}{6 \text{ counts/rev}} = 10 \times \text{counts} .$$

Pulses from the same counters are also fed into a two-channel "Ratio Speed Control" which is an adaptation of a Shell designed Ratio Flow Control which had been developed for another purpose. In this system, an oscillator was adjusted to produce a frequency in the neighborhood of the pulse rate from either the driving or driven side, whichever was higher. The incoming pulse rate was compared electronically with the oscillator frequency, and any deviation from the desired ratio produced an error voltage. This voltage was converted to a pneumatic signal, which caused a change in the position of the corresponding motor valve topworks on the pump, so that a correction in speed resulted. The desired ratio of oscillator frequency to pulse rate is separately adjustable for the driving and the driven side.

In any test, it is necessary that the specimen with the higher peripheral speed be mounted on the driving side, and the one with the lower peripheral speed be mounted on the driven side. When the machine is started up at no load, the control system brings the two shafts to the desired speeds; the hydraulic system is required to develop enough power to overcome the friction in the motors, seals and gearboxes. When a load is applied between the specimens, the one with the higher peripheral speed begins to deliver power to the one whose peripheral speed is lower. This requires the control system to readjust, which it can do quickly. However, at some load level, the driving disk is able to deliver enough power to the driven disk to overcome all the friction in the system. At this point, the demands on the driven-side hydraulic motor become nil, and the electronic speed control system no longer

has the ability to reduce the speed on that side. The tendency, then, is for the driven side to increase in speed until the disks are rolling, and of course, the test is invalidated. In this state the driven side motor acts as a pump. To prevent this, a special back pressure valve is installed in the outlet line of the driven side hydraulic motor, as previously mentioned. This valve is adjusted to produce a pressure drop, so that the total power requirement for operation of the driven side is increased to a level beyond the ability of the driving side disk to deliver by friction, so that some power is always required from the driven side hydraulic pump. As long as the driven side pump is delivering power to the system, the digital speed control can control the speed.

The friction measuring system operates from the reaction of the driven side assembly to friction at the disk contact. This assembly is mounted on anti-friction bearings on the axis of rotation of the specimen. The hydraulic inlet and outlet tubes are arranged to act as springs, so that the torque developed by the friction force produces a rotation of the entire assembly. A differential transformer converts this motion to an electrical signal, which is amplified and displayed on a recorder.

Certain difficulties with the operation of this system interfered with the accuracy of the data, so the system was not used in this study, except to allow the operator of the machine to monitor the friction as the tests were conducted. The difficulties apparently stemmed from distortion in the machine base and the transducer supports due to the loading forces of the tests, and from thermal effects.

The lubricant circulation system included an electric motor-driven gear pump, which delivered oil under pressure to two jets pointed toward the disks. Lubricant flows over the disks, and is retained within a chamber mounted around the disks. This chamber has moving parts and seals which cause the oil to be collected without undue waste, without interference with the movement of the driving side carriage in loading, or the driven side carriage in friction measurement. From the bottom of this chamber the oil flows through a filter, which removes metal particles and into a vacuum chamber, containing a number of trays. Air, which is entrained in the oil in contact with the disks and in the test chamber, is removed as the oil flows by gravity over the trays. This chamber, with a conical bottom, is mounted directly over the lubricant pump. Since the deaeration chamber is under vacuum, a gravity feed is necessary. An electric heater and a water cooled heat exhanger are inserted in the line between the pump and the test chamber, to maintain the lubricant at the desired temperature.

One of the oil jets delivers a stream of approximately 25 cc/sec directly from above into the space where the disks are approaching contact. The lubricant flow rate has not been precisely measured, and it probably varies somewhat with oils of different viscosity. However, experience with this and other systems has indicated that the response to increasing lubricant flow rate is such that once an abundance is present, additional amounts do not make a significant difference. The disks (or gears), operating at a certain load and speed, and with a lubricant of a certain viscosity, develop an oil film of a certain thickness. Any lubricant beyond that required to maintain the oil film must flow around the test specimens, and have no effect except cooling.

With respect to cooling, it was found in previous work that the oil jet was insufficient, even with flow rates of two or three times the present one, to cool the disks. It appeared that this was caused, basically by the same fact which was just described: high flow rates of oil introduced from above cannot pass through the contact zone. The metal surface emerging from the contact zone is coated with a very thin layer of oil, and because of the centrifugal force field, there is no opportunity for the surplus oil from the stream above to wet and cool the surfaces. As a result, the temperature of the disks rises to values which affect the properties of the metal. To combat this problem, a secondary oil jet was installed, pointing upward into the region where the metal surfaces are emerging from the contact zone. This provides cooling directly on the surfaces which are carrying the heat out of the contact zone, and proved quite effective in eliminating the problem.

Experimental Procedure and Results

The first step in performing a test on the Rotary Contact Simulator is to determine the proper specimens to use. This is done by determining the radius of curvature of the gear tooth to be simulated at the point of interest. For this purpose the gages shown in Figure 74 were used. The larger of the two gages is designed to be used with our standard 19-tooth test gear, and the smaller one is used with the 17-tooth gear. The outer rim of each gage is eccentrically mounted on the hub and can be rotated on it. One can mount a gage alongside the gear of interest and rotate the rim until the surface of the rim lines up with the area of interest on the tooth. This establishes the distance from the center of the gear to the point on the tooth, which is monotonically related to the radius of curvature. The gages are therefore calibrated directly in radius of curvature, which can be read from the side.

Once the radius of curvature of either member of the pair is known, the other can be calculated from the equation

$$r_2 = 1.026 - r_1$$

which applies only to the test gears. Rotary Contact Simulator specimens are then selected from an assortment, which most nearly approximate the values obtained above. The available sizes are listed below in pairs, along with notations indicating any special significance of certain pairs. In this program, practically all the work was done with pairs having radii of .700-.326 and .800-.226. This arose from the observation that one of the leading problems with helicopter gears was pitting. A photograph of a helicopter gear tooth which was submitted to us as an example of this is shown in Figure 75. Our gear tests were therefore conducted in a manner designed to produce similar pitting, if possible. This was not entirely successful, but in some instances our test gears developed pits as shown in Figure 76. In this case, the pit was located at a radius of curvature on the pinion of .700", which corresponds to a radius of .326" on the gear. The gears had been run at a transmitted load of 177 lb, and 6400 rpm with MIL-L-7808 D oil.

	Pinion	Gear
Start of Contact	.1047	.921
	.200	.826
	.300	.726
Start of Single-Tooth Contact	.3648	.661
	.400	.626
Pitch Line	.4845	.542
	.500	.526
End of Single-Tooth Contact	.5968	.429
	.600	.426
	.700	.326
	.800	.226
End of Contact	.8569	.169

The speed of operation of the Rotary Contact Simulator was matched to that of the gear machine. The disk representing the pinion addendum was operated at 6400 rpm, while the gear dedendum simulator disk was operated at a speed of 17/19 x 6400 = 5726 rpm. The disk with the higher peripheral speed in this case is the pinion simulator disk, so it was mounted on the driving side, and the gear simulator disk was mounted on the driven side of the machine.

Some eccentricity is always present between the mounting shank and the test surfaces of the disks themselves. There is also some eccentricity present in the collets which hold the disks, and the shafts and bearings themselves. In mounting the disks, it is necessary to check with dial indicators reading to 0.0001", and to rotate the disks within their collets to a position in which the eccentricity is minimized.

The lubricant is circulated and brought up to temperature, and then the shafts are brought up to speed. Load is applied by application of air pressure to a loading cylinder which has already been described. Pressures are controlled by regulators and read from laboratory test gages. The radial force developed between two specimens is proportional to the pressure in the loading cylinder and has by calculation and calibration been shown to be very close to

$$F = 30\ P\ (psi)\ .$$

In order to apply the correct load for simulation, it is necessary to examine the actual load existing in the gear machine and the Rotary Contact Simulator. As pointed out earlier, parts of the contact in a set of gear teeth are in single-tooth contact, and part in double. For the test gears, the fraction of the transmitted load being carried by a pinion tooth vs X is shown in Figure 4. At a radius of curvature of .7,

$$X = \frac{.7}{1.026} = .68 .$$

At X = .68 the contact carries 53% of the transmitted load. Since the damage had occurred at a transmitted load of 177 lb, the actual tooth load at that point was 53% x 177 = 94 lb. Since the gears are operated with an effective face width of 0.10", this corresponds to a load per unit width of 940 lb/in. The disks are operated with a contact width of .250", which would indicate that the force between them ought to be 2-1/2 times as high as on the gears, or 235 lb. However, earlier work with the high-speed gear machine has shown that for mineral oil, for speeds ranging from 1000 to 10,000 rpm, the factor to convert score-limited loads from 0.1" to 0.25" varies from 1.25 to 1.6, with 1.4 being a reasonable average value. No information is available at the present time to explain why this effect exists, and several hypotheses have been proposed. In the absence of better data, we are forced to use the experimental data available, so the factor of 1.4 will be used to relate loads carried at .25" face width to those at .1". The load required for simulation is therefore 94 x 1.4 = 132 lb.

Each of the lubricants used in the spur gear tests was also run in the Rotary Contact Simulator. Several of the tests were started with a break-in period of from 15-30 min at very light load, after which the load was raised to 105 lb. Inspection of the disks after this load revealed no damage, after which the load was increased to 150 lb. This resulted in a type of damage which has typified the results of study on the Rotary Contact Simulator, and which are shown photographically in Figure 77 through 79. These figures require some interpretation for a full understanding. Figure 78 is an enlargement of a portion of a dedendum simulator specimen. The illumination is so arranged that the smooth, work surface appears dark and the depressions are illuminated. Cracks can be seen on the dark background, across the direction of sliding, and parallel to the axis of the specimen. On one side of the contact zone the contact pressure was apparently heavier, probably as a result of a small amount of misalignment of this specimen with the addendum simulator. On this side the damage became heavier, and pits were formed along the edges of the cracks. The observation that the pits developed from the cracks is supported by the fact that the pits appear in lines across the contact surface and are in line with cracks. Figure 79 is a photograph of the same specimen taken with a special camera. This camera uses a special combination of a knife-edge slit and moving linkages to develop an image on the film which, in effect, is the "unrolled" surface of the specimen. This produces a photograph in which all portions are uniformly lighted and in focus. Furthermore, the lighting can be controlled in such a way that defects are emphasized. In this case the worn surface was illuminated in such a way that it appears bright and the pits and cracks are dark. Figure 77 is a similar photograph of the addendum simulator, showing a multitude of short scored streaks.

The significance of the evidence shown in these photographs will be more fully developed in a later section, but at this point it must be taken up briefly because the choice of further experiments hinges on it.

Previous work had led to a hypothesis that scoring in gear teeth was related to fatigue effects. It had been found that scoring and gear pitting were represented by curves of the type shown in Figures 55 through 59. Difficulty in the inspection of gear teeth, particularly in the dedendum, made the investigation of this hypothesis difficult. The evidence in the current study is a major advance because it establishes a connection between cracking of the dedendum, which is presumably a fatigue effect and scoring of the addendum. It is believed that the increase in friction which results from the cracks causes the contact temperature to go up, producing scoring.

Pits of the type observed in the helicopter gears and in a few of our tests gears are believed to be an extension of fatigue cracking. During each revolution the teeth undergo bending stresses, Hertz stresses, and probably also high thermal stresses, which being cyclical, can cause cracks to develop and propagate. When cracks develop it is likely that some of them will start beneath the surface because it is known that the maximum shear stress develops some distance below the surface (hard materials fail in shear). The continued propagation of a crack can isolate a fragment from the parent metal and leave a pit. Inasmuch as pits are induced by cracks and the fatigue-scoring hypothesis indicates that scoring is frequently also produced or hastened by cracks, it appeared that we could profitably continue the investigation of crack-induced scoring as a means of learning about pitting. At the same time, scoring is a form of damage of gear teeth which must also be protected against, and therefor whether or not one eventually solves the pitting problem by this approach, the information on scoring which is developed has potential value.

At this point we can return from the digression on scoring and give our attention again to the test results. Tests were conducted at 3200 rpm with MIL-L-7808 C oil for positions of the pinion tooth with radii of 0.45", 0.7", and 0.8". The first of these is at the pitch line and the other two are on the addendum. In the pitch line simulation the specimens were able to sustain loads up to 2360 lb radial load on 1/4" face width without damage. At the next load step, 2410 lb, the gear simulator specimen developed very fine, evenly distributed pits over its surface. The pinion was also thus affected but to a lesser degree. The loading schedule in this test was similar to a spur gear load carrying capacity test. A second pitch line simulation follows this, in which this break-in schedule was followed:

15 minutes	52.5 lb load
5	105
5	157.5
5	210

Following this, the disks were run at a load of 2410 lb for five minutes without damage. After an additional 45 minutes of running at this load, very fine pitting began to appear on the pinion simulator. After another 15 to 30 minutes this had increased on the pinion simulator and appeared also on the gear simulator. This test was continued for a total of 155 minutes at the 2410 lb load, during which the pitting continued to increase in severity on both specimens but was more severe on the pinion simulator.

Using the previously developed relation that a decrease in contact width from .25" to .1" decreases the load carrying capacity by a factor of about 1.4, one can calculate that the above load is equivalent to a transmitted load on the test gears of 1720 lb. Such a test could not have been run on the gears for two reasons:

1. The required beam load of 97.4 lb is beyond the capacity of the gear machine.

2. Scoring of other portions of the gear teeth would have forced the termination of the tests at much lower loads.

These tests demonstrated that pitting can be produced in a short time in the neighborhood of the pitch line by sufficiently high loads which, however, cannot be applied to the test gears. This suggests an experimental approach for the study of pitch line pitting which can be conducted on the Rotary Contact Simulator, but not on test gears. It is possible to operate pitch line simulations at high loads and high speeds so that the time required to produce pitting is reduced to practical values for laboratory study. This approach has not been used because other areas of very strong interest dominated the program.

The above tests also demonstrated that the damage did not occur instantaneously, but required an induction period of approximately 45 minutes at a load of 2410 lb. This confirms the argument that such pits are produced by metal fatigue.

From the above tests it may be seen that MIL-L-7808 C does not show a very strong break-in sensitivity. Damage occurred at the same load in a test with only modest break-in as in a test which followed the entire LCC type schedule. The fact that the specimens survived longer at a given load in the constant-load type test than in the LCC type indicates, on the other hand, that the stepwise loading schedule of the LCC test may have been producing some fatigue damage.

Four tests were made to simulate the pinion addendum at .8" radius, with a loading schedule comparable to that used in the spur gear LCC tests and with the same oil and at the same speed as in the previous tests. The results are tabulated here:

Loading Pressure, psi	Force Between Specimens at Failure, lb	Equivalent Gear Tooth Load, lb	Equivalent Transmitted Load, lb	
14	420	300	698	Uniform damage
14	420	300	698	Uniform damage
10-1/2	315	225	524	Slight nonuniform
7	210	150	349	Very nonuniform

The nonuniformity referred to in the above table describes the fact that the damage did not extend entirely across the contact width. In the last test the damage occupied only a narrow bank on the edge of the contact path. The degree of variation in stress across the contact is not known, but the dependence of failure load on this nonuniformity is obvious, and is to be expected. When the equivalent transmitted loads are plotted on a graph of LCC vs score load obtained for spur gears at this speed, Figure 80 is obtained. It can be seen that the two failures at 698 lb transmitted load are well above the curve, while the one at 540 lb is in agreement with it. The point at 349 lb falls well below the curve.

Thus, the load-carrying capacity for disks brackets the load-carrying capacity curve obtained for gears; the actual values for the disks correlate with the uniformity of loading. When the uniformity of loading was poor, the value obtained falls below the curve, and when the uniformity is good, the values are above the curve. A slight amount of nonuniformity was present in the test which produced a load-carrying capacity which agrees with the curve. This suggests that the load-carrying capacity of gears may also be affected by the uniformity of loading, and that the curve is drawn from data for which some non-uniformity existed. This reasoning is consistent with our knowledge about the rating of gears in load-carrying capacity tests. The first trace of scoring on the addendum of the pinion is used to assign the score load. Any non-uniformity across the tooth face or around the pinion on various teeth would tend to lower the load at which traces of scoring occur. Such nonuniformities have been observed.

In each of the tests listed in the above table, the observation of scoring on the addendum simulator coincided with the observation of axially aligned crack-like defects on the used surface of the dedendum simulator. In those cases where the scoring was non-uniform, the cracks were seen to extend only over that portion of the specimen as had contacted the scored portion of the addendum simulator as illustrated in Figures 77 through 79.

One test was conducted with specimens which simulated the contact conditions at a radius of curvature of .7" on the pinion. The load schedule followed the LCC schedule approximately up to a load of 377 lb and then up to 420 lb in load steps which were maintained for approximately twenty minutes each. No damage to either disk was observed in this test. This indicates a difference in the severity of contact between positions with radii of .7" and .8".

A total of 9 tests were conducted with MIL-L-7808 D at 6400 rpm. One was at a pinion radius of .8". The pinion simulator scored at the first load step of 52.5 lb, within the first five minutes. The gear tooth dedendum simulator exhibited cracks at the same time. The test was continued for ten more minutes at the same load with no substantial change in the appearance of the specimens. This score load is substantially below that obtained in gear tests.

The other eight tests were conducted to simulate .7" pinion tooth radius. The score loads ranged from 158 lb down to 105 lb, corresponding to 212 lb down to 141 lb transmitted load in the gears. The highest value obtained still fell below the curve of spur gear load-carrying capacity vs speed for this oil.

The tests with MIL-L-7808 E were conducted at 6400 rpm and 12,800 rpm. In the first such test, at 6400 rpm, the point simulated was at a pinion radius of .7". This test produced a high wear rate, scoring of the addendum simulator at a load of 105 lb and cracks on the dedendum simulator. This is equivalent to a transmitted load on the gears of 142 lb. By comparison with Figure 50, it can be seen that this point falls well below the load carrying capacity of the test gears at this speed.

The next test was performed in the same manner, but the dedendum simulator specimen was ground down .013" on the diameter, to remove any metal which might have previously been cracked during the manufacture of the specimen, and then heat treated in a furnace for 2 hours at 350°F to remove any residual stresses which might have been introduced in the regrinding operation. The results of this test essentially duplicated those of the previous one, indicating strongly that the cracking and pitting are not due to residual stresses from grinding and that these defects are not present in the unused specimens.

In two tests, loads were applied much more gradually than in those just described. In the first of these, no scoring damage occurred at all even though the load was raised to 345 lb, equivalent to a transmitted load on the gears of 465 lb. In the second test, the load was raised to about the same level at which slight scoring of the addendum simulator was observed. A few cracks of the dedendum simulator were observed at this stage of the test, as well. The test was continued to a load of 585 lb, equivalent to 790 lb transmitted load on the gears at which the scoring on the addendum simulator had become prominent, and the dedendum simulator had become pitted. These results are shown in relation to the load carrying capacity curve for this oil for spur gears in Figure 81.

If these data are compared to the break-in data for this oil, shown in Figure 62, it can be seen that the first onset of scoring on the contact simulator occurs at an equivalent transmitted load which is approximately the same as that reached by the gears with suitable break-in.

One test at 6400 rpm which simulated the contact at a pinion radius of curvature of .8" gave essentially the same results as those at .7" radius. This indicates that for this lubricant the difference in severity between these two positions on the gear tooth is not substantial.

Four tests were conducted at 12,800 rpm simulating the contact at a pinion radius of curvature of .8". In three of these tests the first load step was sufficient to cause scoring of the addendum simulator and cracking of the dedendum simulator. This is equivalent to a load of 52.5 lb, which is equivalent to a transmitted spur gear load of 87 lb. In the fourth test, the

first load step was reduced to 15 lb which corresponds to 25 transmitted load on the gears. Even at this light load the addendum simulator scored in the first five minutes of running. In Figure 50 it can be seen that the spur gear load carrying capacity decreases rapidly with speed and this qualitative fact has been substantiated with the contact simulator, but the actual value of the curve at 12,800 is well above the equivalent load level at which the simulator specimens were damaged. The cause of this discrepancy is not known.

On MIL-L-21260 (Grade 2) oil, three tests were conducted at 1600 rpm, and six at 6400 rpm. All tests were in simulation of the contact at a radius of curvature on the pinion tooth of .8". The tests at 1600 rpm were essentially similar to the spur gear break-in tests, shown in Figure 64. In these tests the load was increased in steps of 15 lb (25 lb spur gear transmitted load equivalent) with ten minutes at each load step. When a load of 285 lb (475 lb spur gear transmitted load equivalent) was reached, the tests were continued at this level for lengths of time which varied from 419 minutes to 1030 minutes, with inspections every 30 to 60 minutes. Rust was found deposited on the dedendum simulator after the second load step of the test in each case. This rust persisted until the end of each test. The addendum simulator became polished in each of these tests as though through the abrasive action which one might expect from the rust. Scoring occurred in each of the tests at about the load level at which the constant load portion of the tests began, but apparently the rust was able to reduce this to almost invisible traces. In one of the tests, after about 300 minutes, chevron-shaped cracks, with their points away from the direction of rotation and from the direction of sliding, appeared on the dedendum simulator; this was follows in about 120 minutes by complete scoring of the addendum simulator. In each of the tests, the dedendum simulator became gradually covered with small pits as the constant load portion of the test continued. In two of the tests the chevron-shaped cracks did not appear, and the sudden catastrophic scoring did not occur.

In the load carrying capacity type tests conducted at 6400 rpm with MIL-L-21260, it was found that the addendum simulator scored at loads from 30 lb (50 lb spur gear transmitted load equivalent) to 135 lb (224 lb spur gear transmitted load equivalent). The higher score load just cited agrees well with the spur gear score load vs speed curve taken from Figure 51, as shown in Figure 82. Since the maximum score load one obtains is probably the correct one, it is reasonable to suppose that some sort of disturbances in the other tests may have caused the specimens to score earlier. On the other hand, it is possible that the gears may have become slightly scored earlier than was noticed. Disk specimens are much to be preferred for the observation of small, elusive effects since they are much easier to evaluate, as discussed earlier. Rust deposits on the dedendum simulator frequently appeared at a load level of about 30 lb, and cracks or pits generally occurred just prior to scoring, or were discovered at the same inspection as scoring.

Some Incidental Observations on Rust

In many of the Rotary Contact Simulator tests deposits of rusty material were observed on the specimens. These deposits were heaviest on the gear dedendum simulators, but they also appeared occasionally on the pinion

addendum simulators. Deposits on the addendum simulators generally were thinner and were visible primarily in the spaces between the grinding marks, as though rubbed in by the action of the addendum simulator. These observations were made in tests of MIL-L-7808 D and E at 6400 rpm with addendum simulators having a radius of .7". Such deposits were also observed in tests of MIL-L-21260 oil at 1600 rpm and 6400 rpm with an addendum simulator radius of .8". These deposits were visible both to the naked eye and through the microscope when illuminated by incandescent light, but they became nearly invisible under fluorescent light. Under the latter condition, the deposits appear transparent and blue-black in color.

Organic solvents have been found not to remove the deposit which rules out the usual gums and varnishes which often form from lubricants. Dilute hydrochloric acid dissolves the deposit readily. The deposit is too thin to be removed by scraping for chemical analysis and it was found that an electron microprobe could not analyze it.

The most telling test was that of dissolving the deposit in oxalic acid and adding a weak solution of sodium ferrocyanide as an indicator. Oxalic acid dissolves iron rust but is not a good solvent for iron. Therefore, it was expected that if the material was rust, that this acid would remove it selectively. However, it was found that to completely eliminate the solution of iron, cathodic protection could be applied. A positive indication by the sodium ferrocyanide is shown by the appearance of a blue color when it is added to the test solution. Since the cathodic protection prevents the direct solution of iron from the steel, the only source of iron is in the deposit which has been dissolved. It was found that the deposit did, indeed, produce the blue color whereas an unused specimen, tested in the same way, did not.

The technique of the test may usefully be described here. The specimen was placed on a grounded metal block, such as a vee-block. A short length of platinum wire was adjusted, so that less than one millimeter gap appeared between the specimen and the end of the wire. A battery with about three volts potential was connected between the platinum wire and the vee-block with the positive connection on the platinum. A drop of oxalic acid was then allowed to run down the platinum wire to the gap between it and the specimen. This was held in the gap by surface tension and it completed the electrical circuit. The evolution of bubbles within the drop could be observed and this served as an indication that current was flowing through the circuit. After approximately half a minute, the drop was then removed with a dropper and transferred to a white porcelain dish where the indicator solution was added. Any change in color was clearly visible against the white background.

The series of tests described do not prove conclusively that the deposit is actually iron rust. However, it is quite clear that it is a compound of iron, and most likely it is red iron oxide. The significance of the formation of this material in the contact zone of operating gears has not been established. Since no wear rate measurements are available, it is not possible to state whether this phenomenon is accompanied by an increase in wear, in comparison to those conditions in which no such deposite is formed. However, the polished appearance of some of the surfaces suggests that wear may be appreciable.

Such deposits had not previously been observed on the surfaces of gear teeth tested under similar conditions, so special effort was made during subsequent test to observe any evidence of rust colored deposits on the teeth. It was found that these deposits do occur but on the gears there are so many distracting roughness elements due to original grinding marks, abrasion and scoring, that it had gone undetected before. Furthermore, the rust appears to be generated under some operating conditions, but not all. In the tests with MIL-L-7808 D and E referred to above, the deposits occurred at radii of .7" and not at .8". This means that only certain parts of the contact zone on a gear tooth produce this material.

Further work is needed to determine whether this is an important effect from the standpoint of gear operation. If it develops that such an abrasive material as this can be continuously produced in the contact zone of gear teeth, and that this has an influence on the wear rate, then possibly the specifications on such MIL-SPEC lubricants ought to be reviewed to determine whether this effect can be insured against.

Discussion

The results of Rotary Contact Simulator Tests have agreed reasonably well with the values of score load obtained directly from spur gears in a number of instances, and have disagreed in certain cases. The fact that agreement has not been exact in all cases is not surprising since all disturbances tend to lower the failure load. Only when the gears and the disks used in testing a certain lubricant are perfectly made and perfectly aligned can one expect both to reach the same ultimate failure point. Since this ideal is not possible, it is to be expected that in various cases one or the other of the systems will give higher score loads.

The valuable observation from these experiments has been, however, the degree to which trends in effects have been reproduced in the two systems, and the degree to which the Rotary Contact Simulator has been instrumental in the discovery of effects which were not previously observed in the gears. For example, in facilitating the observation of cracks and pits on the dedendum simulator specimens, the Rotary Contact Simulator has performed a function which was not possible with the gears alone. The observations are a subject of considerable importance to this entire project, and it will be taken up in greater detail here.

Fatigue-scoring hypothesis:

It has been known for some time that the failure patterns of gears is not completely consistent with the assumption that each oil possesses a unique "score load" beyond which the lubricant cannot protect the gear tooth surfaces. Data which were obtained prior to this project on the high-speed gear machine had indicated that certain lubricants, when tested at constant load on the spur gear machine, permitted failure to occur after a delay period even though the loads were below those obtained from the formal Load-Carrying Capacity Test. Furthermore, it was also known that the lubricant could be made to carry load for short periods above those obtained from load-carrying

capacity tests. These observations, together with the fact that data plotted in the form of load vs time to failure, fell reasonably close to straight lines on log-linear plots (Figure 57) suggest that a fatigue mechanism is somehow coupled to the mechanism of scoring. The hypothesis is therefore proposed, that scoring can come as a result of an increase in the severity of contact conditions accompanying the sudden appearance of fatigue cracks or pits on one of the surfaces of the contacting pair. This would explain the appearance of scoring after a delay period, and it would explain the fact that in the original data of this type, both scoring and pitting type failures were correlated by the same curves.

In order to understand how the appearance of cracks or pits might participate in the scoring phenomenon, let us first examine the scoring phenomenon itself. If the load in the contact zone is gradually increased, as in a load carrying capacity test, the lubricant film becomes thinner, and the amount of energy generated in the sliding process goes up. This results in a higher contact temperature, which tends to lower the viscosity of the lubricant, resulting in a tendency toward a still thinner lubricant film. Ultimately, a load level is reached at which the metal asperities begin to contact each other, resulting in a further increase in contact temperature. At some level, the increase in temperature becomes suddenly very large; it can exceed the melting point of the metal, and when this happens the surfaces are said to have scored. The throwing off of molten particles of metal, and the welding and tearing of the surfaces as a result of sliding produces a type of surface which can be readily identified as a scored surface by a trained observer.

We propose that this simple view of scoring can be complicated by fatigue. Fatigue in gears can be qualitatively understood if we realize that each time a gear tooth goes through mesh, it is subjected to a variety of stresses. The stresses come from various sources. It can be shown that when a Hertz stress distribution is developed, a maximum shear stress must also develop a short distance below the surface. In the presence of tangential stress at the surface in addition to the Hertz stress, the shear stress increases and moves toward the surface. These shear stresses are significant because hard materials, like the case-hardened gears, fail in shear. In addition to the stresses just mentioned, tensile and compressive stresses in the tooth surfaces are developed in each load cycle from the bending of the teeth. Finally, it has been suggested by some investigators that the high temperatures which develop in the contact zone contribute thermal stresses to the total picture. Without attempting to analyze the development and interaction of these stresses, which must obviously be very complex, one can readily agree that there are sufficient cyclical stresses present to make fatigue effects probable. If a pair of gear teeth are operating at a load high enough to induce fatigue effects, but not high enough to produce outright scoring, then one might expect that after some delay period, cracks or pits would develop. These would sufficiently change the coefficient of friction to make scoring much more likely than it was in their absence.

There is considerable evidence in the Rotary Contact Simulator data that this actually happens. In all tests where scoring was observed on the addendum simulator, there were associated cracks, or rows of pits present on the dedendum simulator. In those cases where the loading was uneven, due to

misalignment of the specimens, scoring was produced on the more highly loaded side of the addendum simulator specimen and cracking/pitting damage was confined to that portion of the contact zone on the dedendum simulator which had been running against the scored portion of the addendum simulator.

Further evidence of a relationship between cracking and scoring consists of the observation that a line on the dedendum simulator contacts a certain distance on the circumference of the addendum simulator as they pass through contact together. The distance contacted depends on the load and on the relative rotative speeds. This was calculated, and it has been found that the length of the scored streaks on a typical addendum simulator specimen agrees approximately with the distance contacted by a line element of the dedendum simulator. Thus, in some cases at least, it is believed that scoring may be fatigue induced.

EP agents are added to lubricants to increase score loads. The addition of extreme pressure agents to the lubricant produces surface films on the metal which have lower friction than the metal asperities themselves, and they thus put off scoring to higher loads. Their ability to do this is generally evaluated in short term tests, similar to the load carrying capacity test. However, lubricants in service are generally called upon to provide their protection for long periods, for which even the constant load tests are only a short approximation. In this case, EP agents by virtue of the higher loads that they allow may accelerate cracking. What is one to expect of an EP agent which is so effective that in spite of the advent of fatigue cracks, it can still prevent scoring? Since cracks, once formed tend to grow and produce pits, it ought to be expected that such effective EP agents as these would prevent scoring, but allow instead pitting to develop in long-term service.

Two other areas may be discussed briefly. When gears are constructed according to the stub-tooth proportions, as are the helicopter gears we are familiar with, the regions of high-sliding velocity are eliminated and the tendency to score is thus reduced. However, the high stress region near the pitch line, where the loads are carried in single-tooth contact is still present, so the effect of operating at high loads for long periods ought to produce pits. In addition, helicopter gears generally operate at fairly low speeds where the contact energy is usually not sufficient to produce scoring. One should, therefore, expect that damage would occur in the form of pits.

It has been reasonably demonstrated that scoring, under the conditions of this test program, is related to the development of fatigue cracks. By investigating fatigue effects through the medium of scoring, we have been able to accomplish a great saving of time. Furthermore, it is believed that the study of scoring is important in its own right. The requirement that gear boxes carry higher and higher loads in the future, and the use of turbine drives both indicate the trend to more severe conditions. Increases in speed have been shown here to be accompanied by reductions in load carrying capacity for every lubricant tested. The fact that scoring is not a current problem does not, in itself, guarantee that increases in speed and load can be made without scoring failures.

So far in this discussion we have been concerned with the relation between fatigue and scoring. Considerable information has also been developed here to indicate that some sort of break-in schedule is highly beneficial in protecting the gears from damage in operation. It has been shown, furthermore, that an optimum break-in exists, at least within the framework of our limited test program. Less than the required amount of break-in results in early scoring of the gears, while a break-in schedule which is too long can begin to produce damage in itself.

It is believed that break-in involves a sort of "competition" between two effects. Break-in, by its very nature, takes advantage of the high stresses produced by the irregularities in the new surfaces to produce localized high wear. To provide maximum advantage, the break-in schedule should be long enough to reduce the roughness to a practical minimum, without exceeding the stress level at which fatigue cracks begin to be produced. Concurrently, with the beneficial effects of break-in, there is the likelihood of the occurrence of fatigue damage.

In the tests which have been conducted here, the really meaningful break-in tests are those for which the results have been plotted in Figures 67 through 71. Here, the survival time of the gearset at a fairly high load is related to the time spent by the gearset breaking in at a load one test-step lower. The survival time of the gears at the "failure" load goes through a maximum as the time spent at the "break-in" load is varied. The time required at the break-in load to produce the maximum survival time at the failure load may be referred to as the optimum break-in time. If less than the optimum break-in time is provided, it appears that insufficient reduction of asperities has occurred. This effect may be considered to continue, at least to the optimum, and perhaps beyond, since there is no reason to believe that the beneficial wear ends at this point. However, the second effect, fatigue, is a function of the break-in program, also. If contact conditions remain constant during the operation of the gears, one might argue that the effect of fatigue accumulates at a fairly uniform rate, until the surfaces fail. However, the rate at which the fatigue effects accumulate is not only a function of load, but is also a function of surface roughness. High surface roughness increases the tangential friction force present on the surfaces which in turn increases the maximum shear stress developed within the metal. Moreover, the higher frictional heating raises the contact temperature which may change the activity of the EP agents, and also any pro-fatigue effect they have. As a result, the damaging effect of fatigue during the break-in load probably accumulates at a decreasing rate. The interaction of a break-in wear process which is improving matters with time and a break-in fatigue process, which is steadily making matters worse, results in the production of a maximum in the survival time at the failure load in these tests. These data are not directly applicable to helicopter gear practice, without further study. They arose in a test program in which they were not fully expected and therefore the information is not fully developed nor fully understood. It is extremely likely, however, that by the further exploration of this avenue of research much can be learned about the properties of lubricants and the safe loading of gears. The development of break-in schedules for new gears, based on laboratory data, must eventually provide gears which have a better chance of survival without pitting than the

present gears. The understanding of the way in which various load schedules, including shock loads, or other momentary overloads may affect the life expectancy of gears should also be useful in machine design.

With the above background some further observations on the complexity of studying gear pitting may be useful. To avoid laboratory runs which last for months it was necessary to operate at loads which accelerate damage. The effect of operation at higher loads is to produce fatigue in fewer load cycles, and therefore sooner, but it also changes the manifestation of damage. At light loads, when cracks develop they may not produce scoring because the loads are not high enough to produce very high contact temperatures. This is particularly true for the helicopter stub-tooth gears, where the regions of highest sliding velocity have been eliminated. Therefore, after small cracks have been produced, these gears may continue to operate until the cracks have grown sufficiently to allow pieces of metal to drop out of the tooth surfaces, producing pits. At higher loads, there is increased likelihood that the cracks will produce scoring.

In laboratory tests with full-depth gears, operation at both high load and high speed to accelerate fatigue, results in scoring because each of these factors brings the contact closer to the scoring limit, and it takes only a small additional energy input to cause scoring. The additional energy comes from an increase in friction at the contact due to the sudden appearance of a surface crack.

Thus, while laboratory tests produced scoring, it is the theme of this arguement that the scoring resulted from cracks (in these tests) which, in another system, would have propogated and ultimately caused pits. Since scoring and pitting arose from the same cause (cracks), we can, with care and alertness to the complexities of the phenomena, use certain kinds of score-limited tests to study fatigue pitting in the laboratory.

Some final comments on laboratory tests can now be made. The phrase "care and alertness" above is not used casually. Valid laboratory work of this kind requires detailed and literally microscopic examinations of the test surfaces so that incipient changes may be detected before they become confused with other events; it requires cross-checking of observations in at least two systems, in this work the gear machine and the simulator, to avoid isolated peculiarities of special systems; and it requires the support of a careful analysis of the mechanics of contacts so that what is discovered in laboratory tests will have a rational foundation for translation to practical systems. The latter requirement is the principle purpose of the analysis of gears presented in this work. The analysis provides a language to relate laboratory and field observations; while it should be useful to designers of gear systems, it is not in itself a guide to gear design.

Summary and Conclusions

1. An analysis has been presented that allows one to calculate the Hertz Stress for a gear contact point at the middle of the line of action by a simple expression. This stress value has been called $\sigma_{.5}$. The Hertz Stress at any other point, σ_X, is shown to be related to $\sigma_{.5}$ by a parameter X, which

is the fractional distance traveled by the contact point from the beginning of the line of action at the base circle of the driver to the end of the line of action. The occurrence of single-tooth and double-tooth contact can also be expressed in terms of the parameter, X. Through use of the ratio, $\sigma_X/\sigma_{.5g}$ and the parameter, X, much of the complex mechanics of involute gears can be reduced to relatively simple forms. Generalized curves have been developed to show the relationship between Hertz Stress, gear ratio, and pitch diameter for any involute gearset of a given pressure angle. Two sets of these curves are given, one for 20° and one for 22-1/2° pressure angle.

2. A study of the relationships revealed by the above analysis suggested that one might establish a balanced stress criterion that would avoid the use of those gearsets having regions of particularly severe contact stress. Such regions can occur near the beginning or end of double-tooth contact for certain choices of gear ratio and number of teeth. Since sliding speed is also high in these regions, it is preferred that the maximum stress in double-tooth contact should be not more than the stress in single-tooth contact, a region of relatively low sliding velocity. The ratio of maximum double-tooth contact stress to maximum single-tooth contact stress has been called m, and plots are presented which show the relation between gear ratio and minimum number of teeth for values of m ranging from $1/\sqrt{2}$, a theoretical minimum for load sharing, to 2. These values bracket the practical range of interest.

3. Spur gear experiments consisted of load-carrying capacity tests, constant load tests, and break-in tests. From the first two of these a hypothesis relating fatigue to scoring was evolved. This hypothesis states that scoring may result from an increase in contact severity arising from the sudden appearance of fatigue cracks in the contact zone. This would explain the appearance of scoring after a delay period, and it also explains why scoring and pitting type failures can sometimes be correlated by the same load vs time curve. The break-in tests suggested that two competing mechanisms are in operation during the early period of gear running. On the one hand, break-in operation reduces surface roughness and thereby reduces both surface stress and surface temperature. These effects, in turn, allow higher loads to be carried for longer periods in subsequent operations. On the other hand, fatigue cycles are accumulating during break-in, and moreover they are accumulating over a high stress (rough) period. The consequences of this stress history will shorten the useful life in subsequent operations. Data are presented which show how these two mechanisms, operating together, result in an optimum break-in for maximum service life.

4. The Rotary Contact Simulator makes it possible to exactly simulate the contact conditions existing at any selected point in a pair of gears. Moreover, it creates a homogeneous sample of surface entirely around the disk which exhibits the characteristics of a single element (Hertz area) on the gear tooth under study. In contrast, each element of a gear tooth exists in a complex gradient of several variables, and any particular element of interest is available as only a very small sample. This availability of a relatively large sample on the simulator lends appreciable power to observations of phenomena with broad statistical backgrounds, such as fatigue. Through the use of the simulator, the fatigue-scoring hypothesis was confirmed in detail; and an

extension of the hypothesis, that is, in the absence of scoring, cracks will degenerate to pits, was also observed.

5. Incidental to the main stream of the work was the observation on the simulator that traces of rust are produced on the working surfaces under some operating conditions. Careful searching for rust on the gears revealed that it was present in that system too, although its presence in gears would not have been detected without guidance from the simulator. This observation was not persued with further experiments, although the implications for gear lubrication and wear are probably quite significant.

Figures 1 through 82 follow

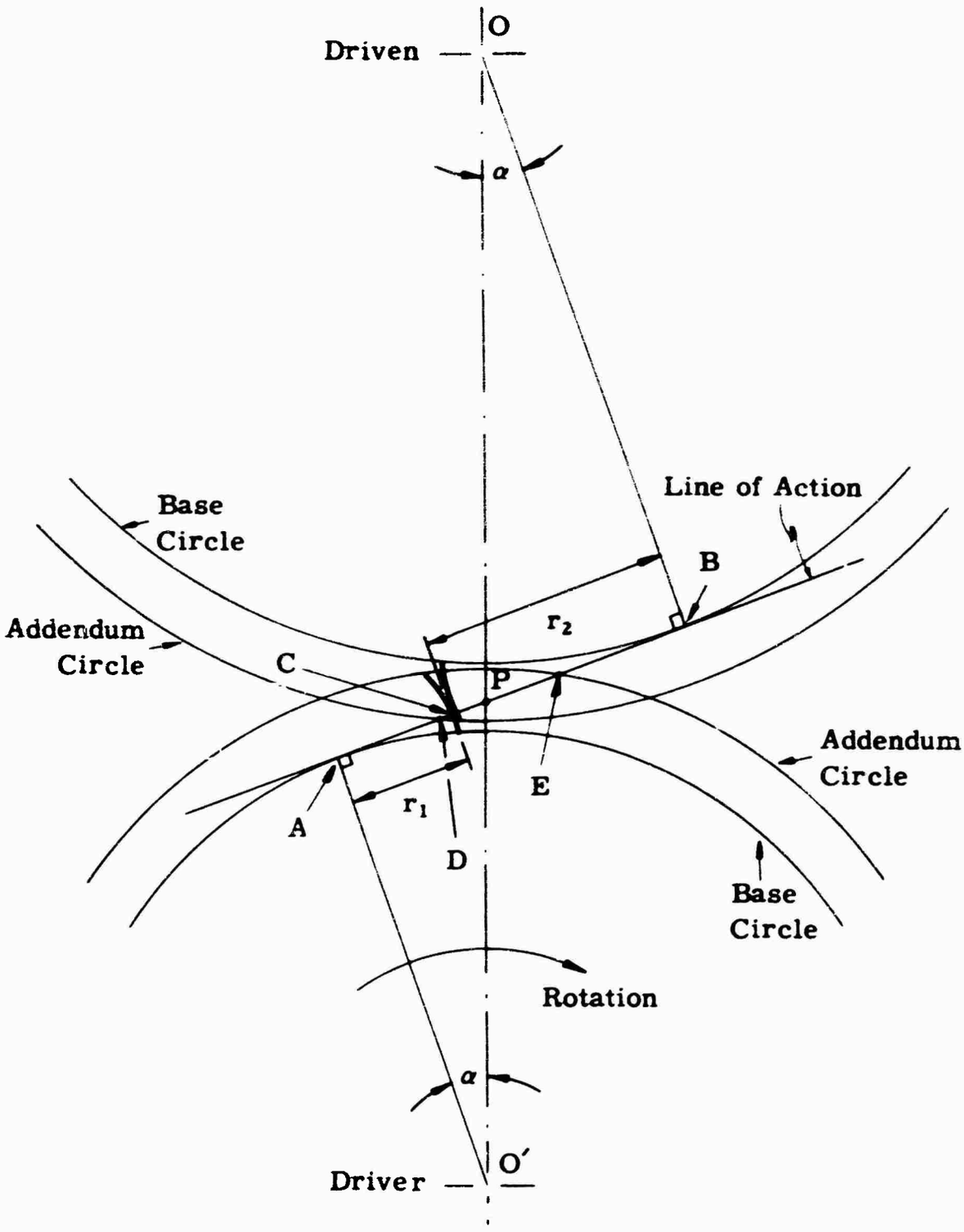

Figure 1. GEAR GEOMETRY DIAGRAM

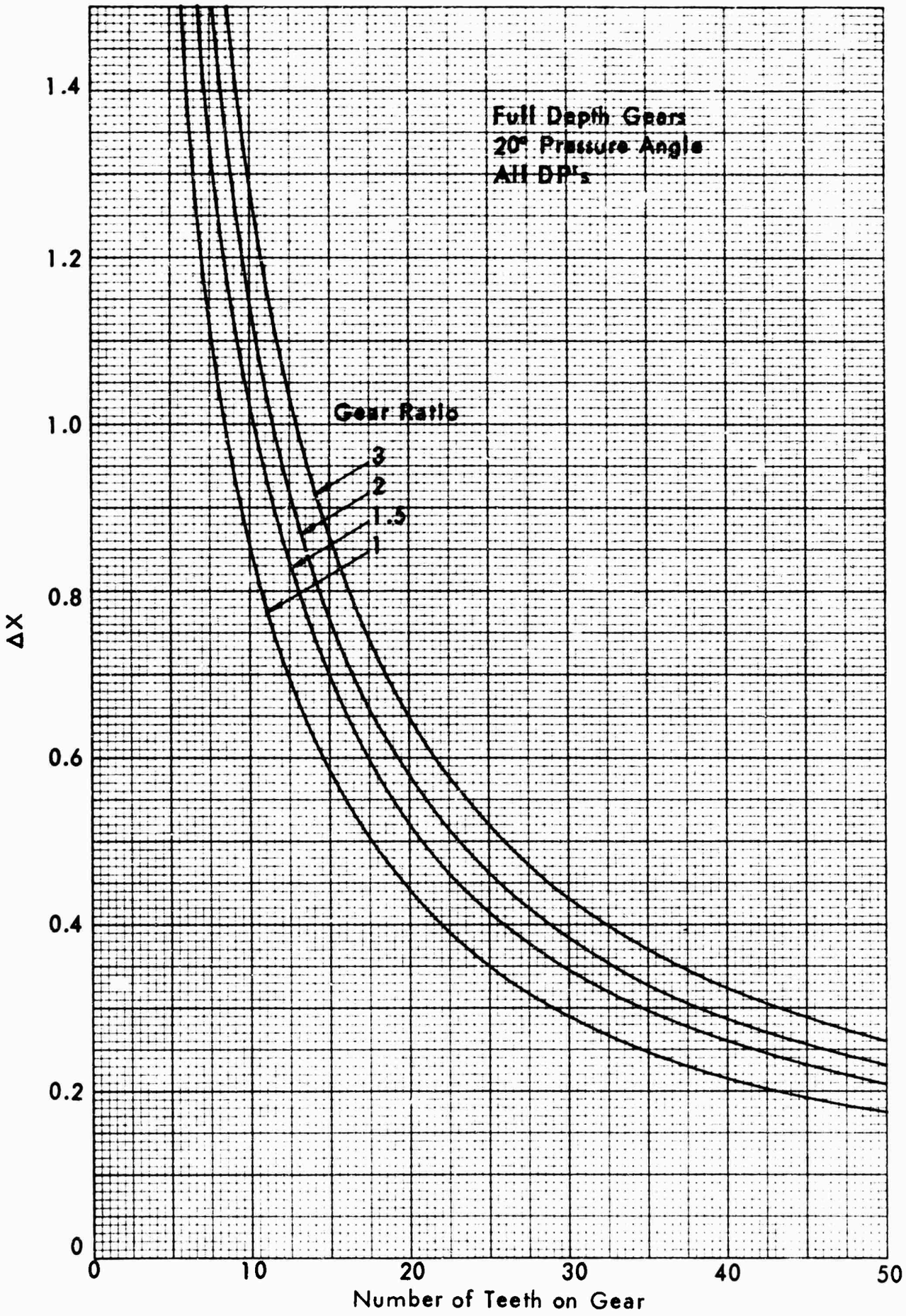

Figure 2. FRACTION OF LINE OF ACTION BETWEEN CONTACT POINTS

A-1510

S-13926
59005

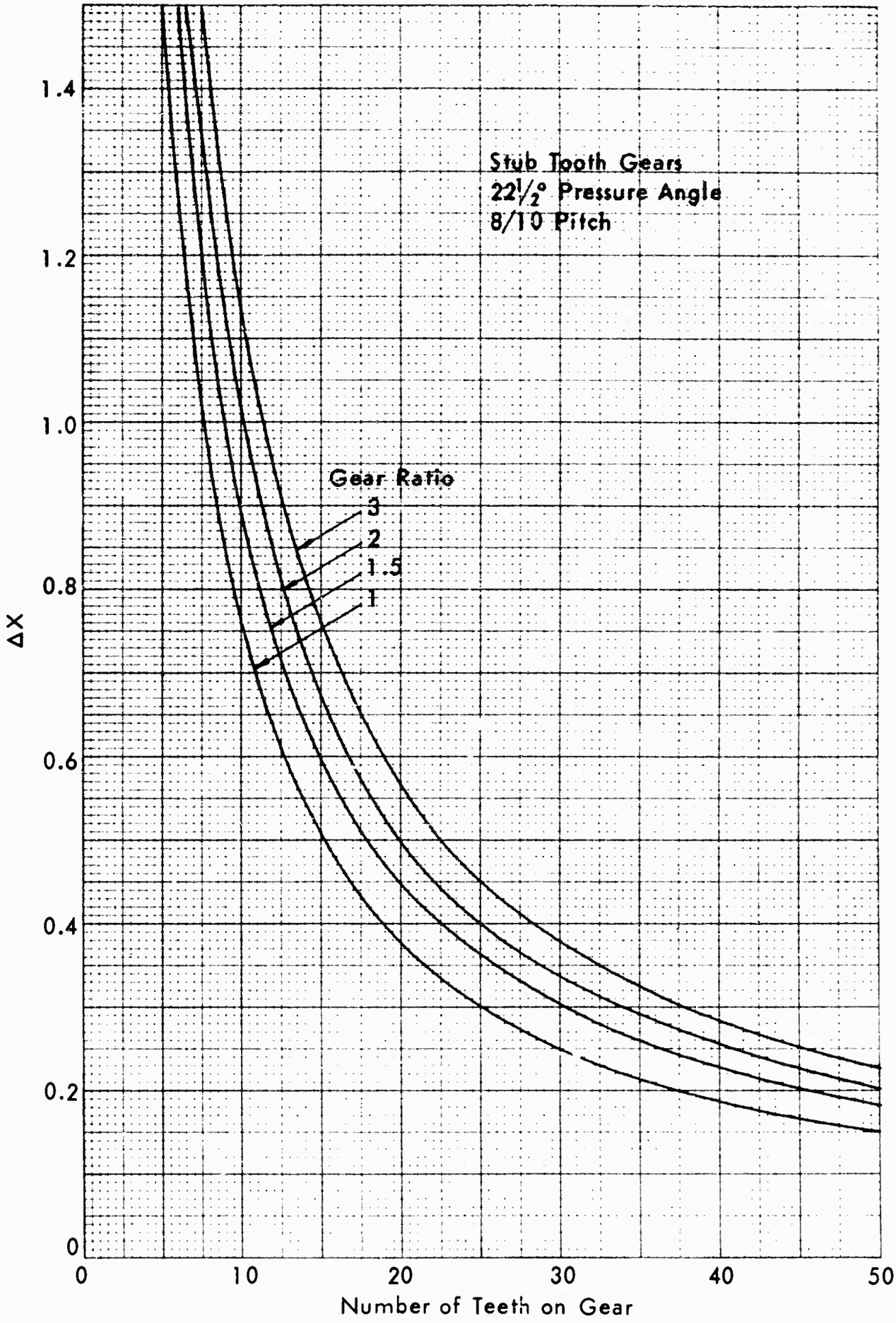

Figure 3. FRACTION OF LINE OF ACTION BETWEEN CONTACT POINTS

S-13926
59926

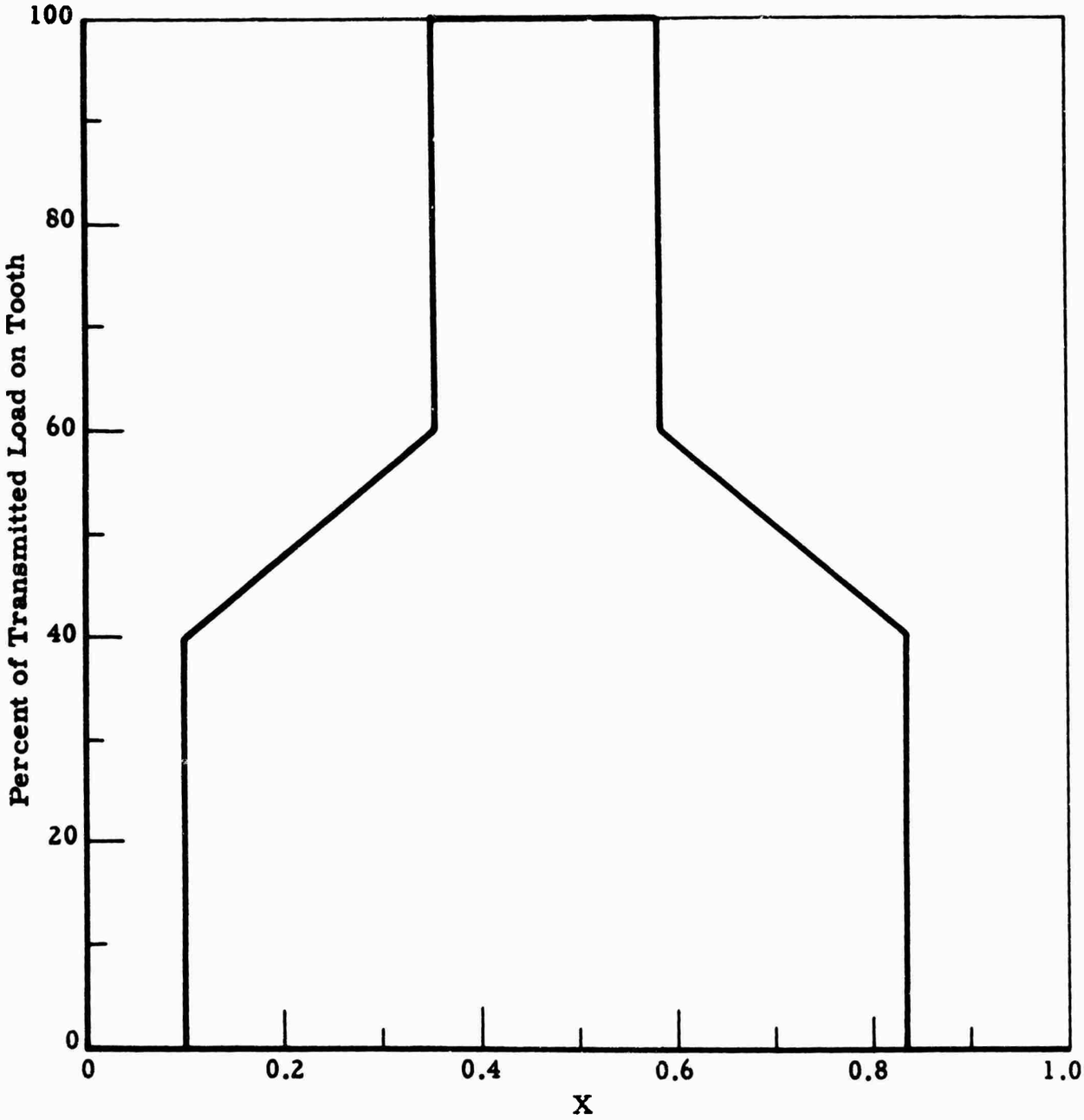

Figure 4. LOAD DISTRIBUTION FOR 17:19 LABORATORY TEST GEARS WITH PINION DRIVING

S-13926
59005

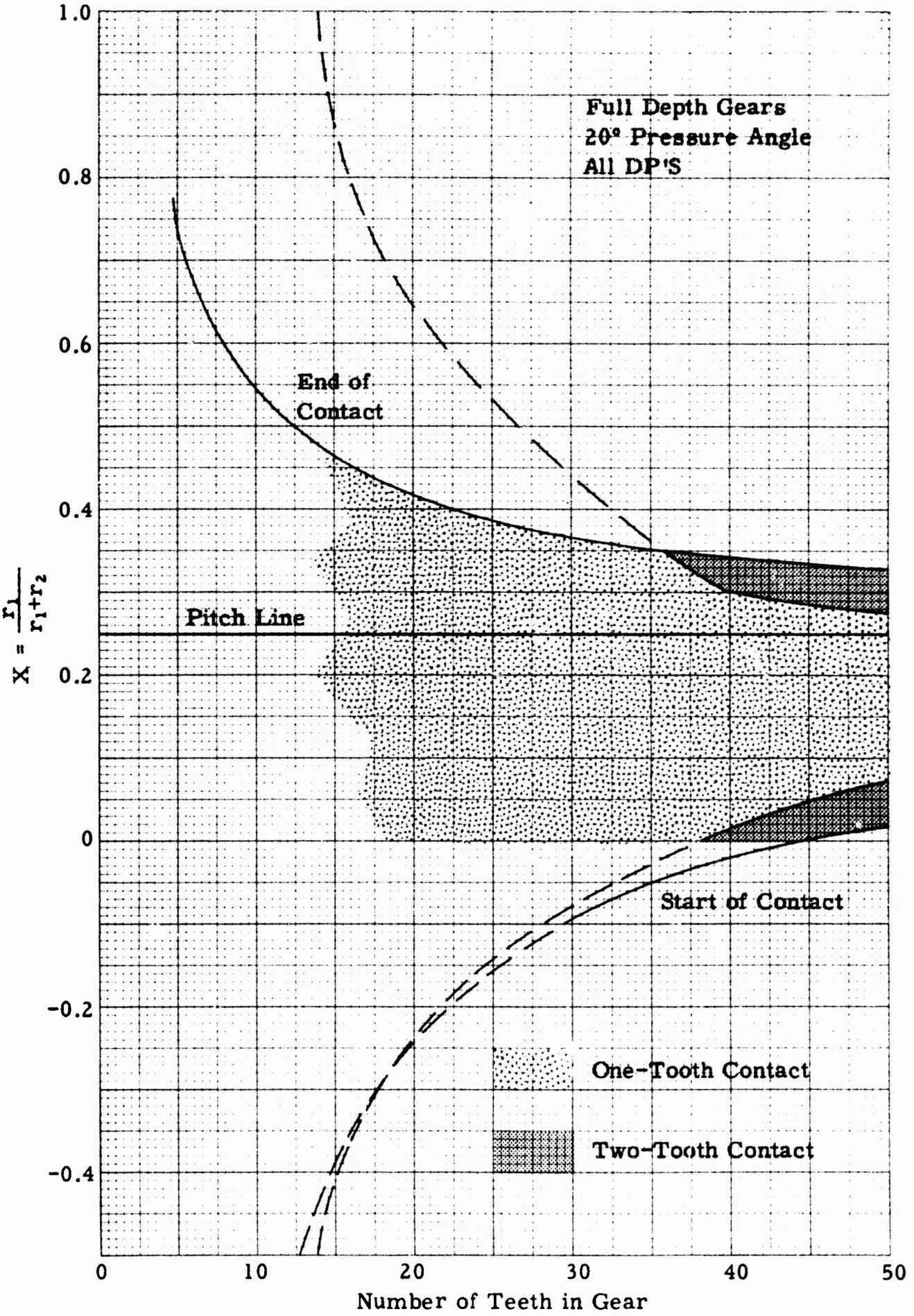

Figure 5. LOCATION OF ONE-TOOTH AND TWO-TOOTH CONTACT ALONG LINE OF ACTION FOR 1:3 GEAR RATIO, PINION DRIVING

S-13926
59005

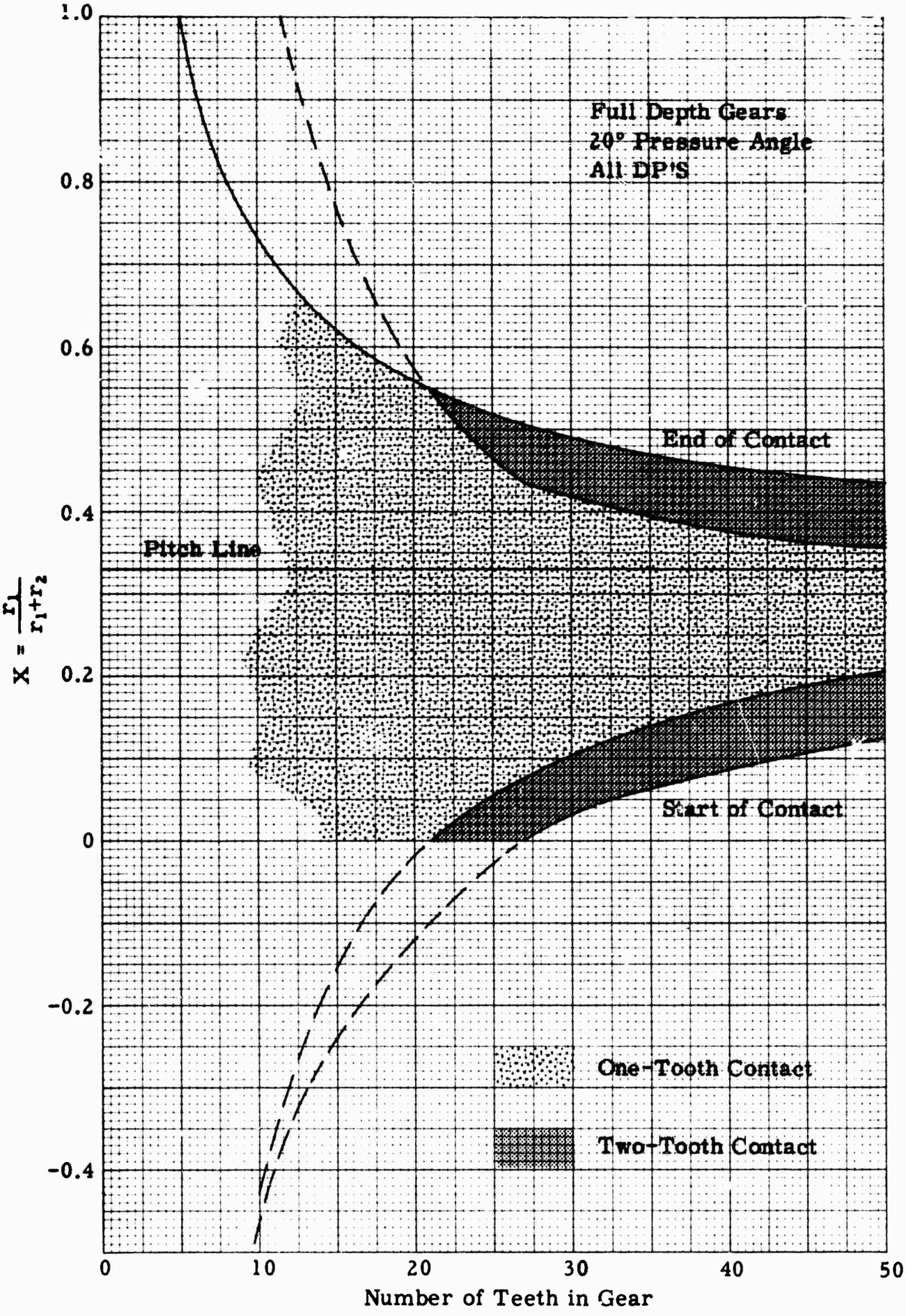

Figure 6. LOCATION OF ONE-TOOTH AND TWO-TOOTH CONTACT ALONG LINE OF ACTION FOR 1:2 GEAR RATIO, PINION DRIVING

A-1510

S-13926
59005

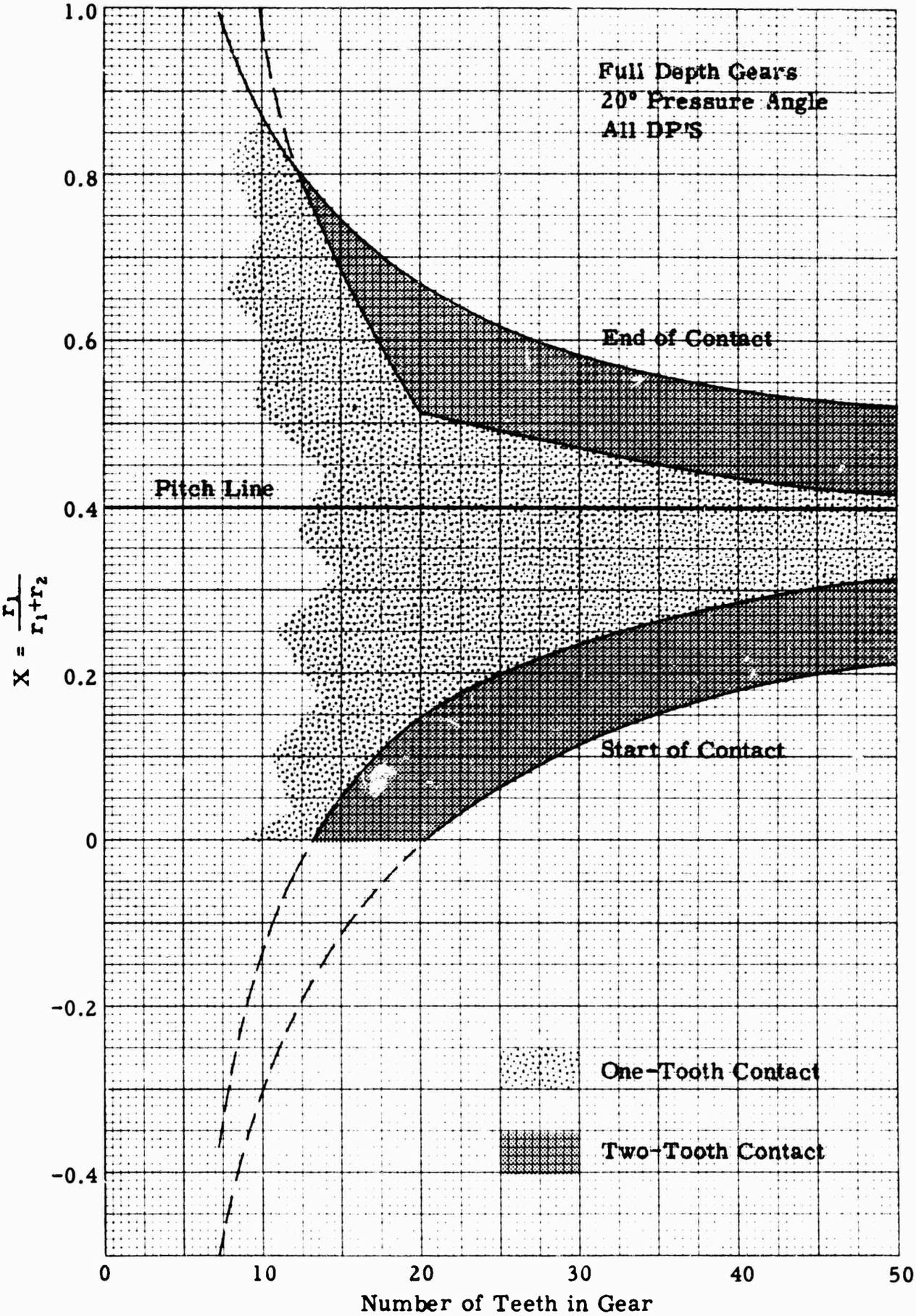

Figure 7. LOCATION OF ONE-TOOTH AND TWO-TOOTH CONTACT ALONG LINE OF ACTION FOR 1:1.5 GEAR RATIO, PINION DRIVING

S-13926
59005

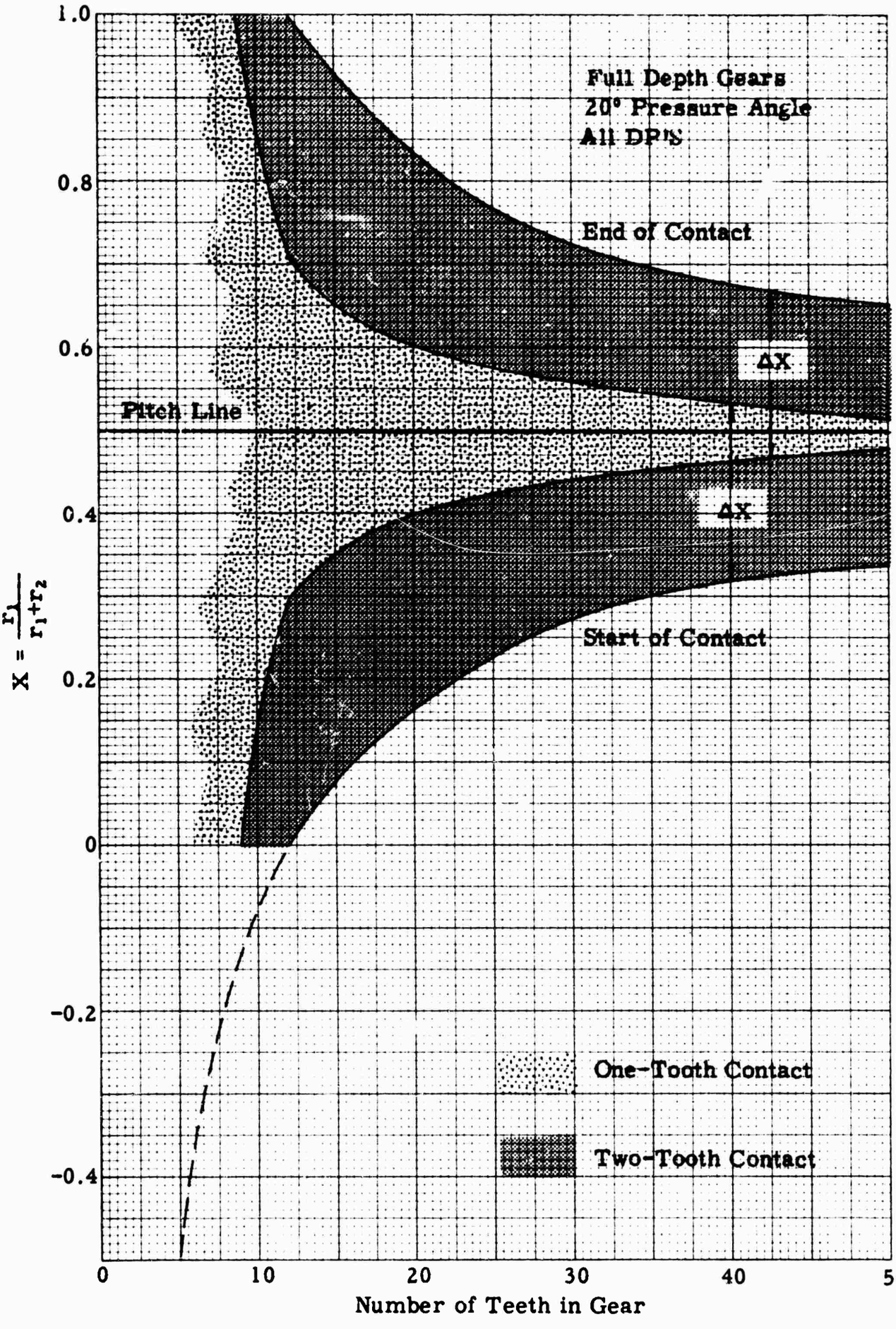

Figure 8. LOCATION OF ONE-TOOTH AND TWO-TOOTH CONTACT ALONG LINE OF ACTION FOR 1:1 GEAR RATIO

A-1510

S-13926
59005

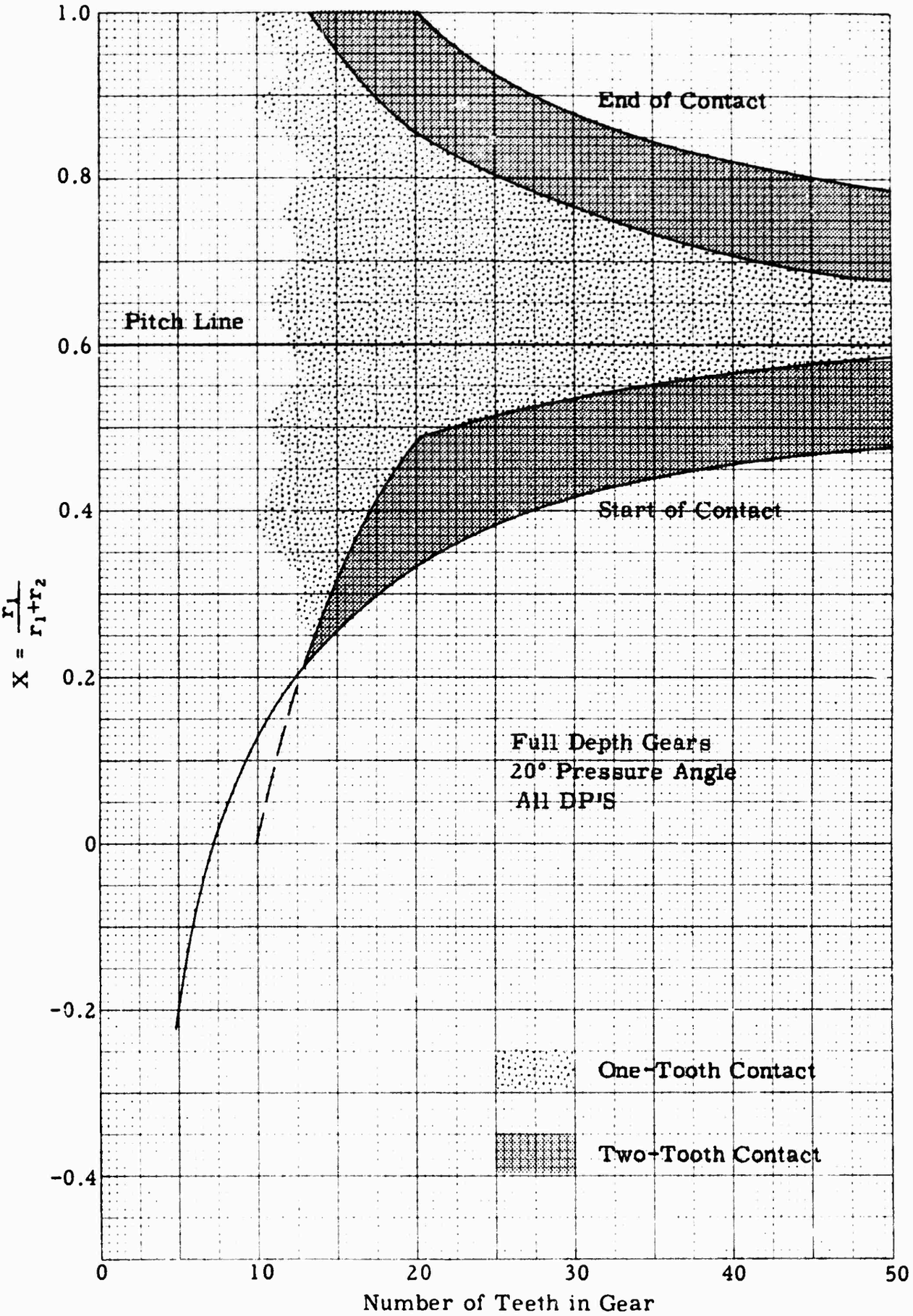

Figure 9. LOCATION OF ONE-TOOTH AND TWO-TOOTH CONTACT ALONG LINE OF ACTION FOR 1.5:1 GEAR RATIO, GEAR DRIVING

S-13926
59005

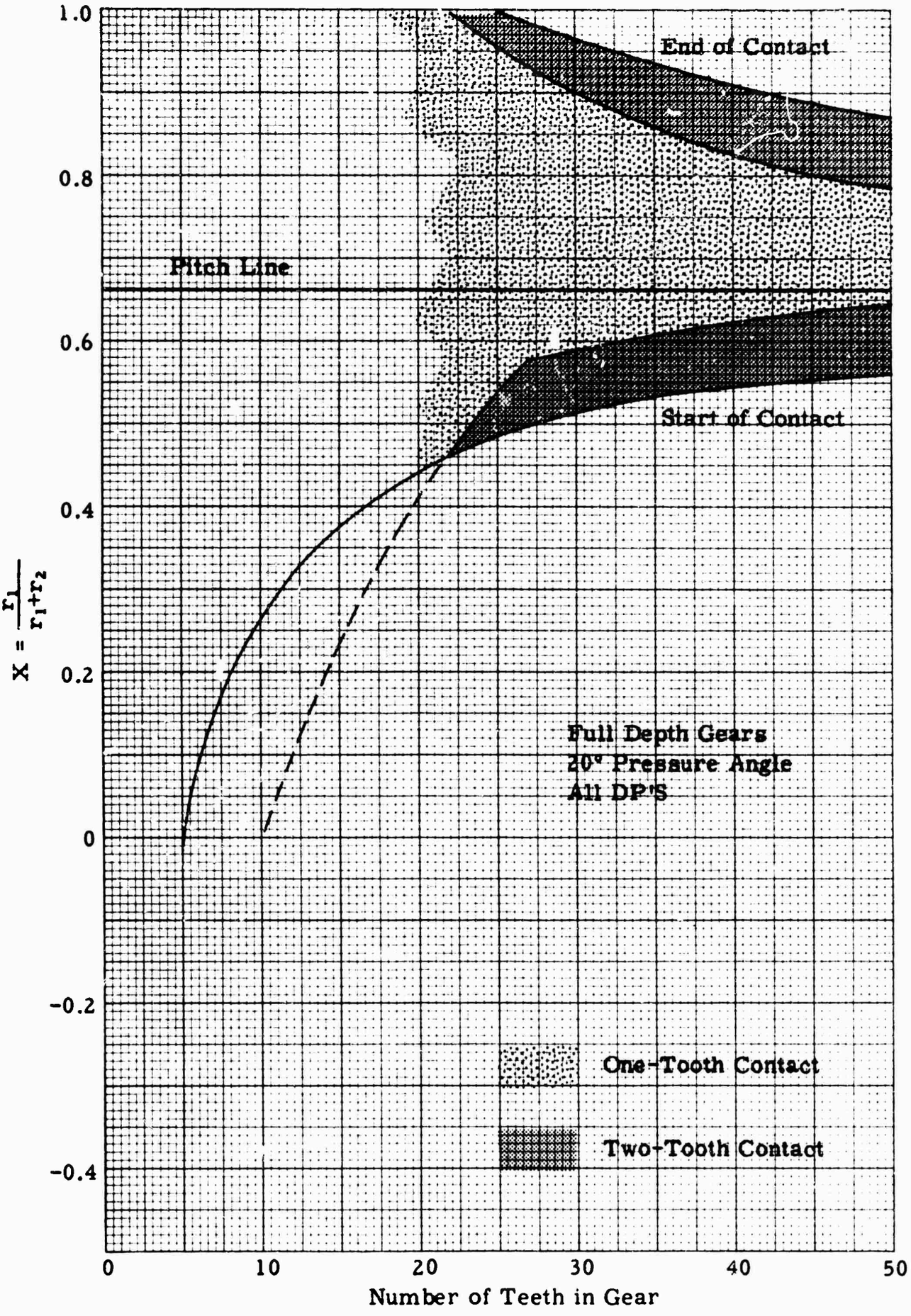

Figure 10. LOCATION OF ONE-TOOTH AND TWO-TOOTH CONTACT ALONG LINE OF ACTION FOR 2:1 GEAR RATIO, GEAR DRIVING

A-1510

S-13926
59005

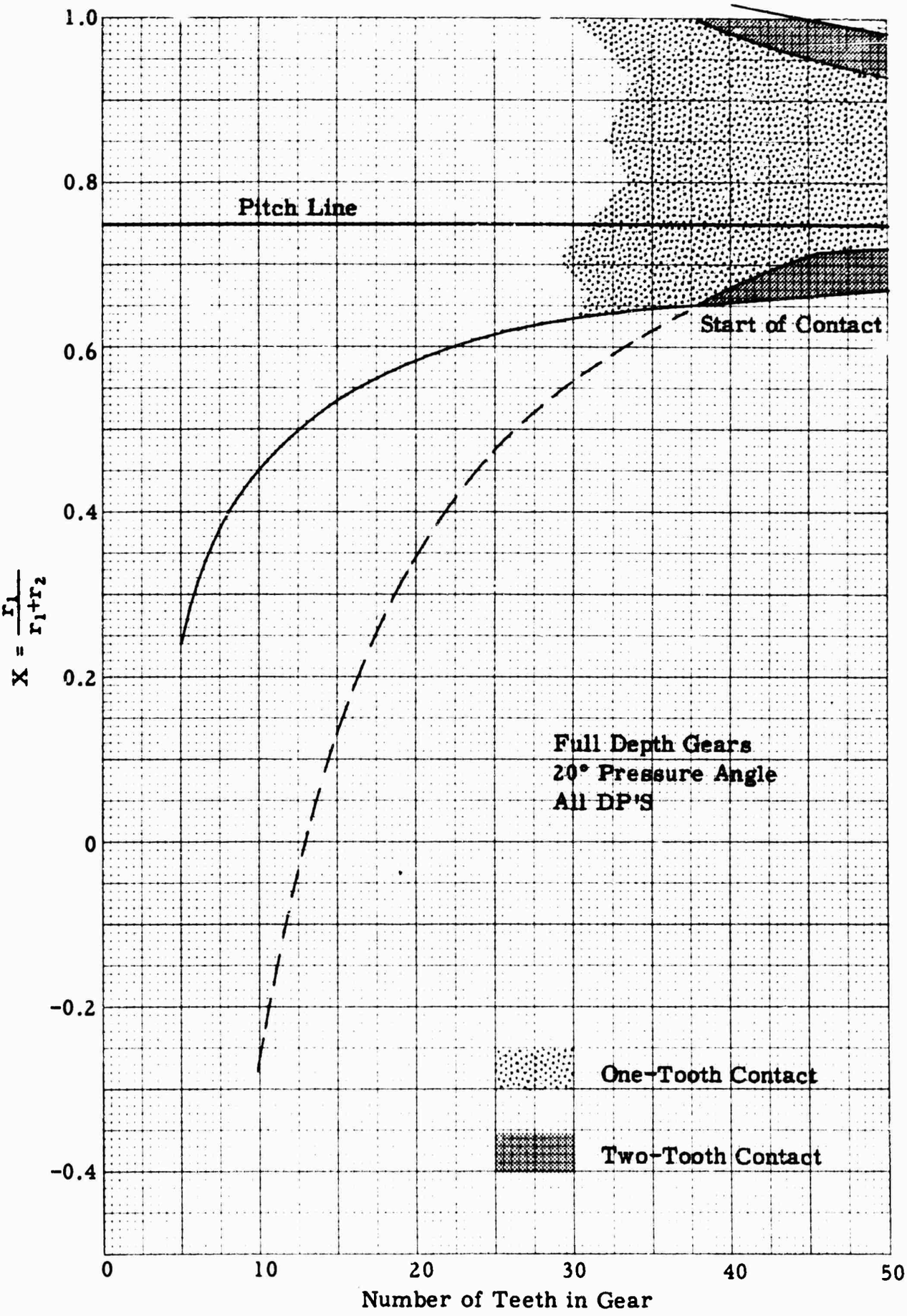

Figure 11. LOCATION OF ONE-TOOTH AND TWO-TOOTH CONTACT ALONG LINE OF ACTION FOR 3:1 GEAR RATIO, GEAR DRIVING

S-13926
59926

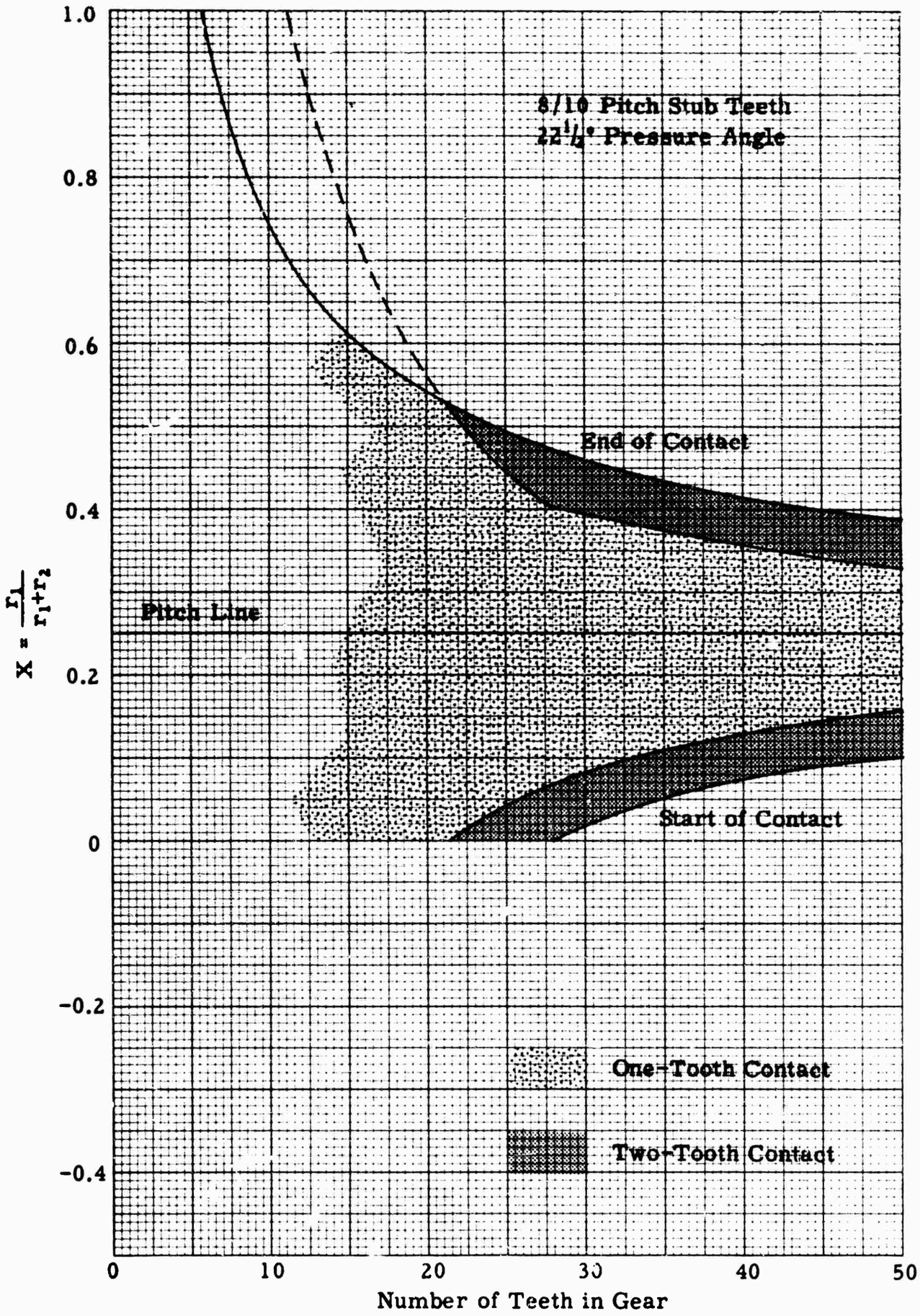

Figure 12. LOCATION OF ONE-TOOTH AND TWO-TOOTH CONTACT ALONG LINE OF ACTION FOR 1:3 GEAR RATIO, PINION DRIVING

-13926
9926

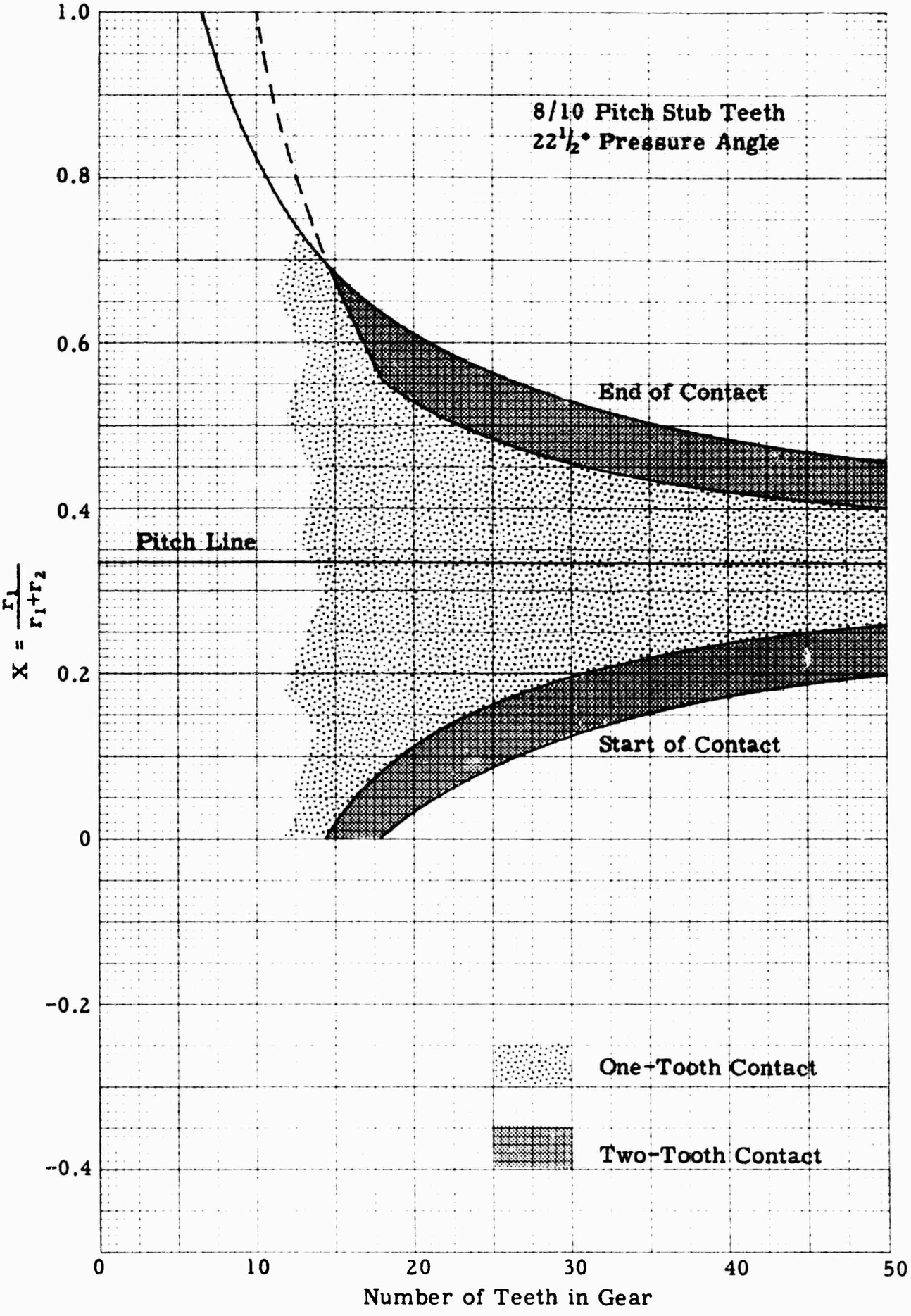

Figure 13. LOCATION OF ONE-TOOTH AND TWO-TOOTH CONTACT ALONG LINE OF ACTION FOR 1:2 GEAR RATIO, PINION DRIVING

S-13926
59926

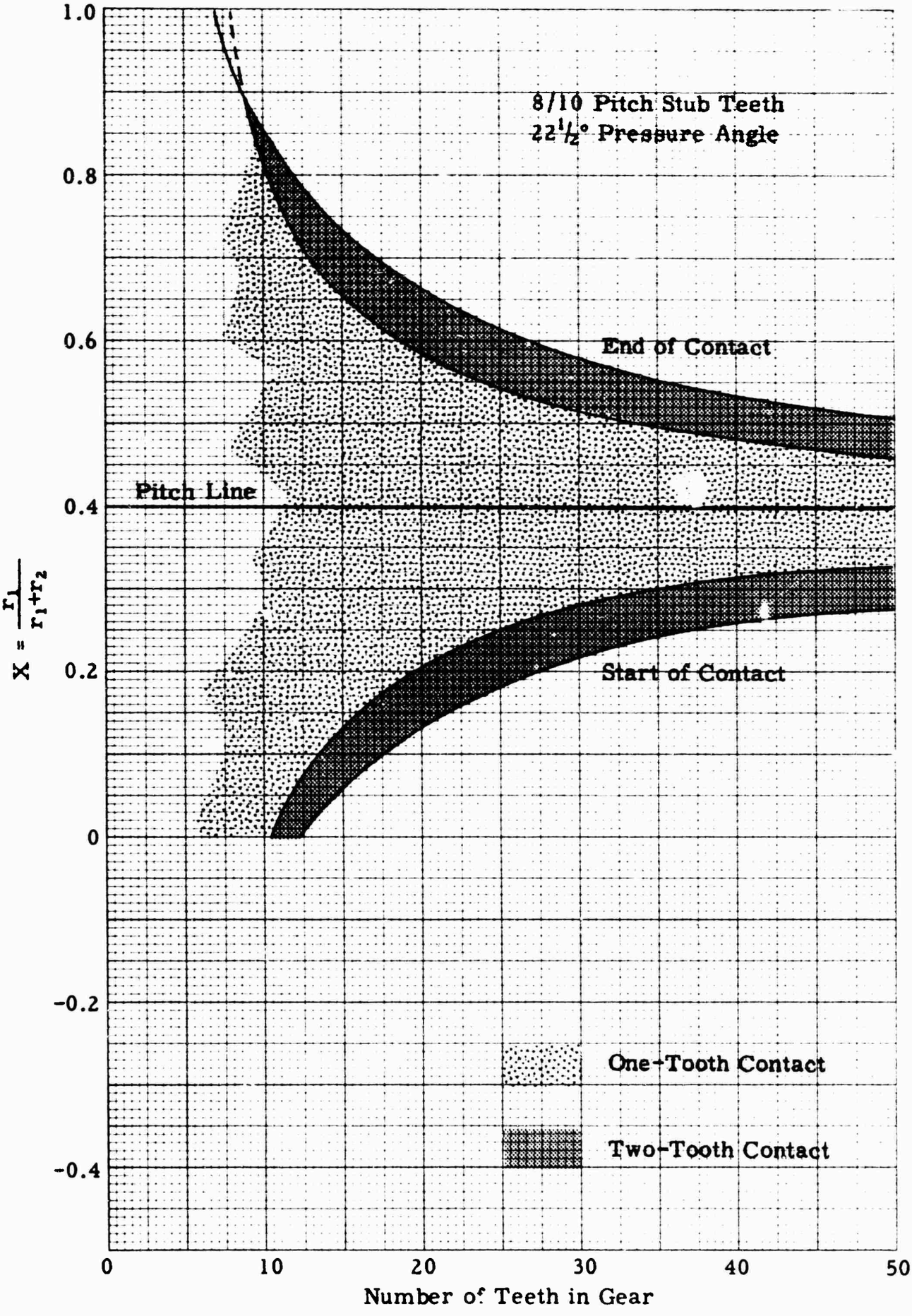

Figure 14. LOCATION OF ONE-TOOTH AND TWO-TOOTH CONTACT ALONG LINE OF ACTION FOR 1:1.5 GEAR RATIO, PINION DRIVING

A-1510

S-13926
59926

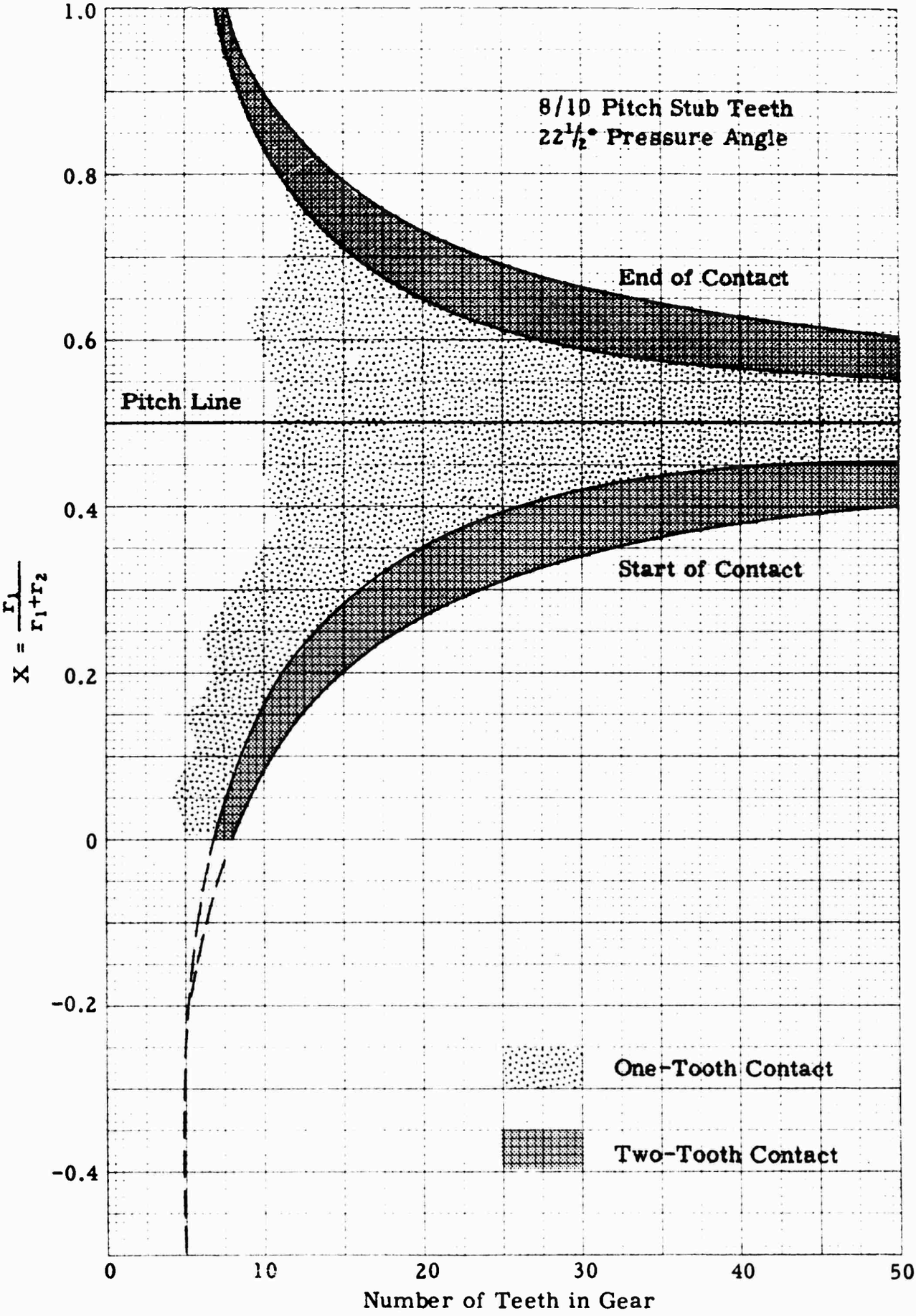

Figure 15. LOCATION OF ONE-TOOTH AND TWO-TOOTH CONTACT ALONG LINE OF ACTION FOR 1:1 GEAR RATIO

S-13926
59926

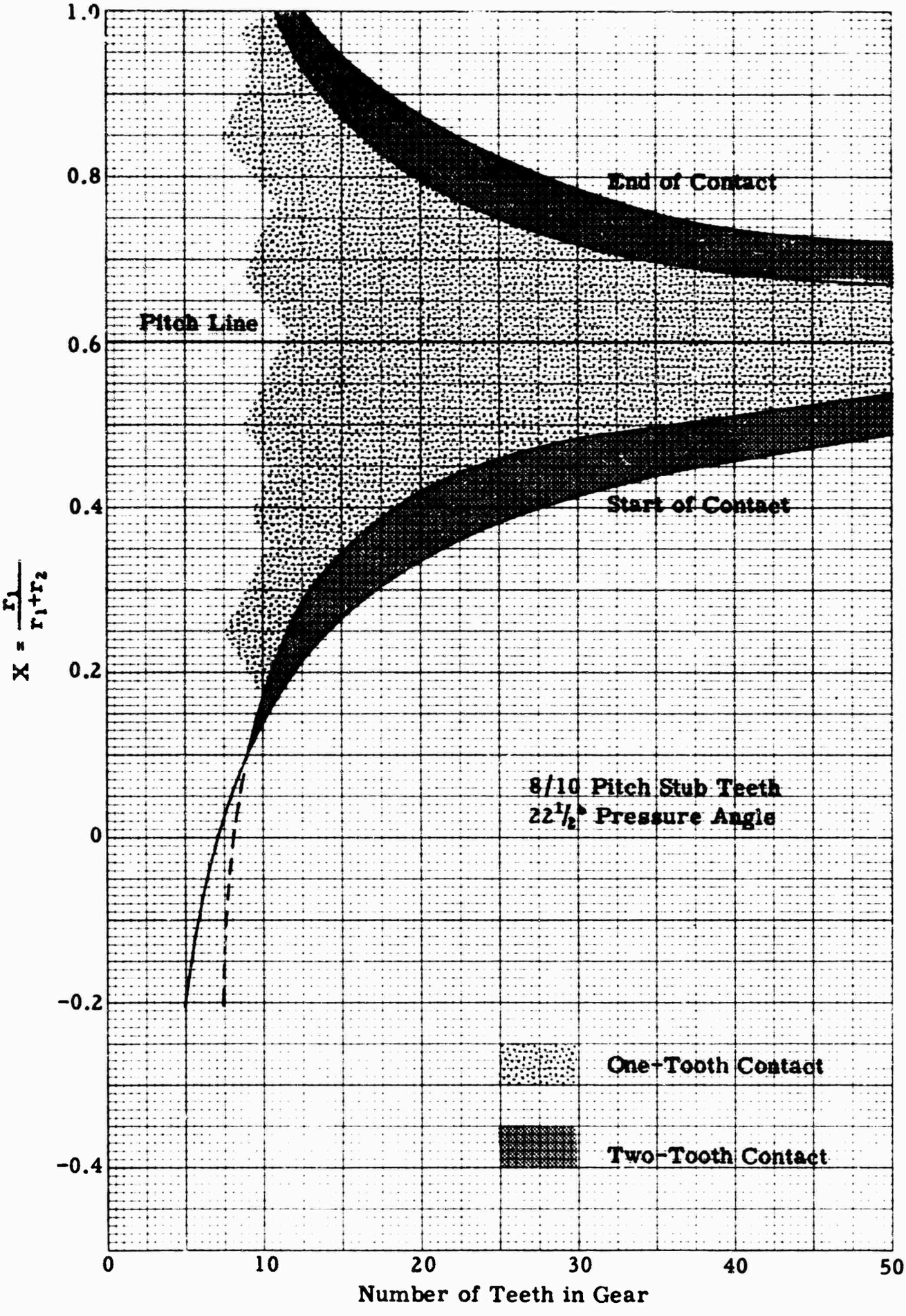

Figure 16. LOCATION OF ONE-TOOTH AND TWO-TOOTH CONTACT ALONG LINE OF ACTION FOR 1.5:1 GEAR RATIO, GEAR DRIVING

A-1510

S-13926
59926

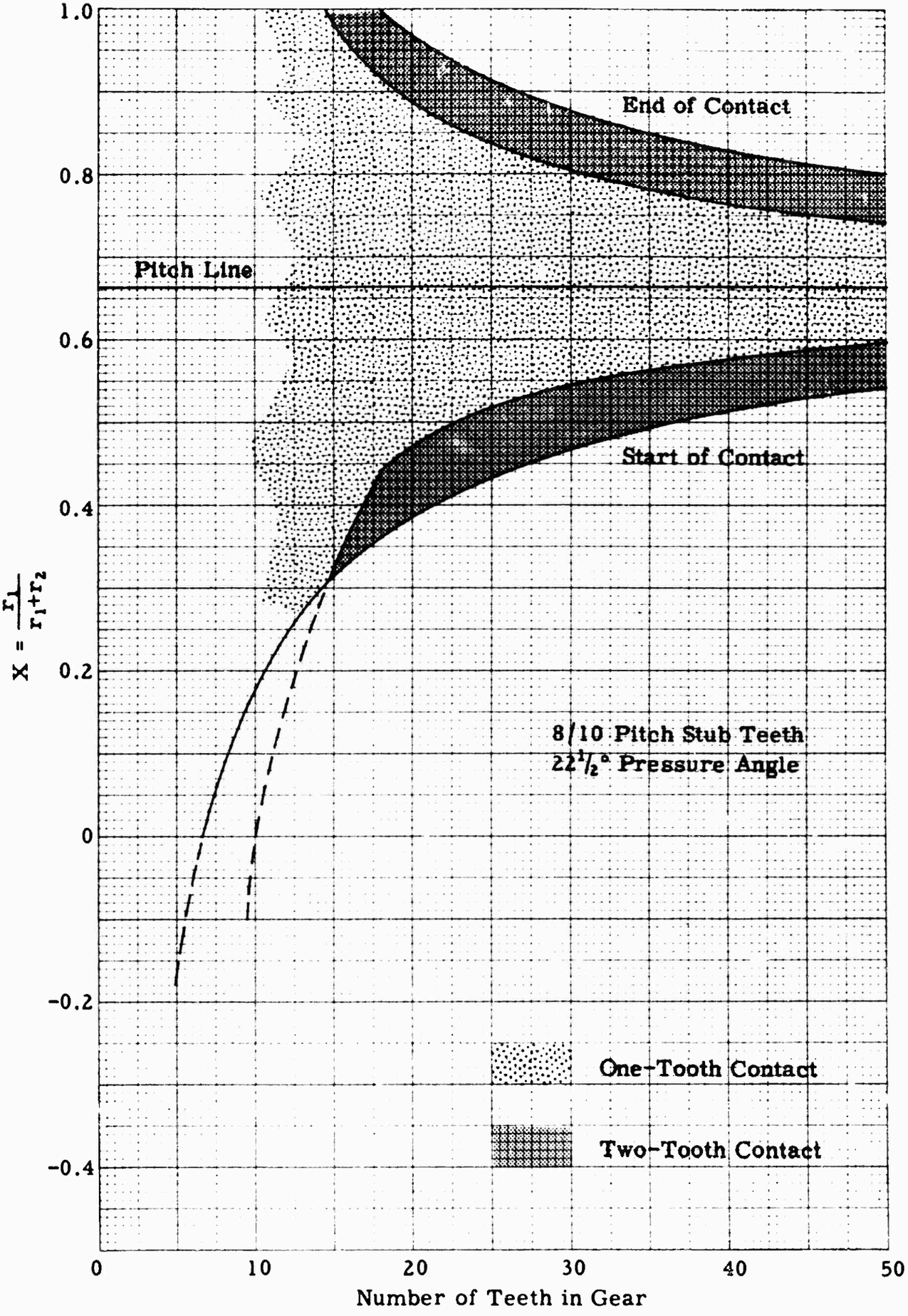

Figure 17. LOCATION OF ONE-TOOTH AND TWO-TOOTH CONTACT ALONG LINE OF ACTION FOR 2:1 GEAR RATIO, GEAR DRIVING

S-13926
59926

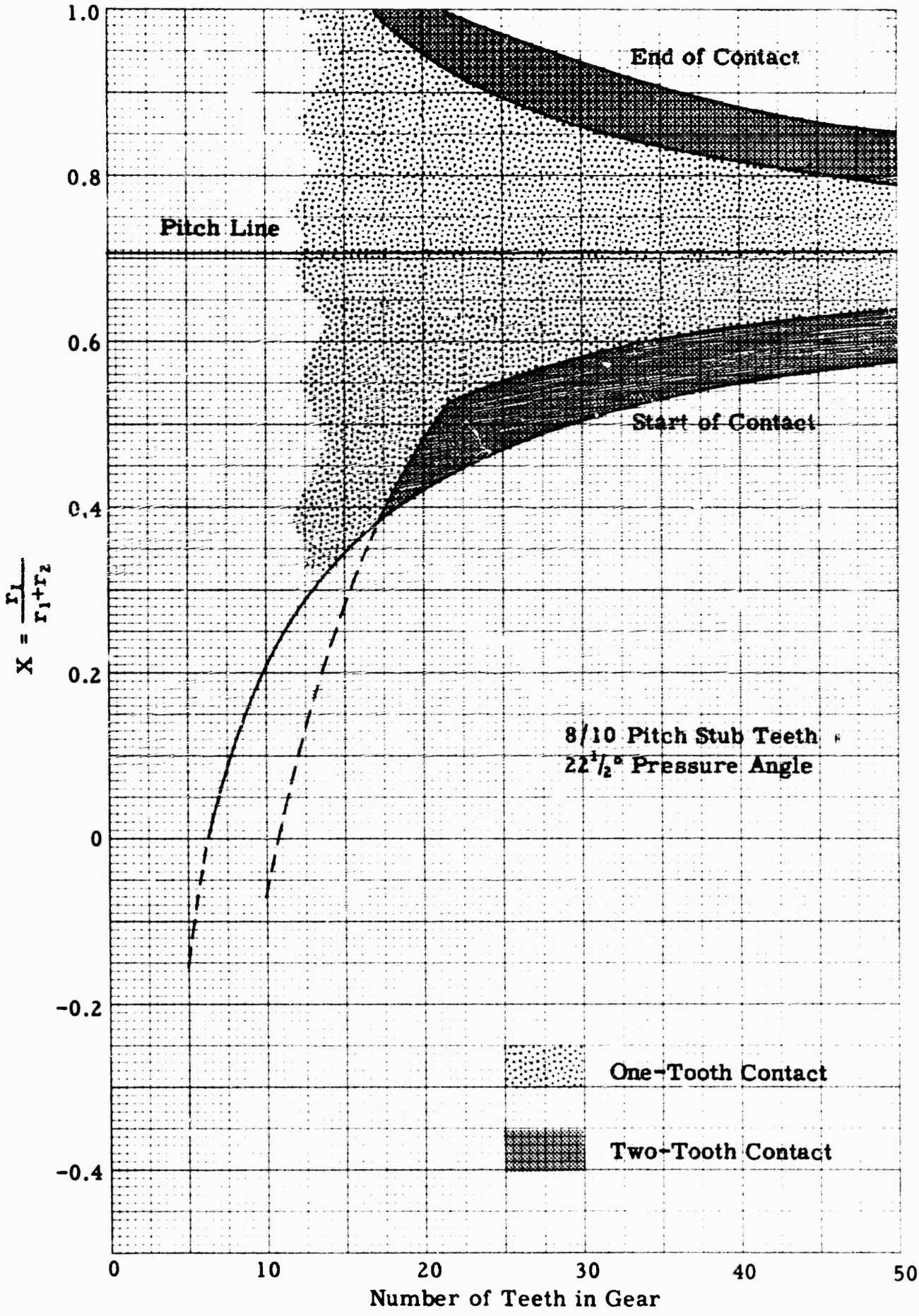

A-1510

Figure 18. LOCATION OF ONE-TOOTH AND TWO-TOOTH CONTACT ALONG LINE OF ACTION FOR 2.43:1 GEAR RATIO, GEAR DRIVING

S-13926
59926

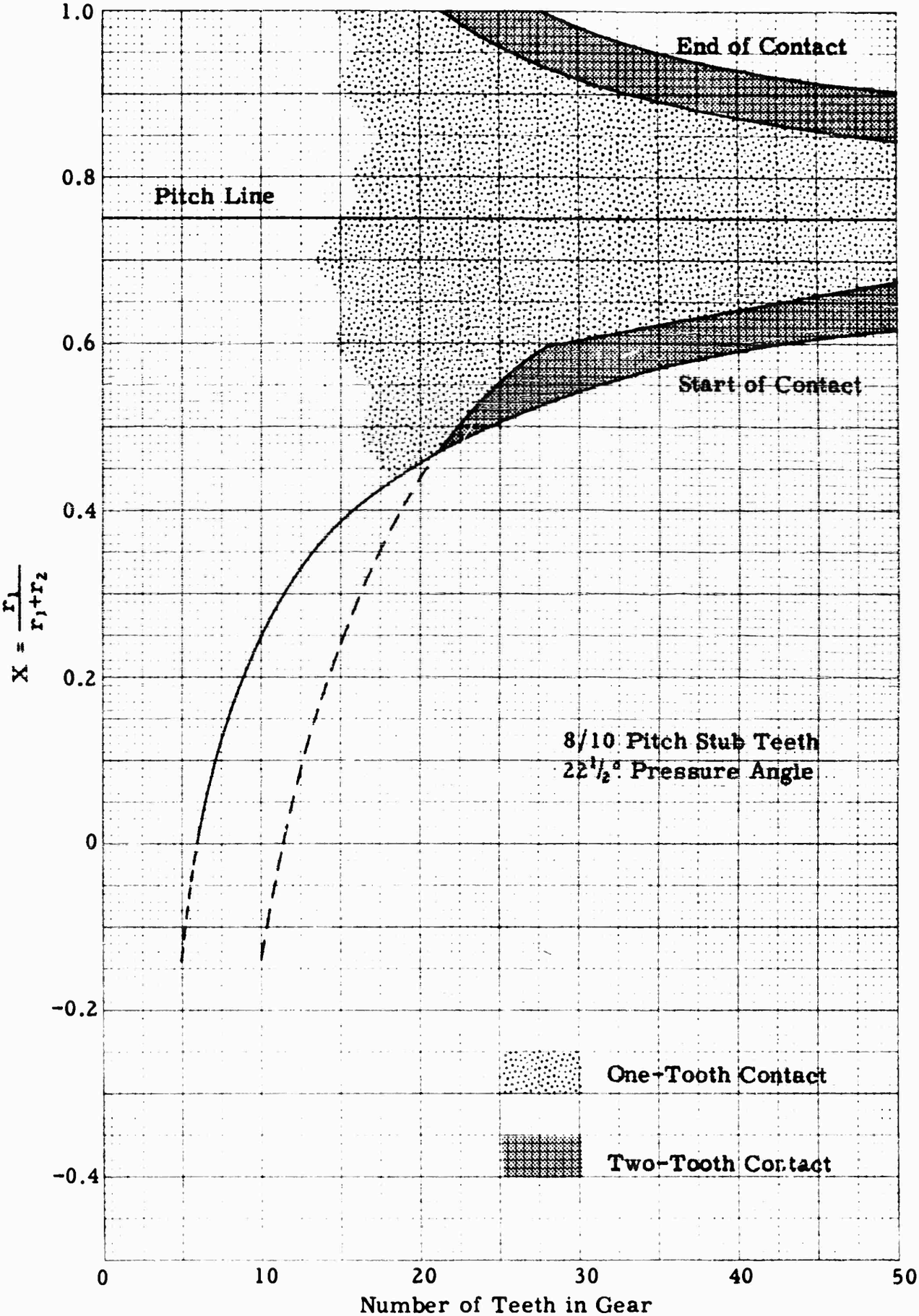

Figure 19. LOCATION OF ONE-TOOTH AND TWO-TOOTH CONTACT ALONG LINE OF ACTION FOR 3:1 GEAR RATIO, GEAR DRIVING

S-13926
59926

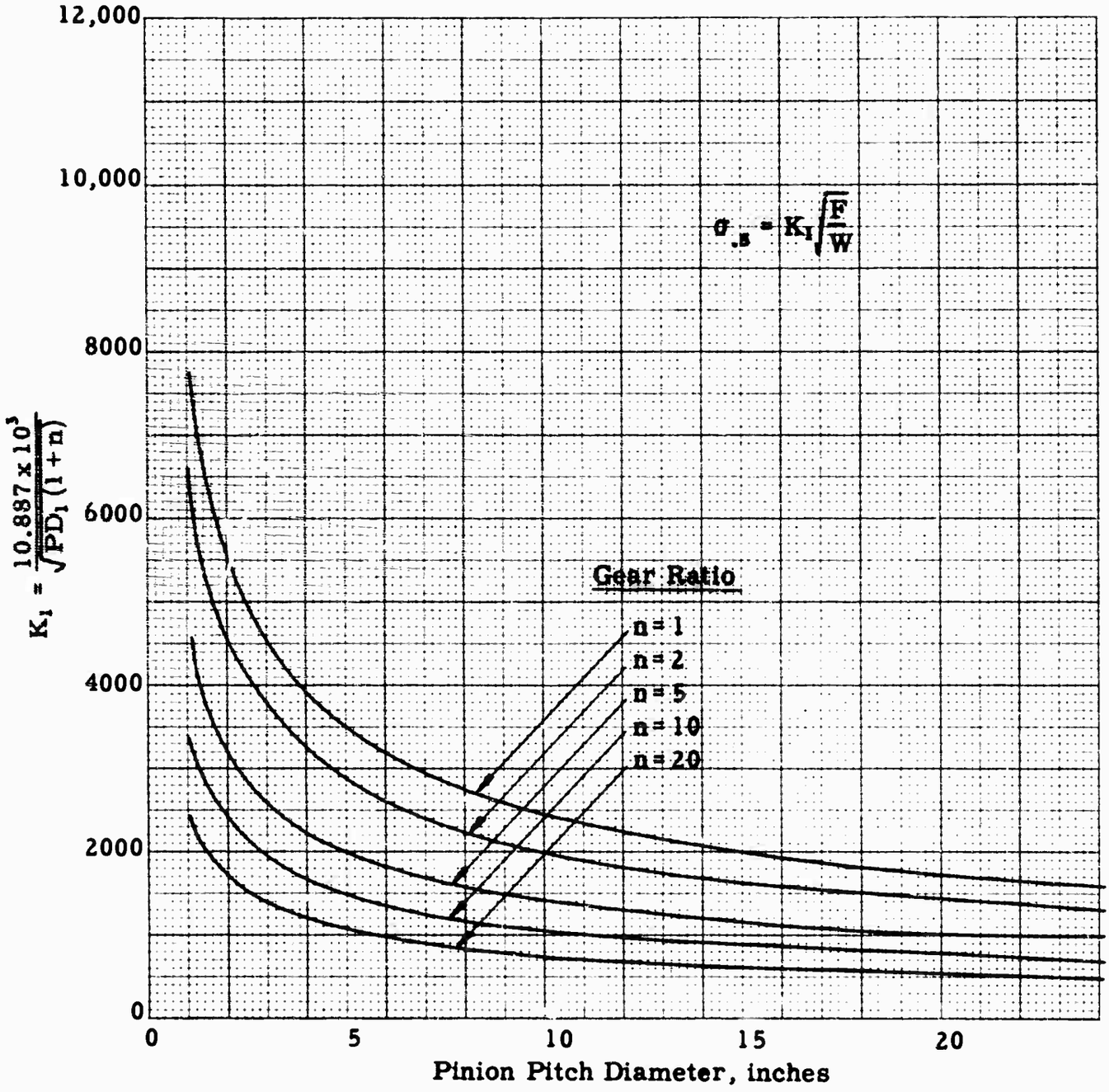

Figure 20. HERTZ STRESS FOR 20° PRESSURE ANGLE SPUR GEARS FOR CONTACT AT THE MIDPOINT OF THE LINE OF ACTION

S-13926
59005

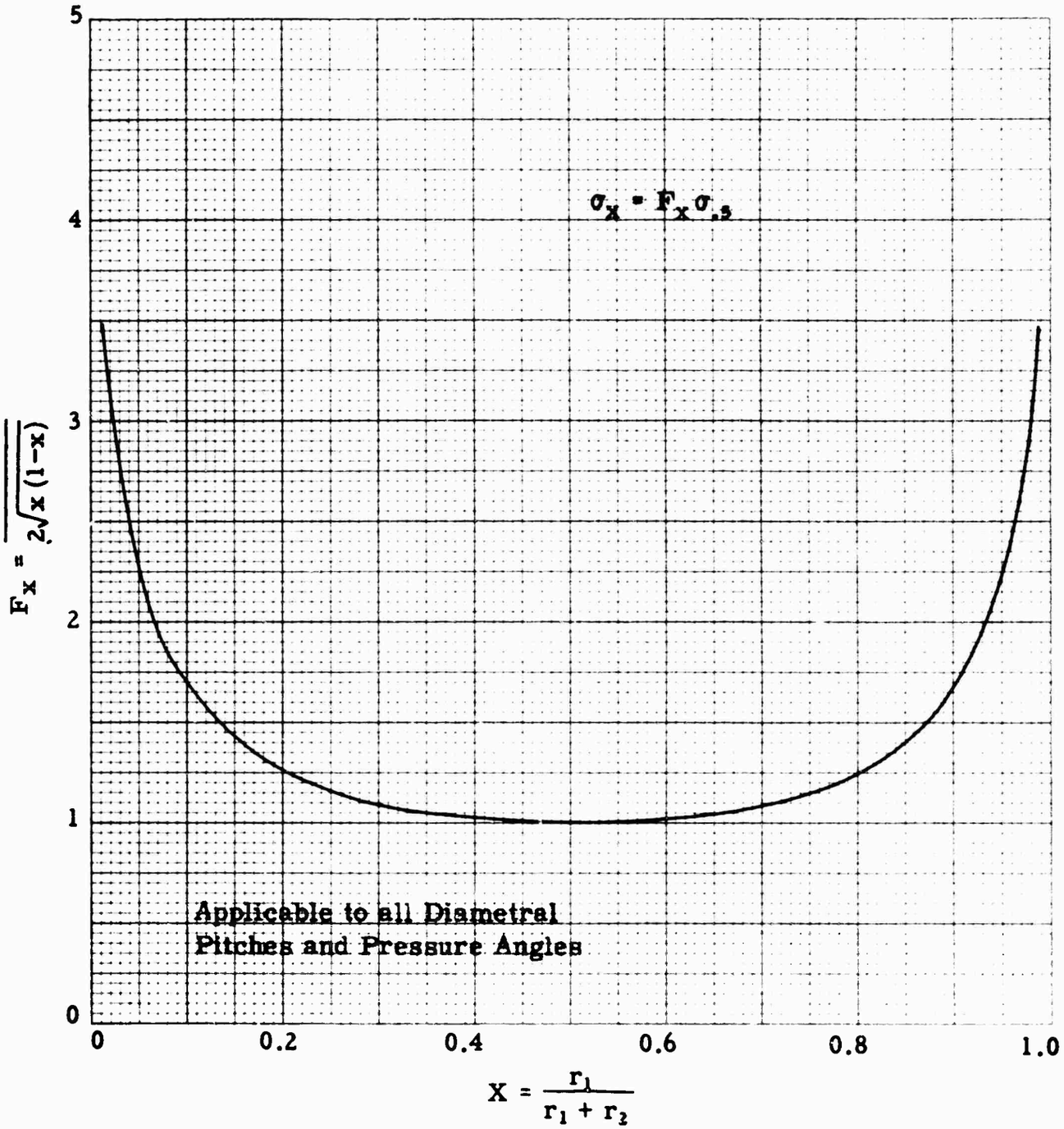

Figure 21. RATIO OF SPUR GEAR HERTZ STRESS AT ANY POINT TO THAT AT MIDPOINT OF LINE OF ACTION

S-13926
59005

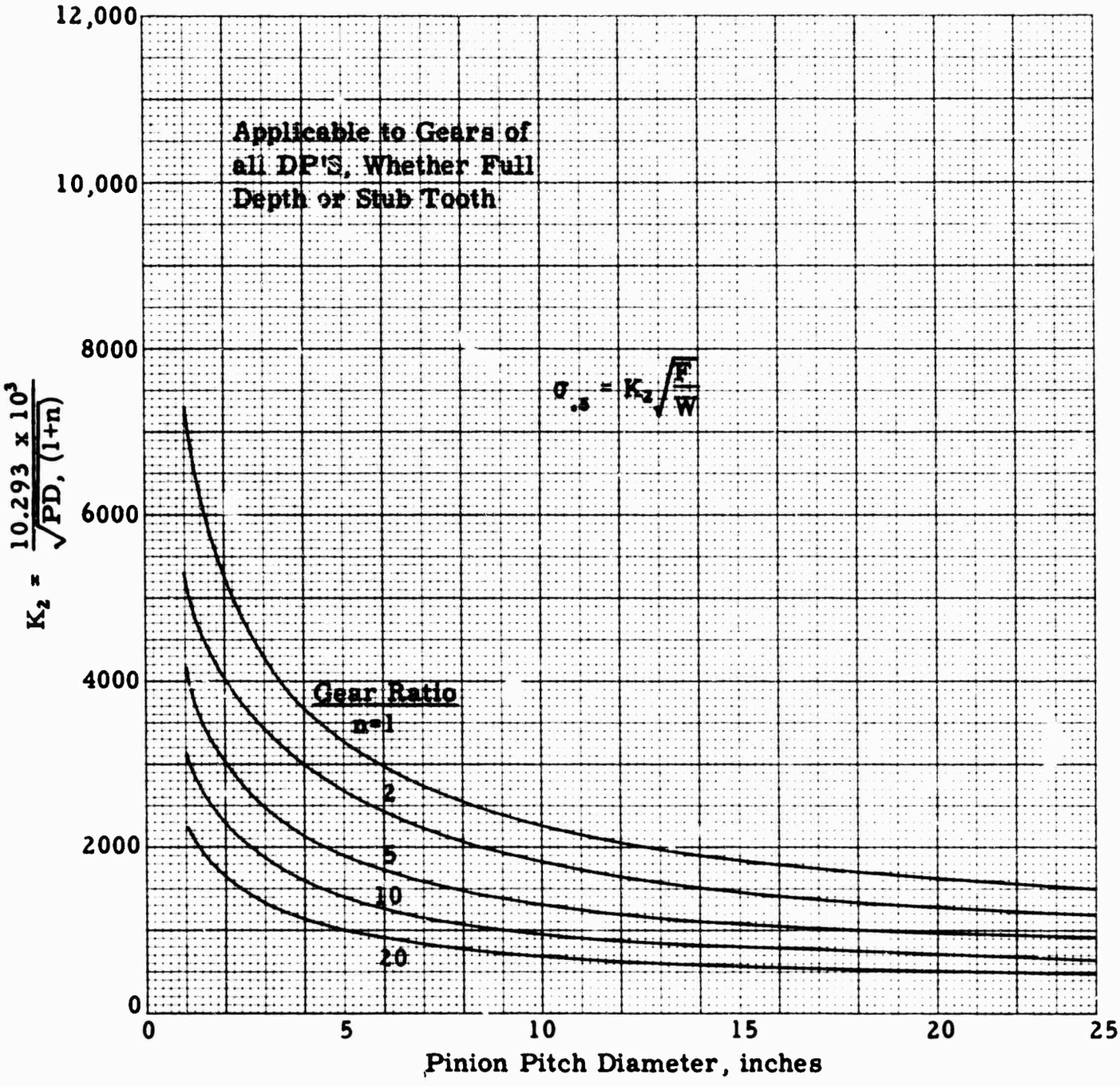

Figure 22. HERTZ STRESS FOR SPUR GEARS WITH $22\frac{1}{2}°$ PRESSURE ANGLE FOR CONTACT AT THE MIDPOINT OF THE LINE OF ACTION

A-1212

S-13926
59926

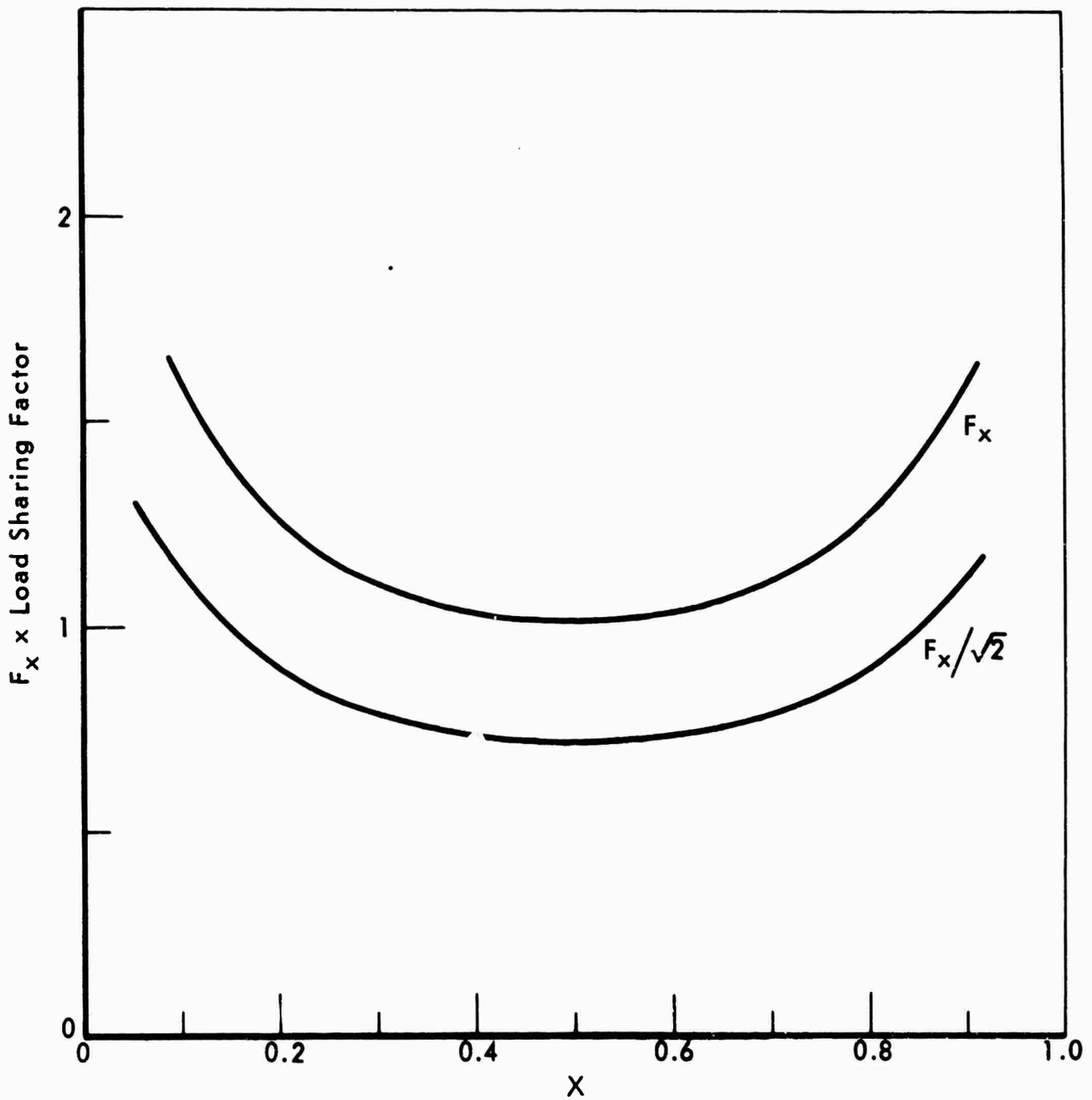

Figure 23. RELATION OF F_x vs X CURVE TO $F_x/\sqrt{2}$ vs X CURVE

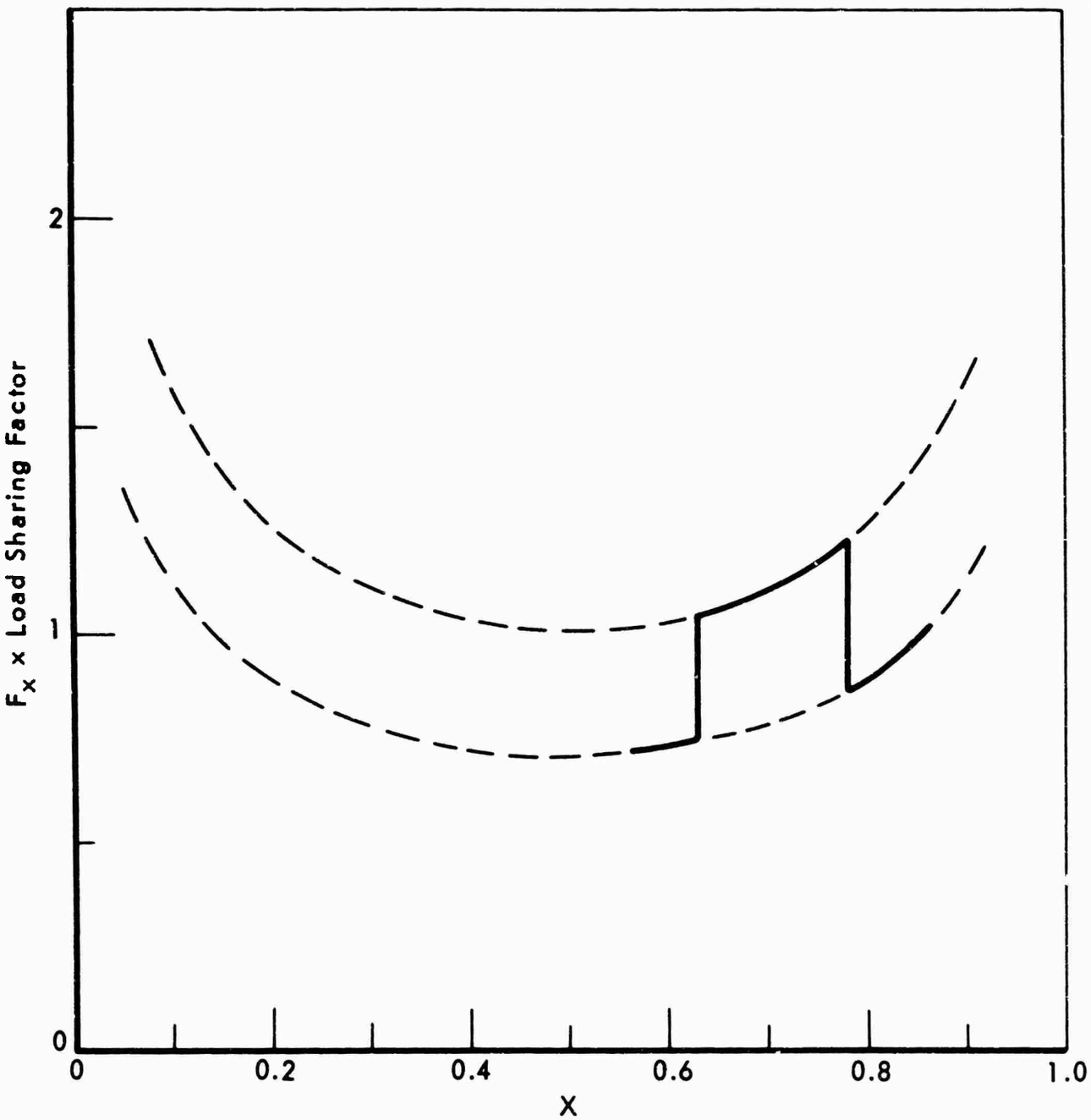

Figure 24. DEVELOPMENT OF LOAD SHARING CURVE FROM FIGURE 23

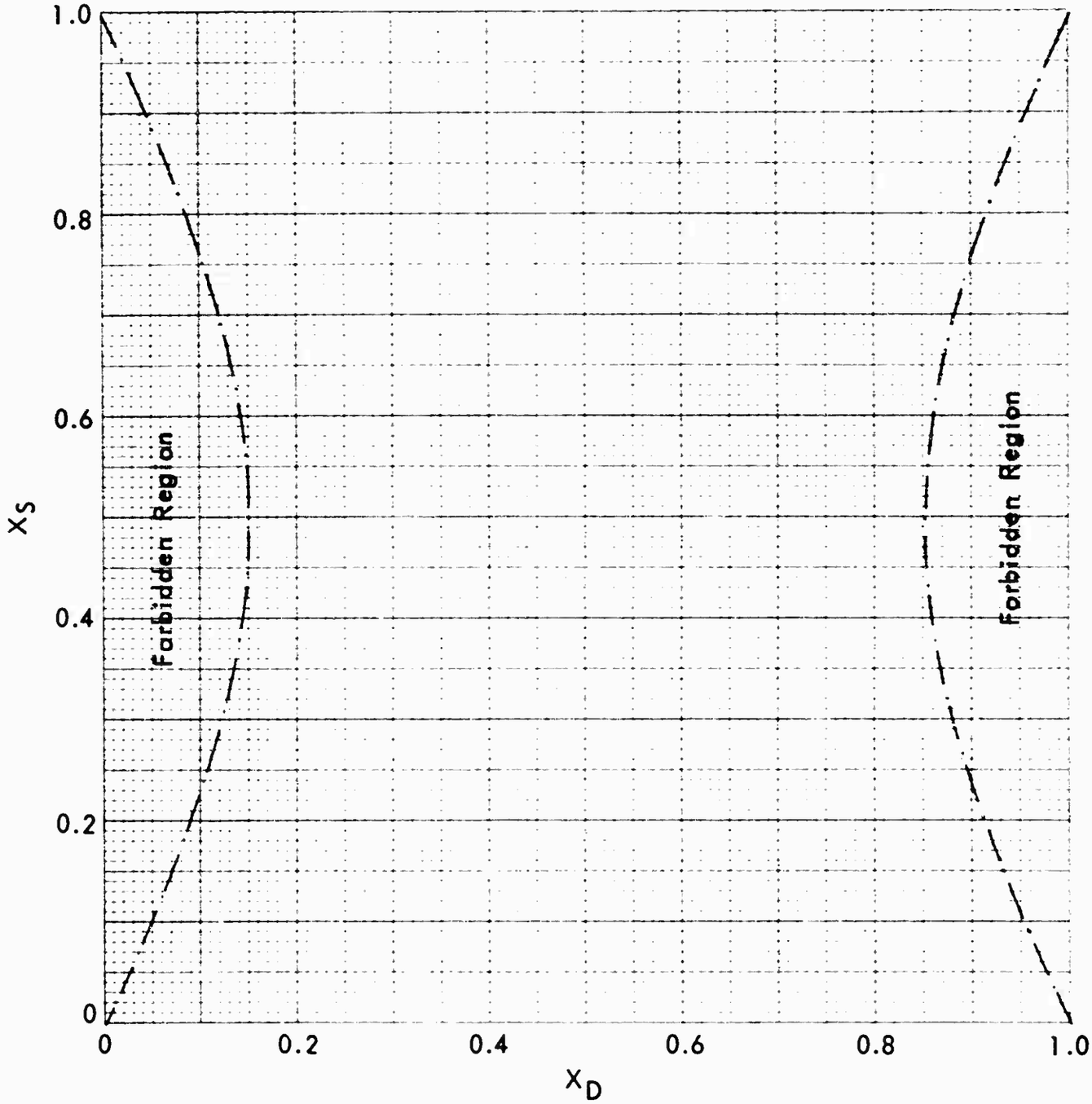

Figure 25. "FORBIDDEN REGIONS" IN X_S-X_D PLANE IN BALANCED STRESS CRITERION WITH m = 1

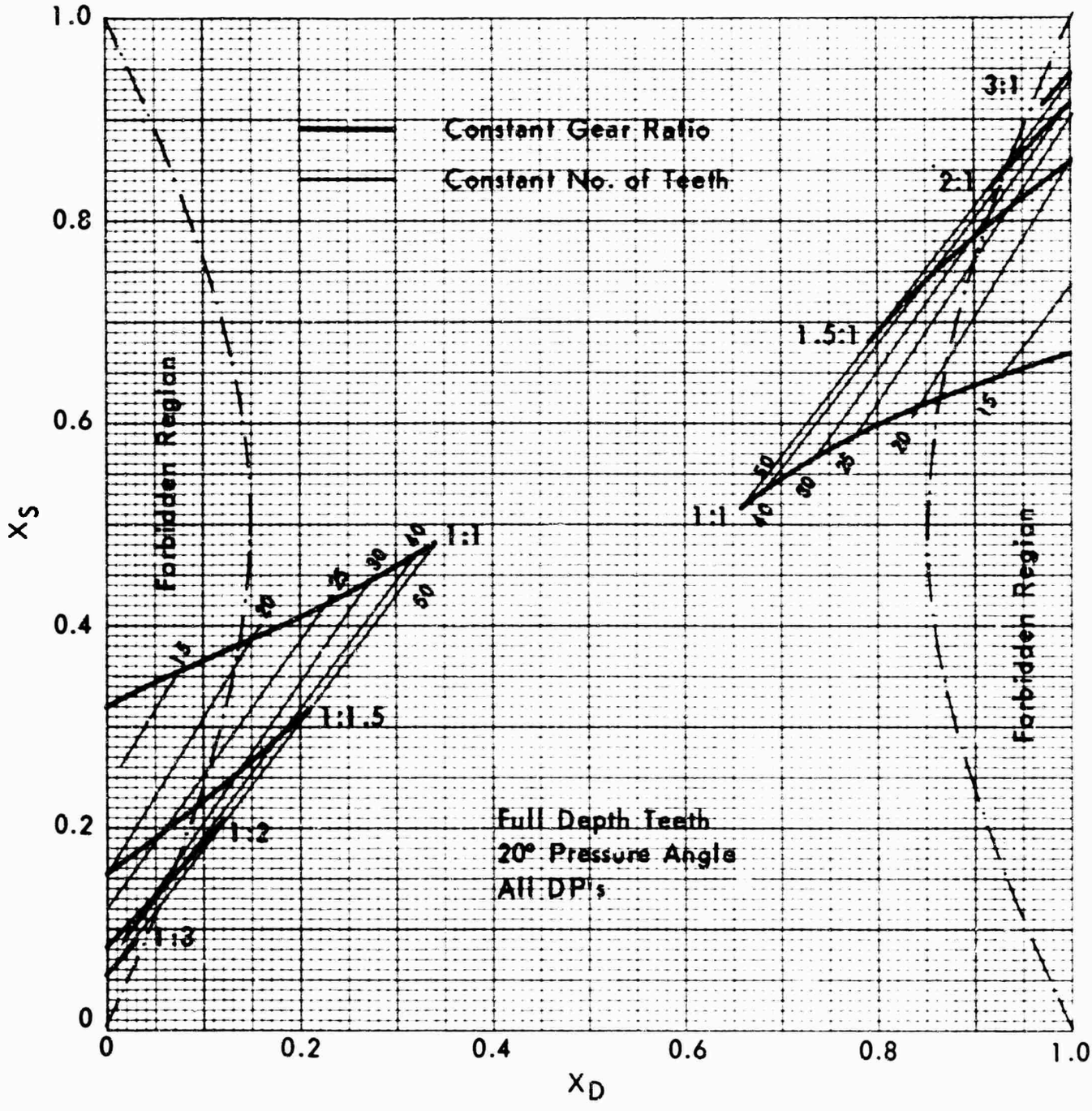

Figure 26. CURVES FOR CONSTANT GEAR RATIO AND CONSTANT NO OF TEETH IN GEAR COMPARED TO FORBIDDEN REGION FOR m = 1

A-1010

S-13926
59926

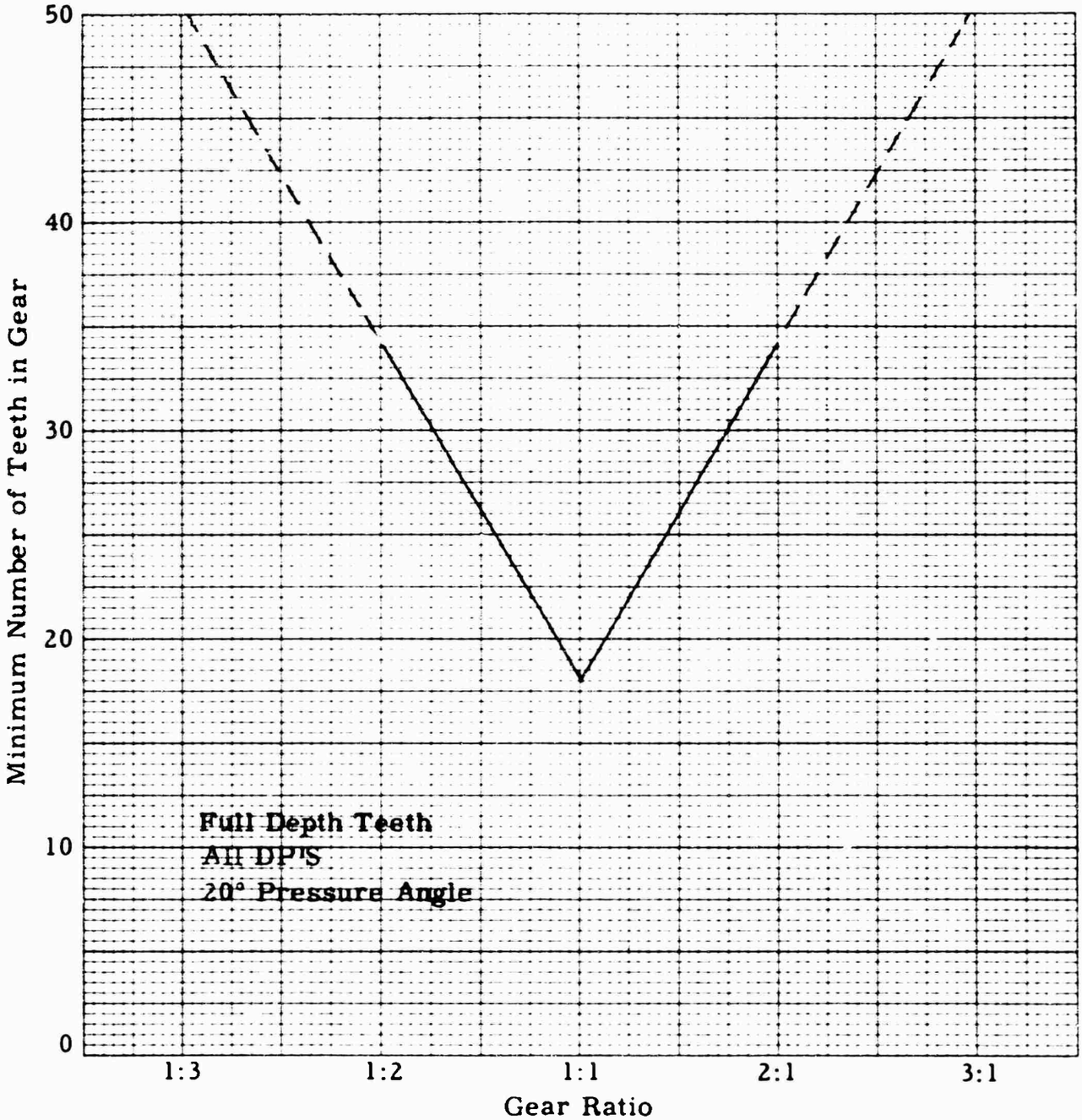

Figure 27. MINIMUM NUMBER OF TEETH REQUIRED BY BALANCED STRESS CRITERION FOR m=1

S-13926
59926

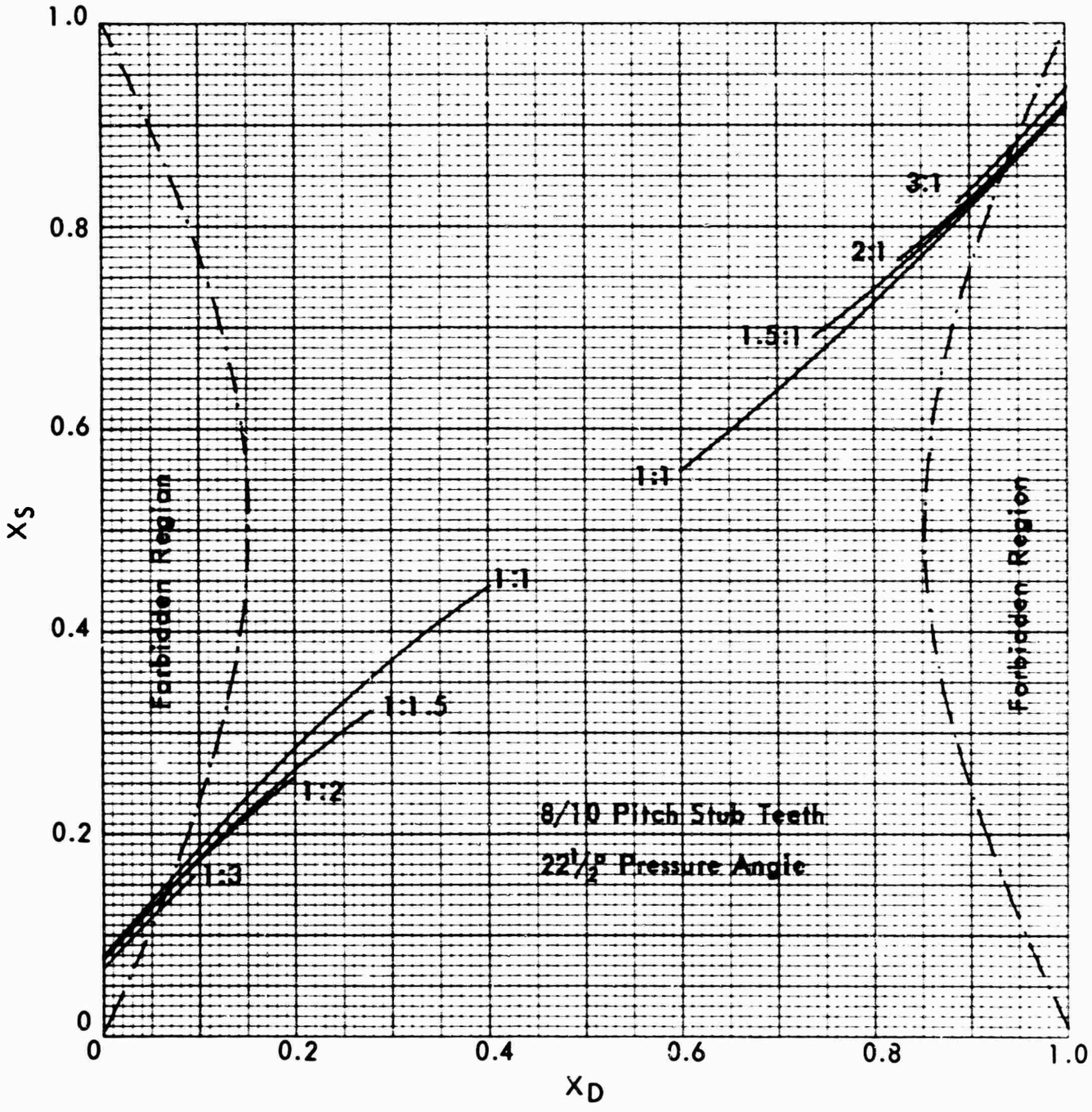

Figure 28. CURVES FOR CONSTANT GEAR RATIO COMPARED TO FORBIDDEN REGION FOR m = 1

A-1010

S-13926
59926

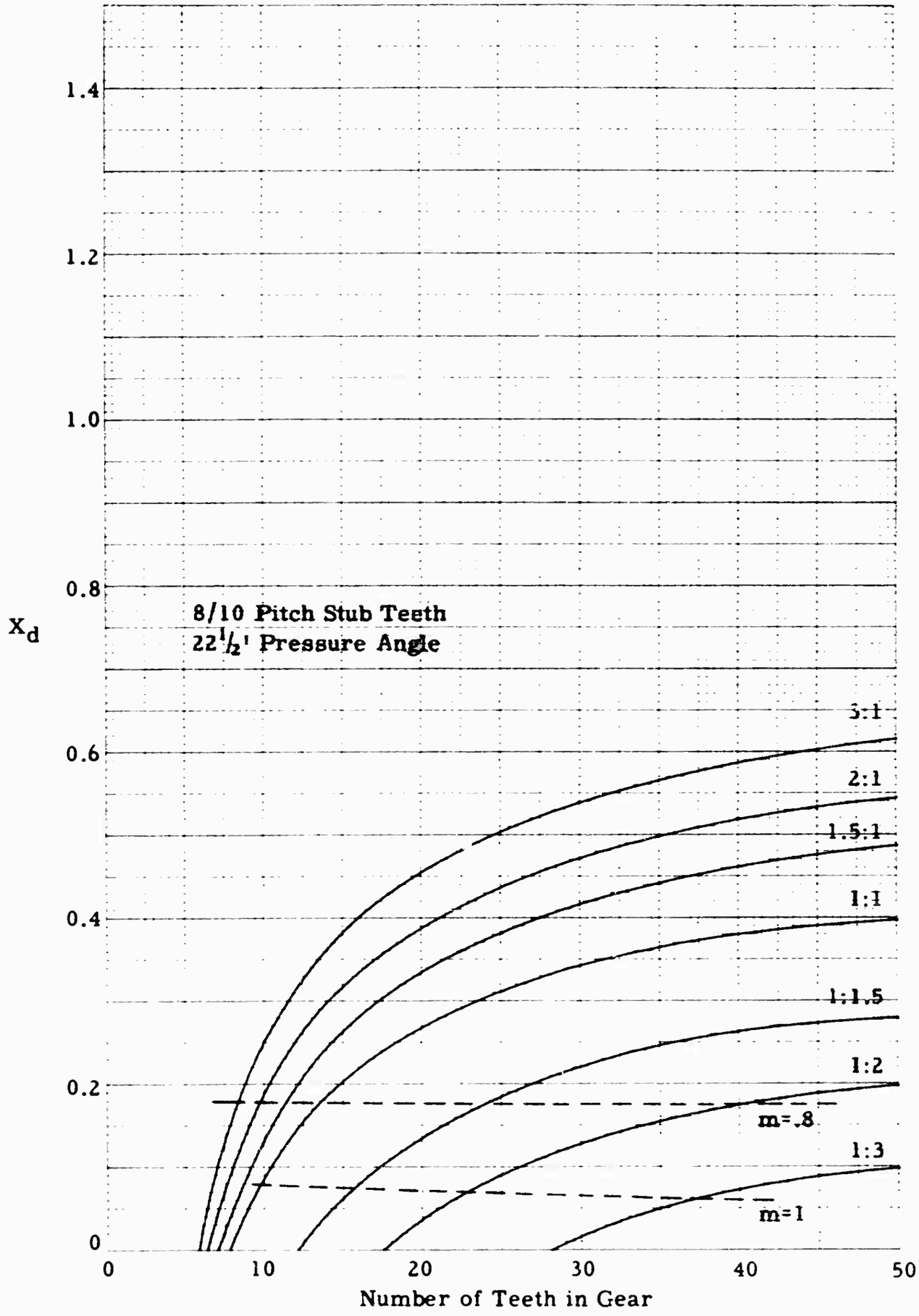

Figure 29. CURVES FOR START OF CONTACT COMPARED TO LIMITING VALUES OF X_d FOR TWO VALUES OF m

S-13926
59926

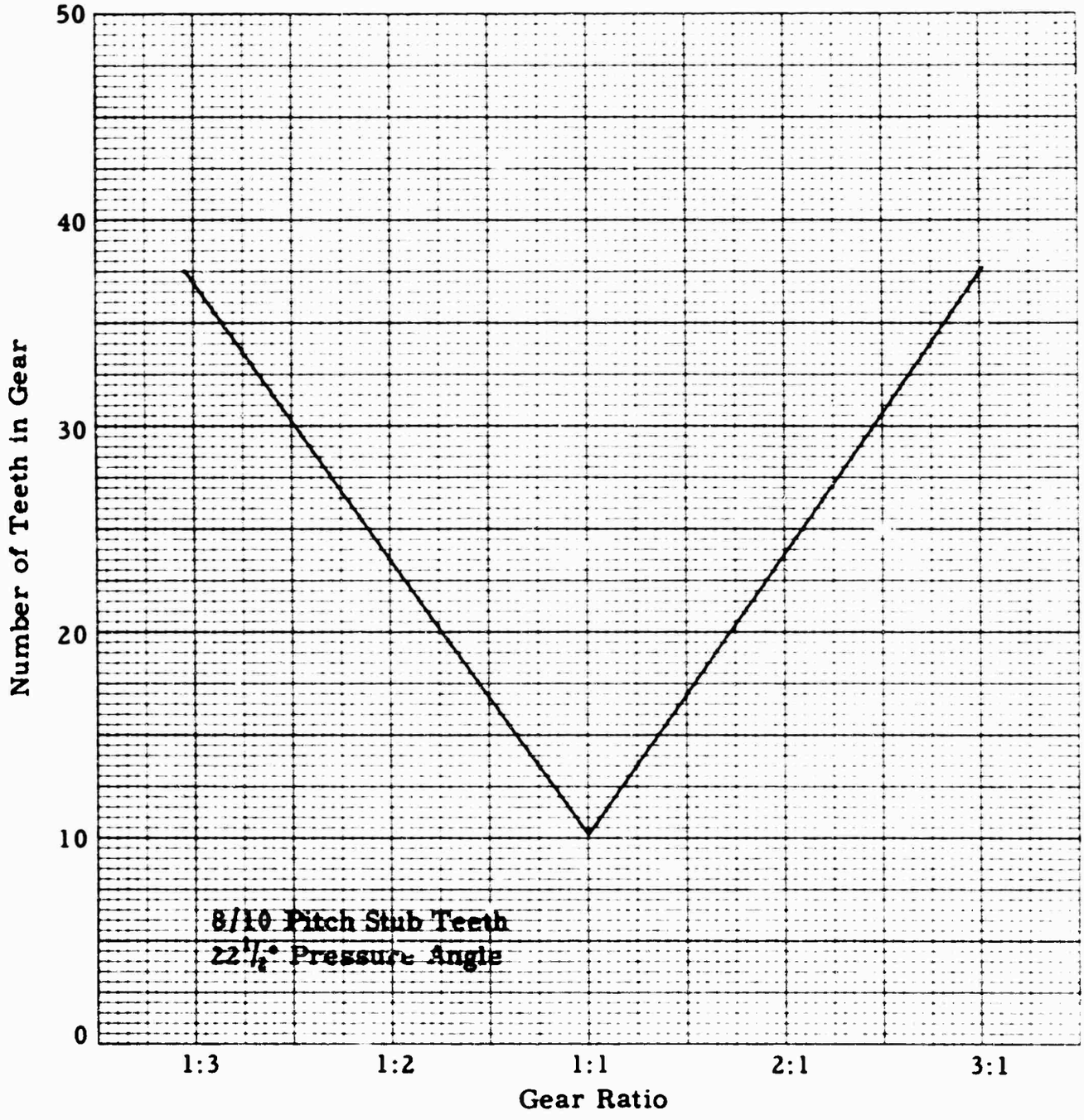

Figure 30. MINIMUM NUMBER OF TEETH REQUIRED IN GEAR vs GEAR RATIO FOR STRESSES OUTSIDE FORBIDDEN REGION WITH m=1

A-1010

S-13926
59926

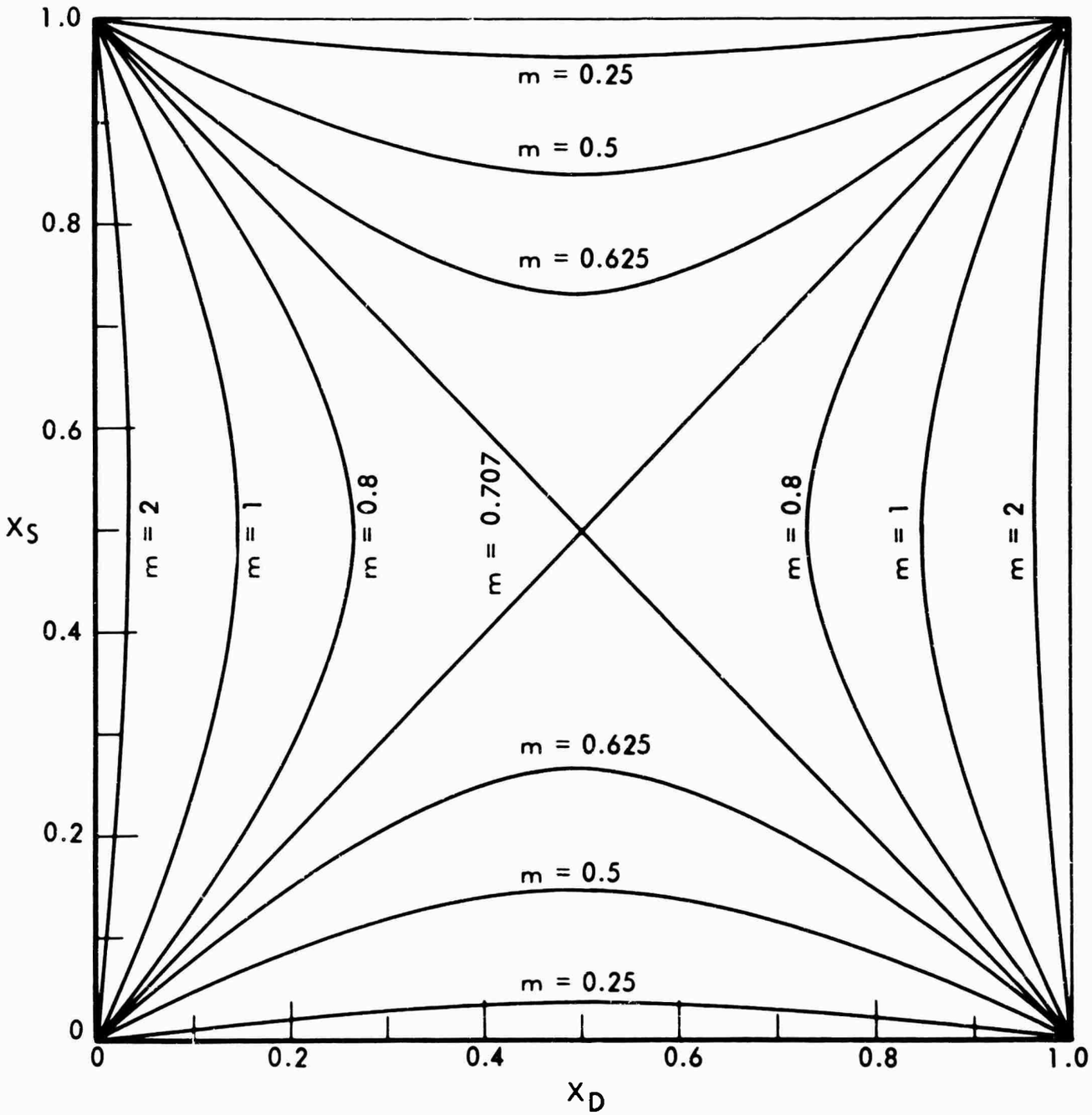

Figure 31. PLOT OF EQUATION DEFINING "FORBIDDEN REGION" FOR SEVERAL VALUES OF m

S-13926
59926

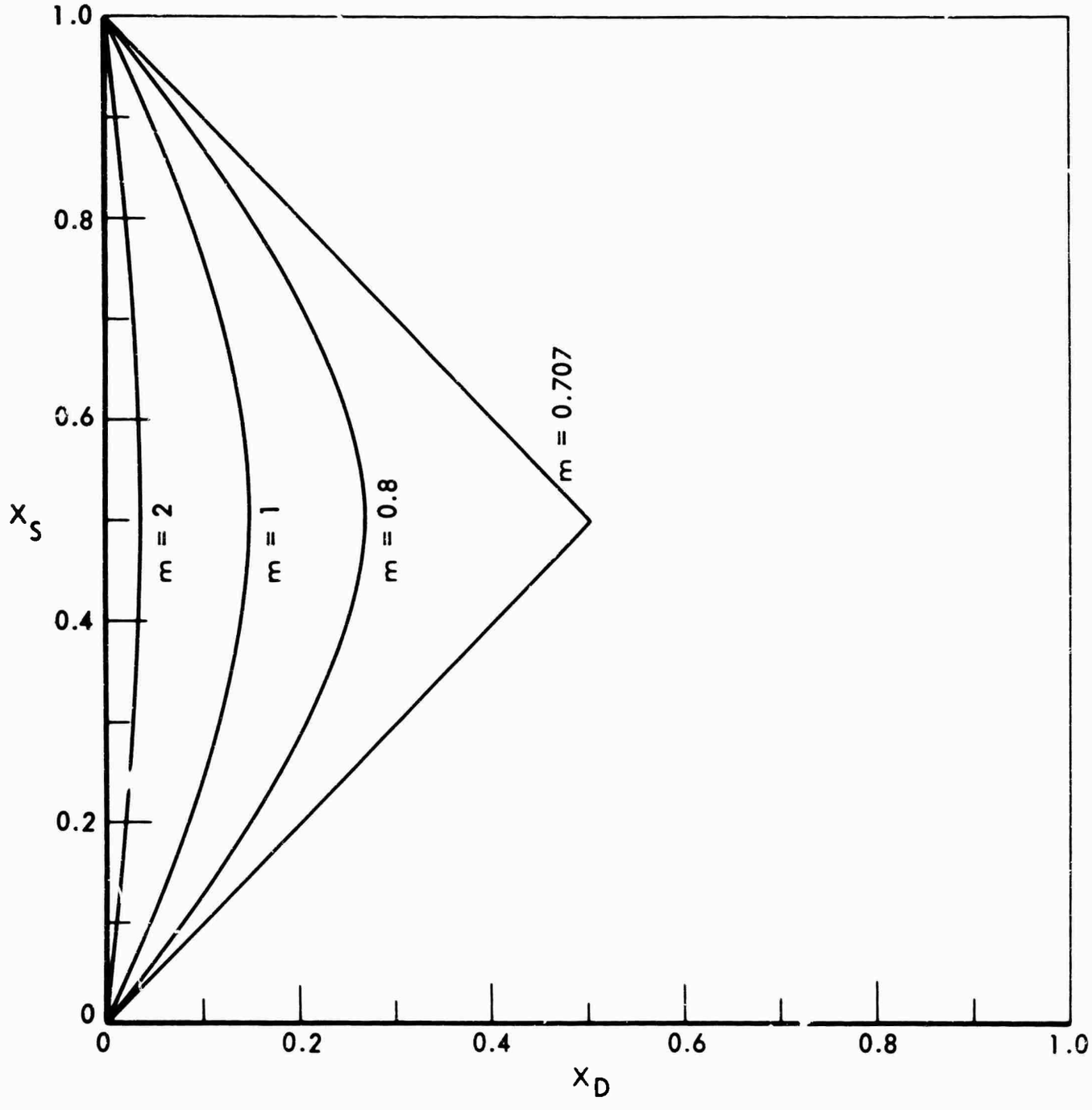

Figure 32. USEFUL PORTION OF FIGURE 31

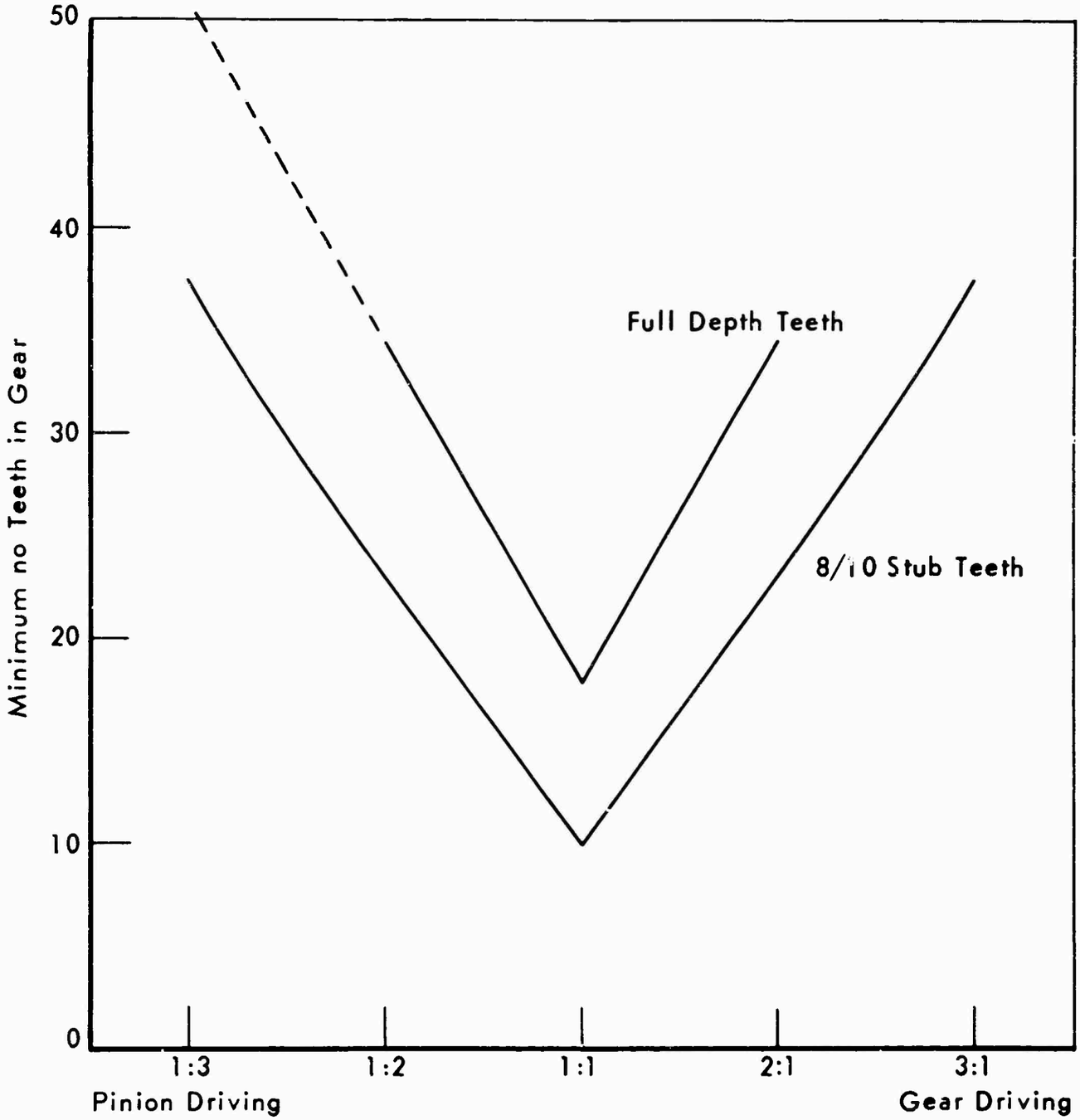

Figure 33. COMPARISON OF MINIMUM NUMBER OF TEETH REQUIRED FOR BALANCED STRESS WITH m = 1 BETWEEN FULL DEPTH TEETH AND STUB TEETH

S-13926
59926

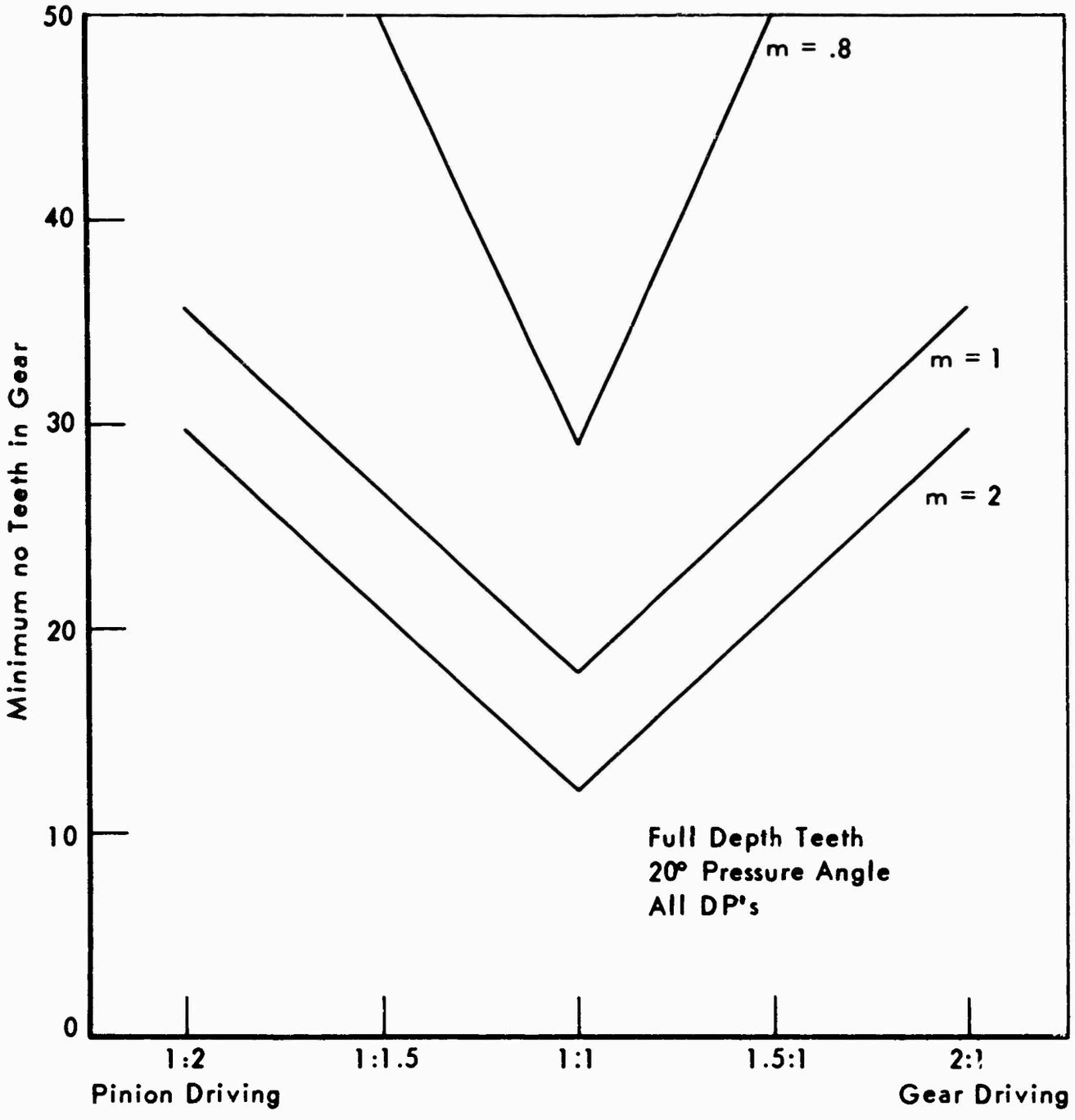

Figure 34. COMPARISON OF MINIMUM NUMBER OF TEETH REQUIRED FOR BALANCED STRESS FOR THREE VALUES OF m

S-13926
59926

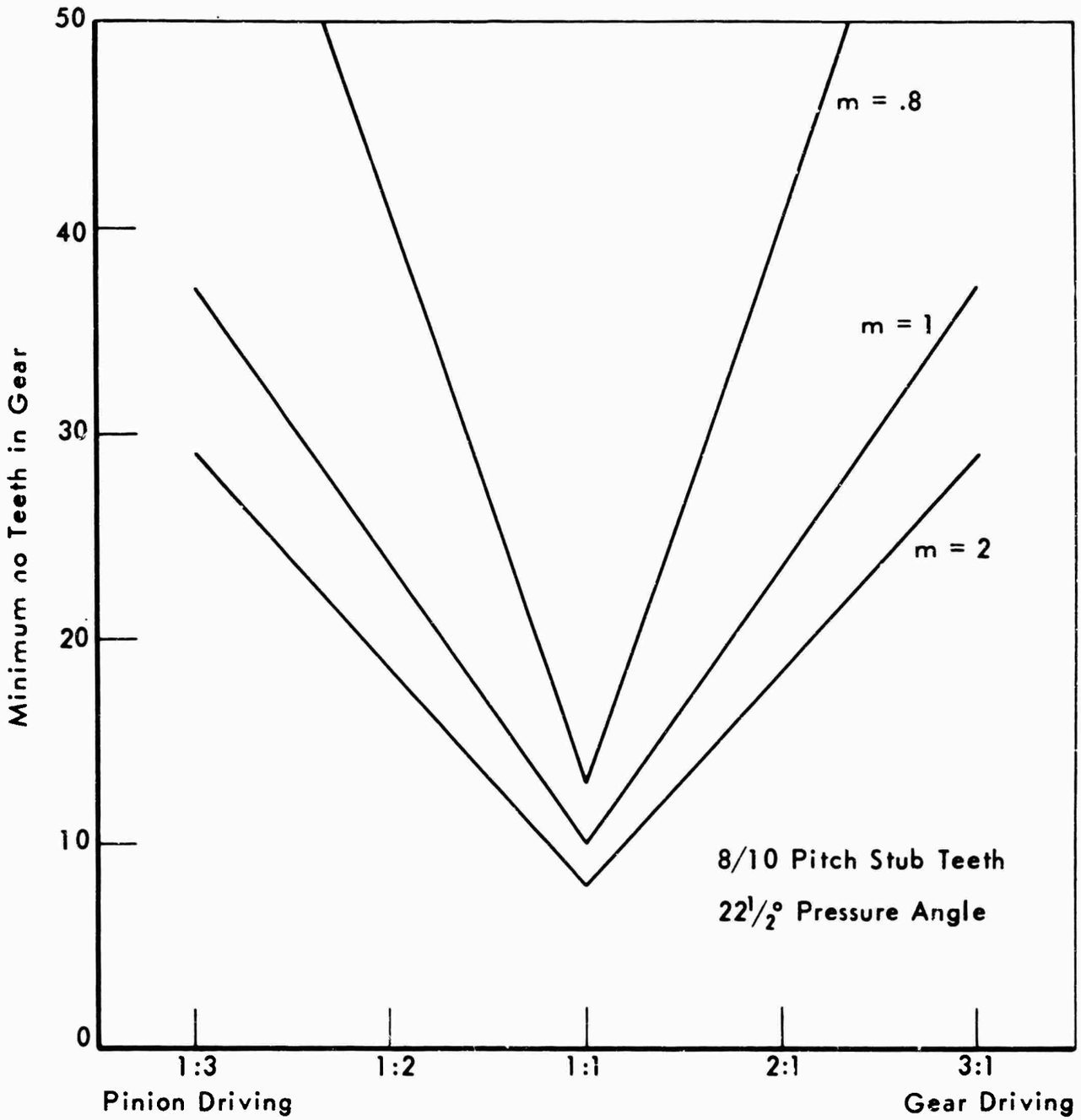

Figure 35. COMPARISON OF MINIMUM NUMBER OF TEETH REQUIRED FOR BALANCED STRESS FOR THREE VALUES OF m

S-13926
59926

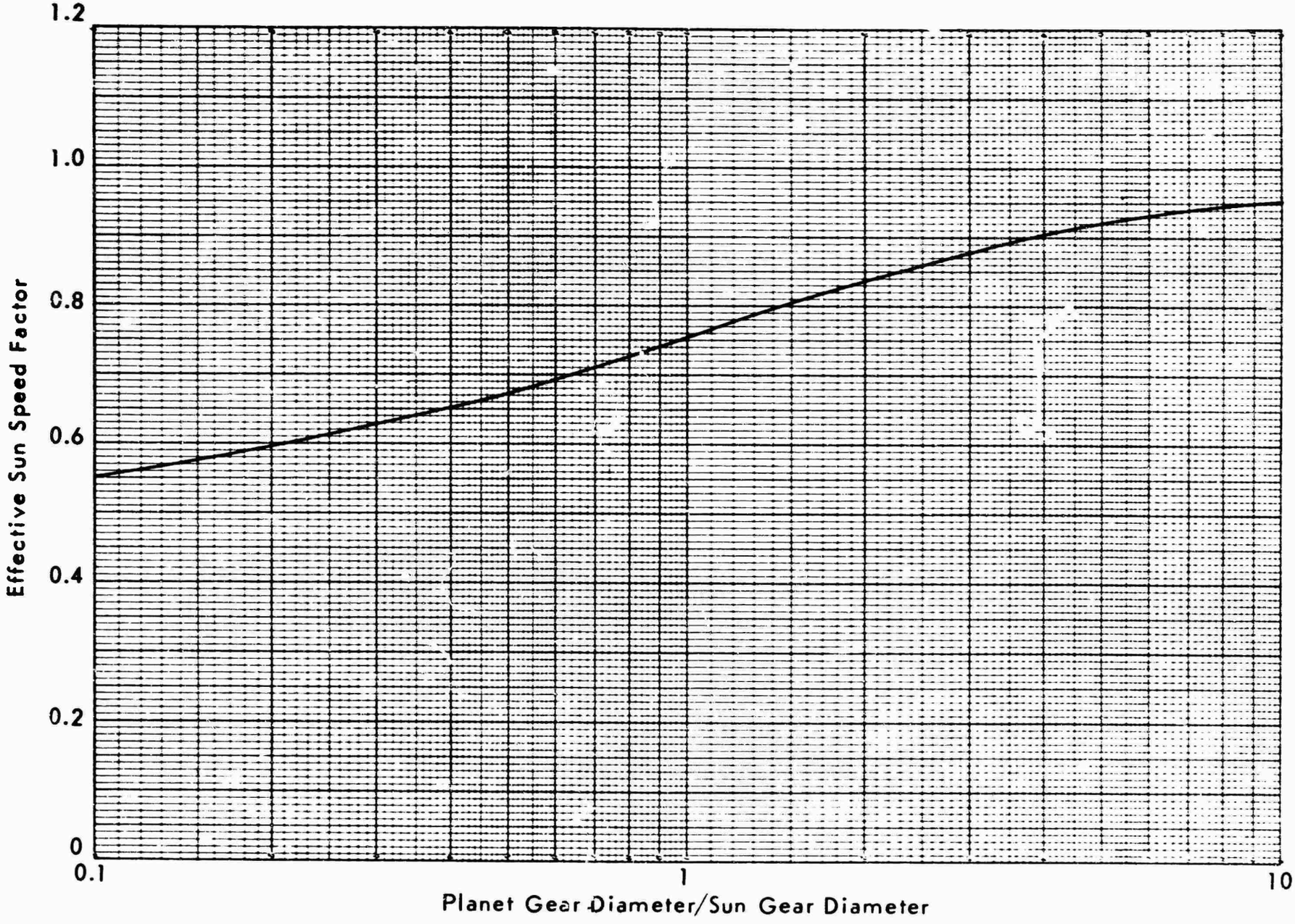

Figure 36. EFFECTIVE SPEED FACTOR FOR PLANETARY SYSTEM vs PLANET/SUN GEAR RATIO

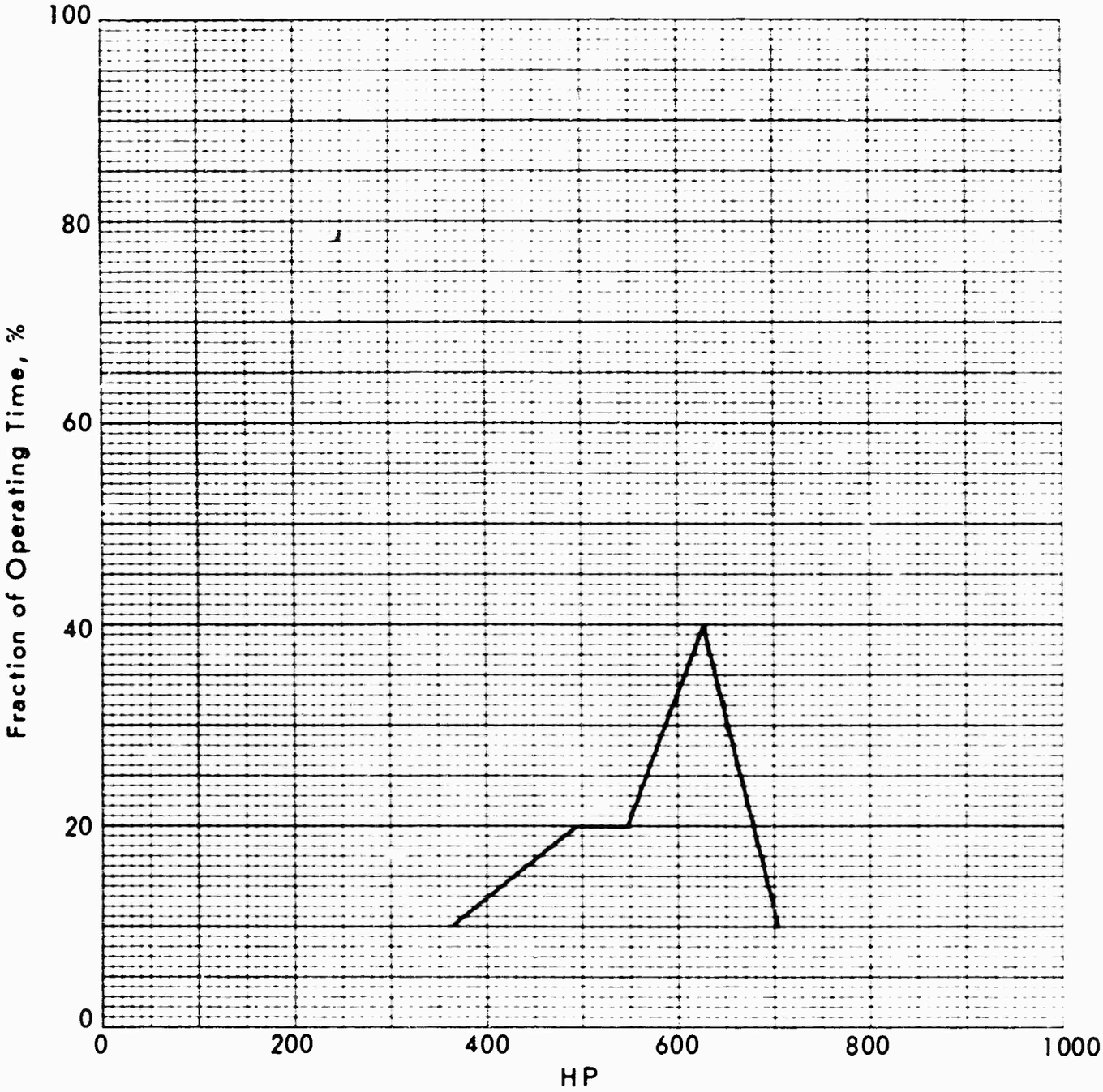

Figure 37. POWER SPECTRUM FOR HELICOPTER PLANETARY TRANSMISSION

A-1010

S-13926
59556

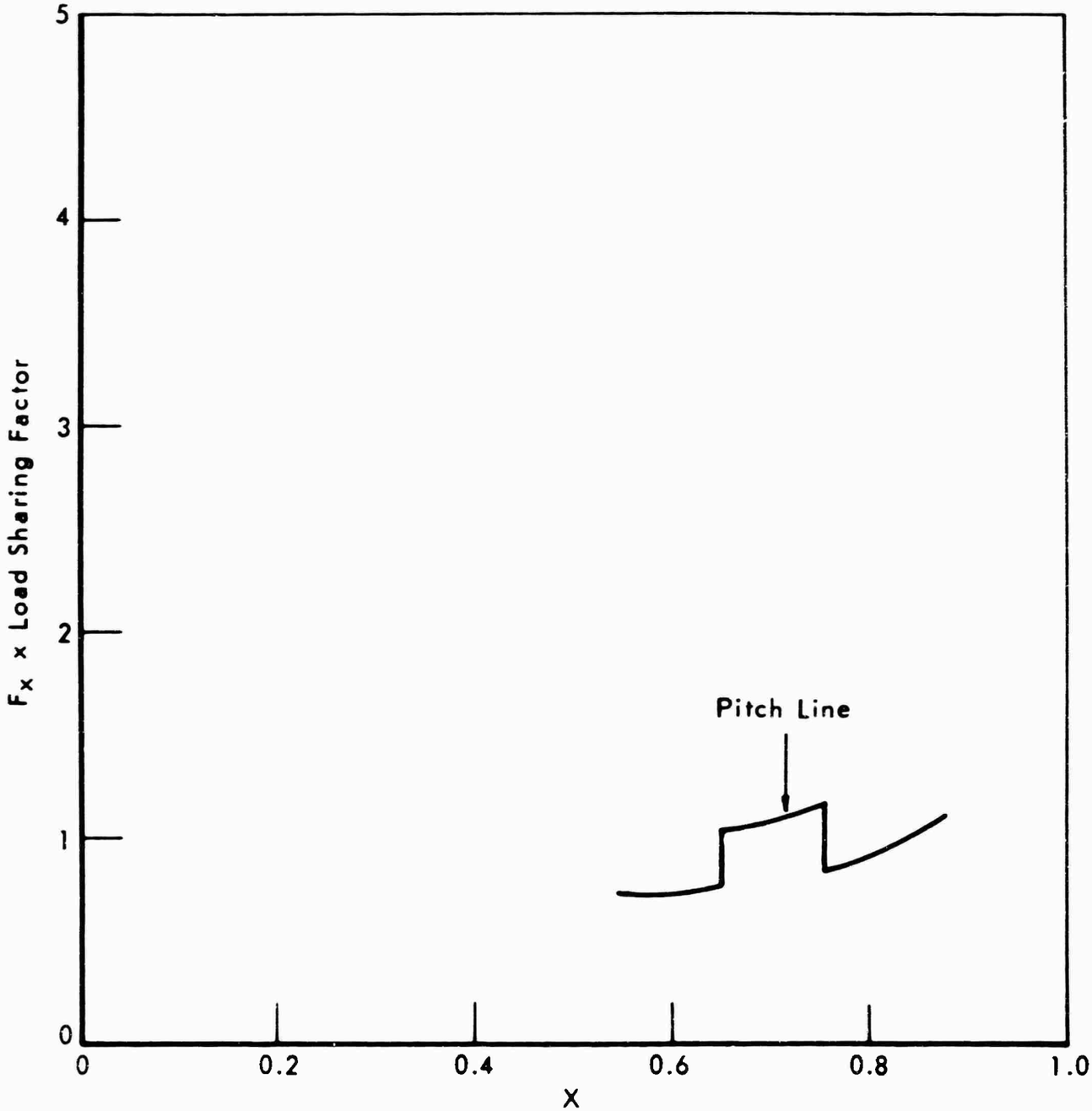

Figure 38. F_x MODIFIED FOR LOAD SHARING

S-13926
59556

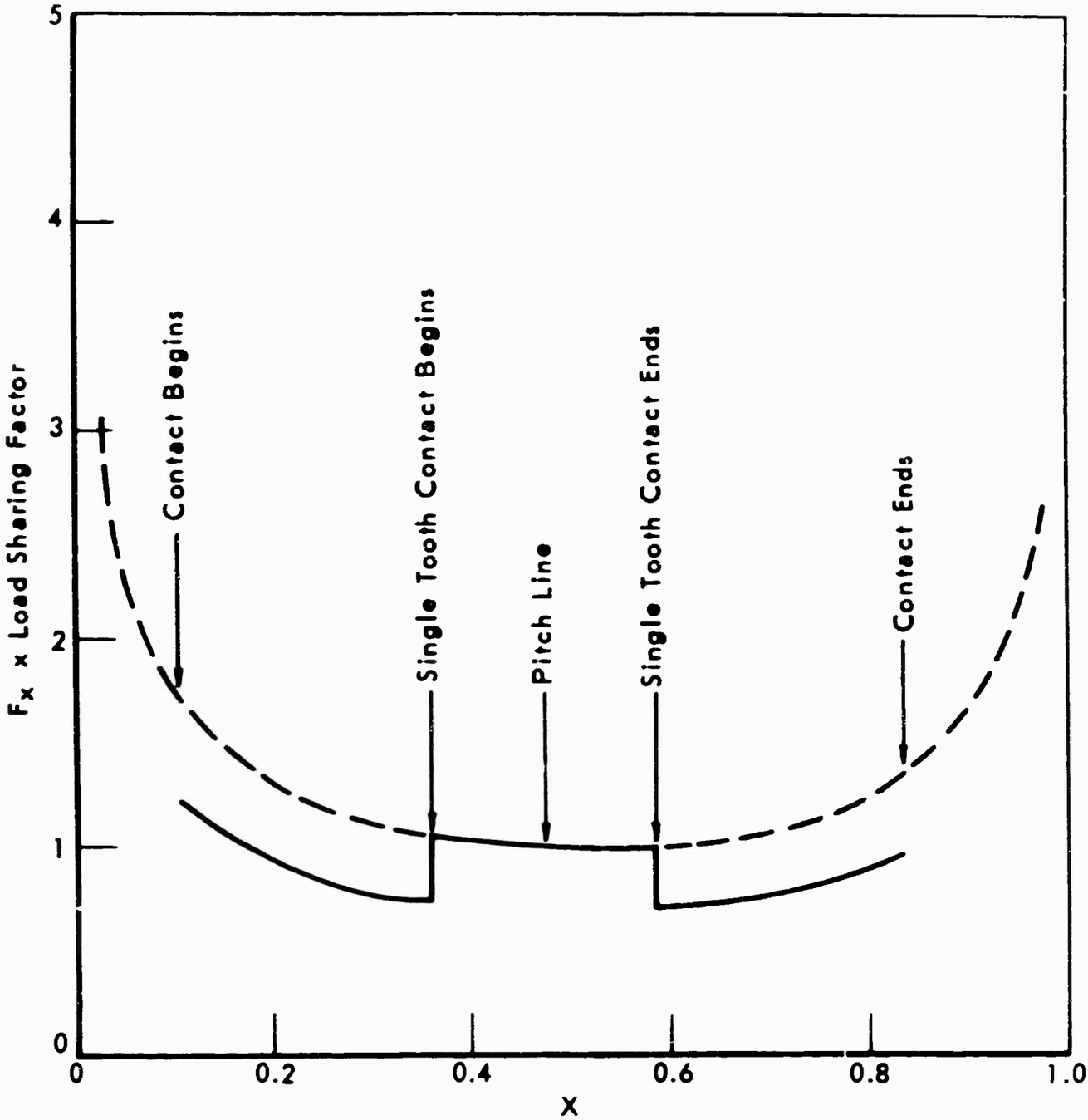

Figure 39. F_x x LOAD SHARING FACTOR FOR TEST GEARS

S-13926
59556

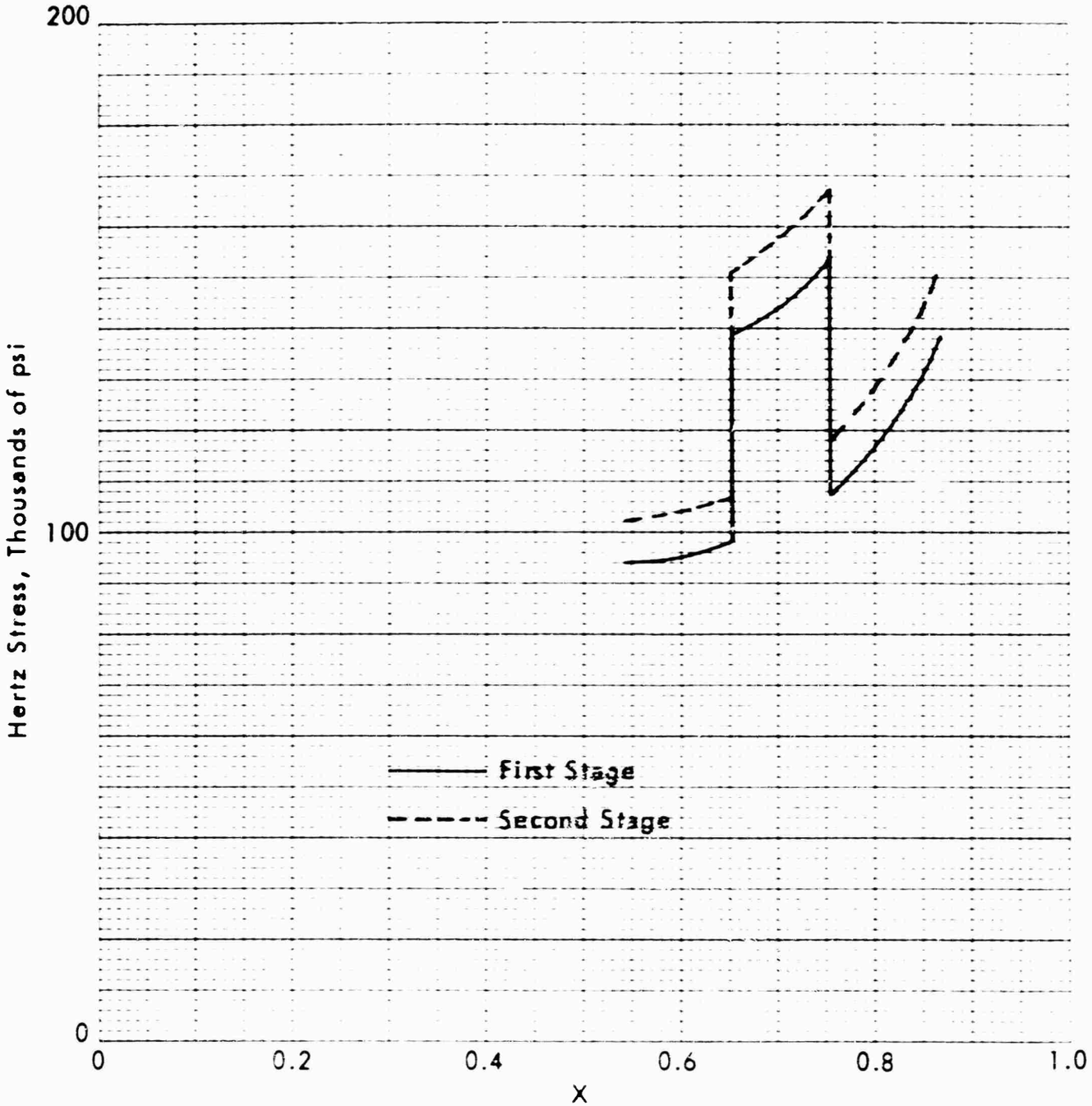

Figure 40. HERTZ STRESS FOR HELICOPTER SUN-PLANET PAIR, FIRST AND SECOND STAGES

S-13926
59556

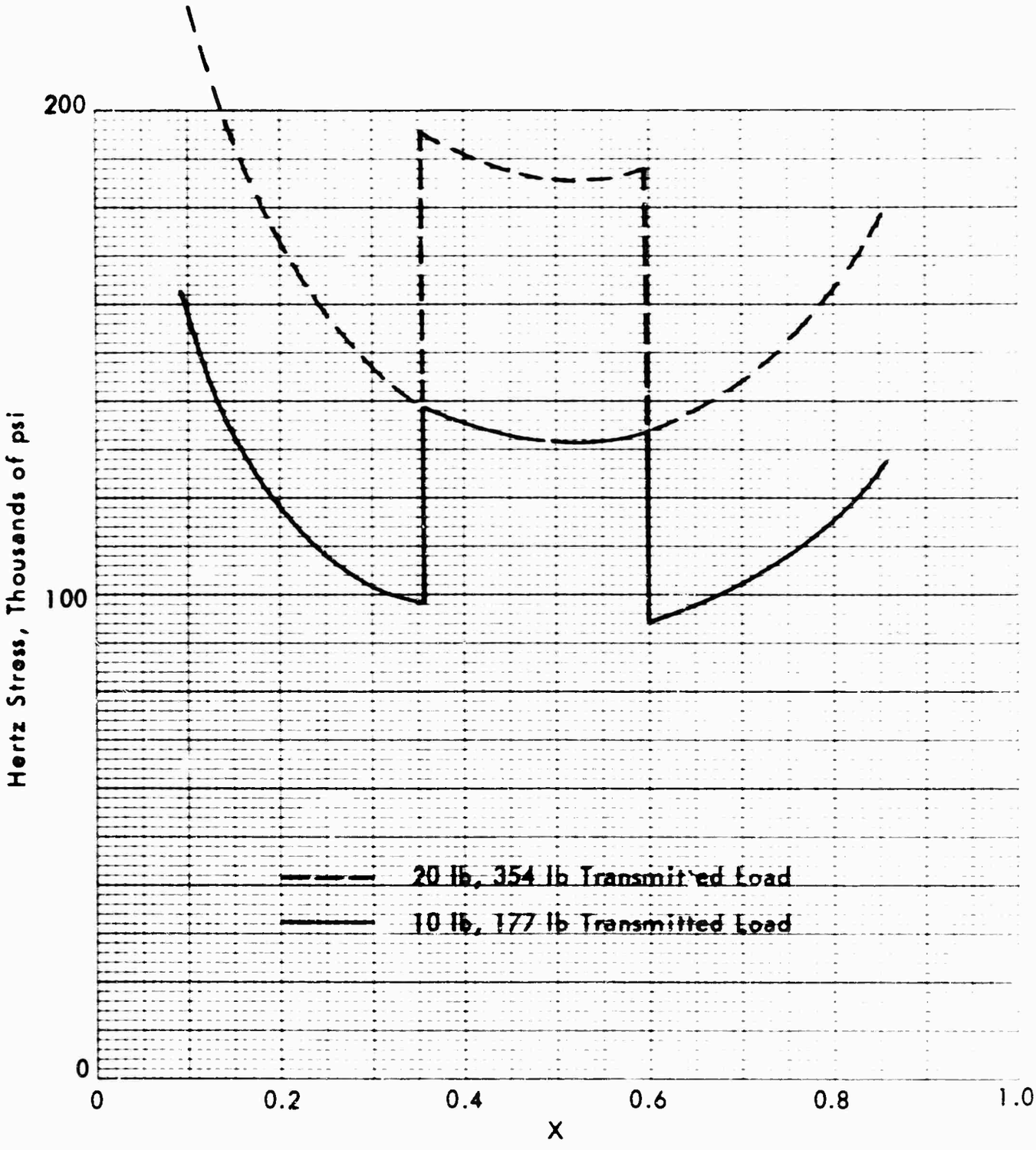

Figure 41. HERTZ STRESS FOR TEST GEARS AT TWO LOAD LEVELS

A-1010

S-13926
59556

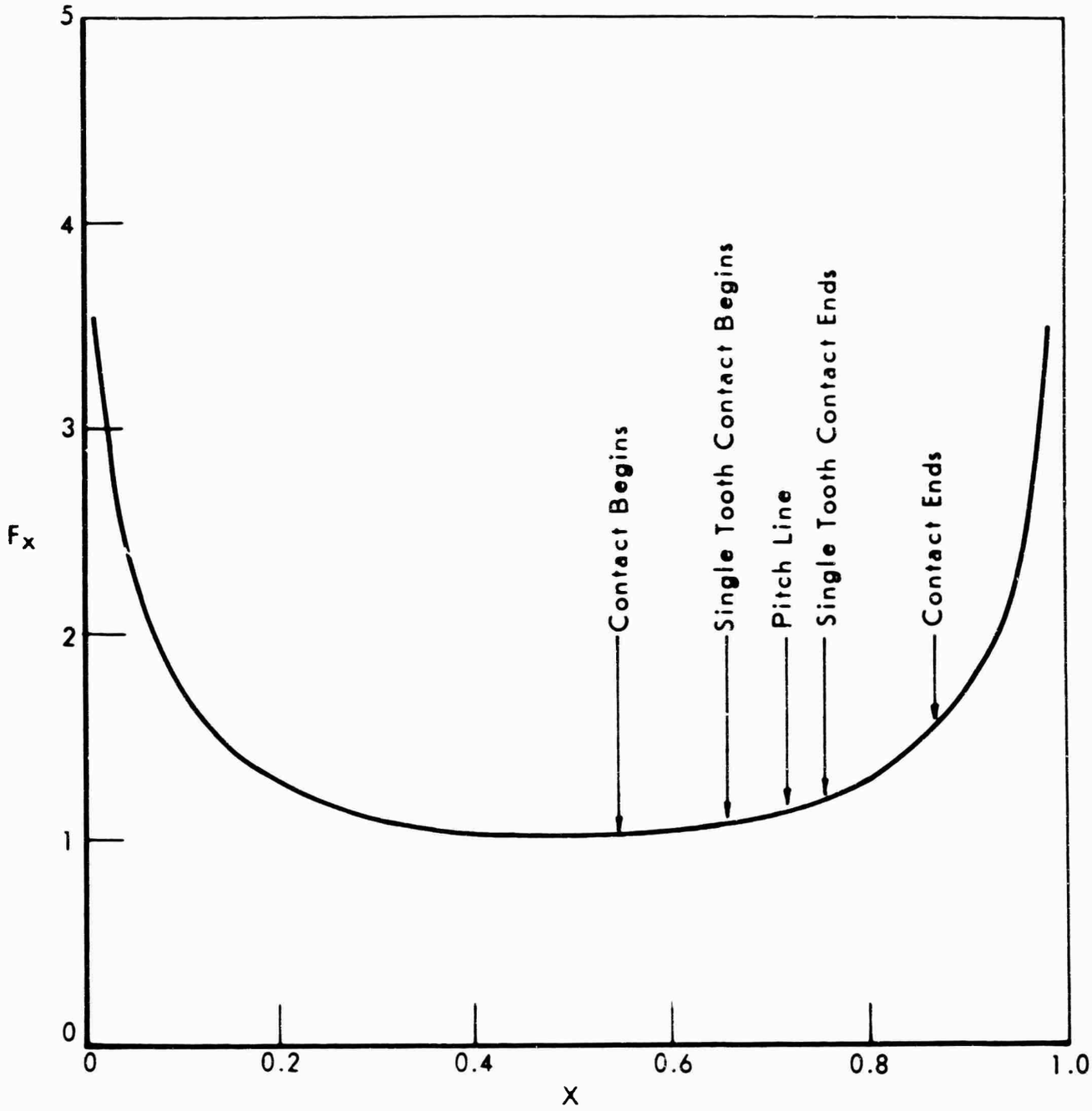

Figure 42. SIGNIFICANT POINTS ALONG F_x CURVE FOR SUN/PLANET PAIR IN HELICOPTER TRANSMISSION

S-13926
59556

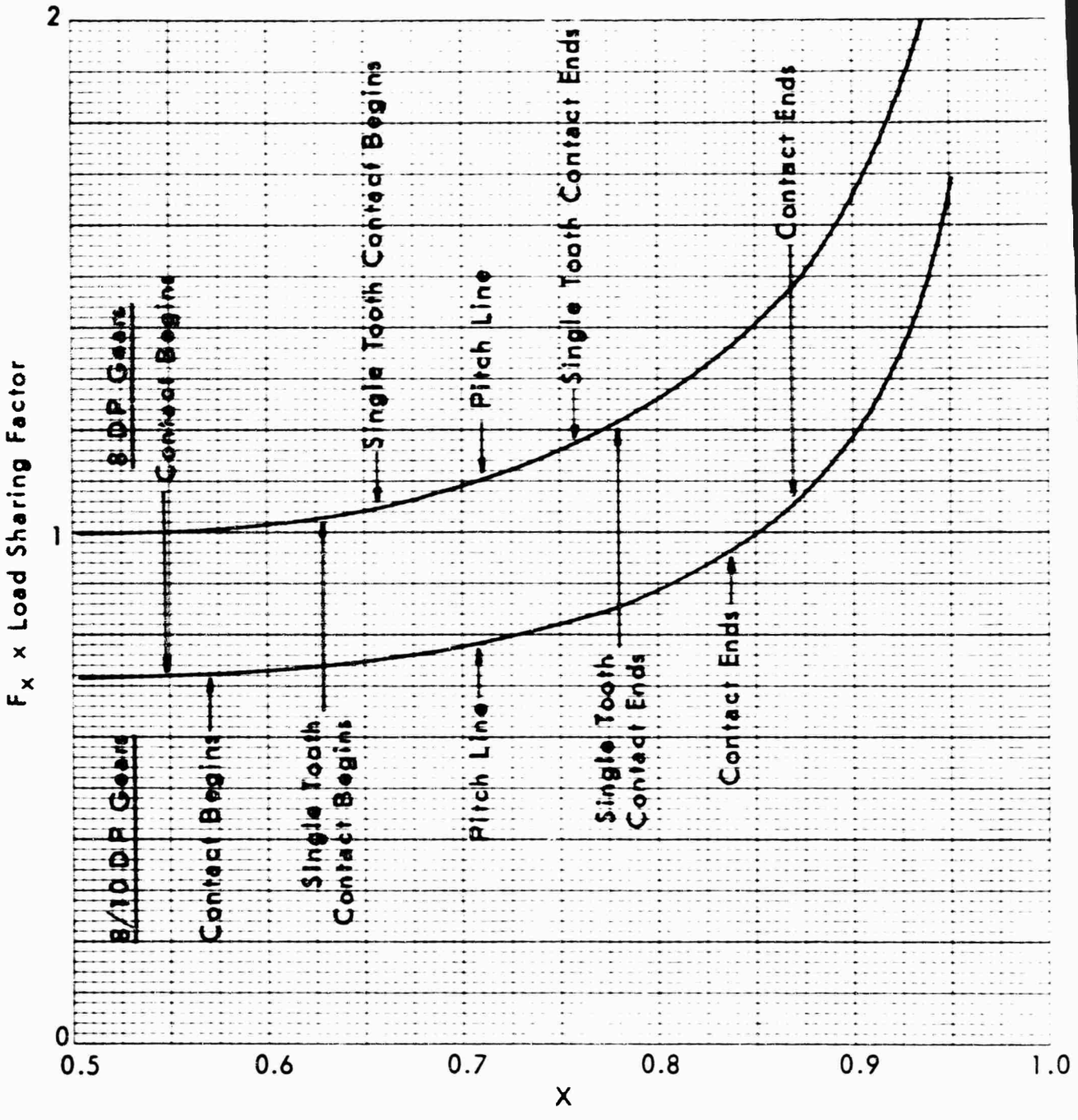

Figure 43. COMPARISON OF CONTACT STRESS CONDITIONS IN 8 DP GEARS AND 8/10 DP STUB TOOTH GEARS

S-13926
59556

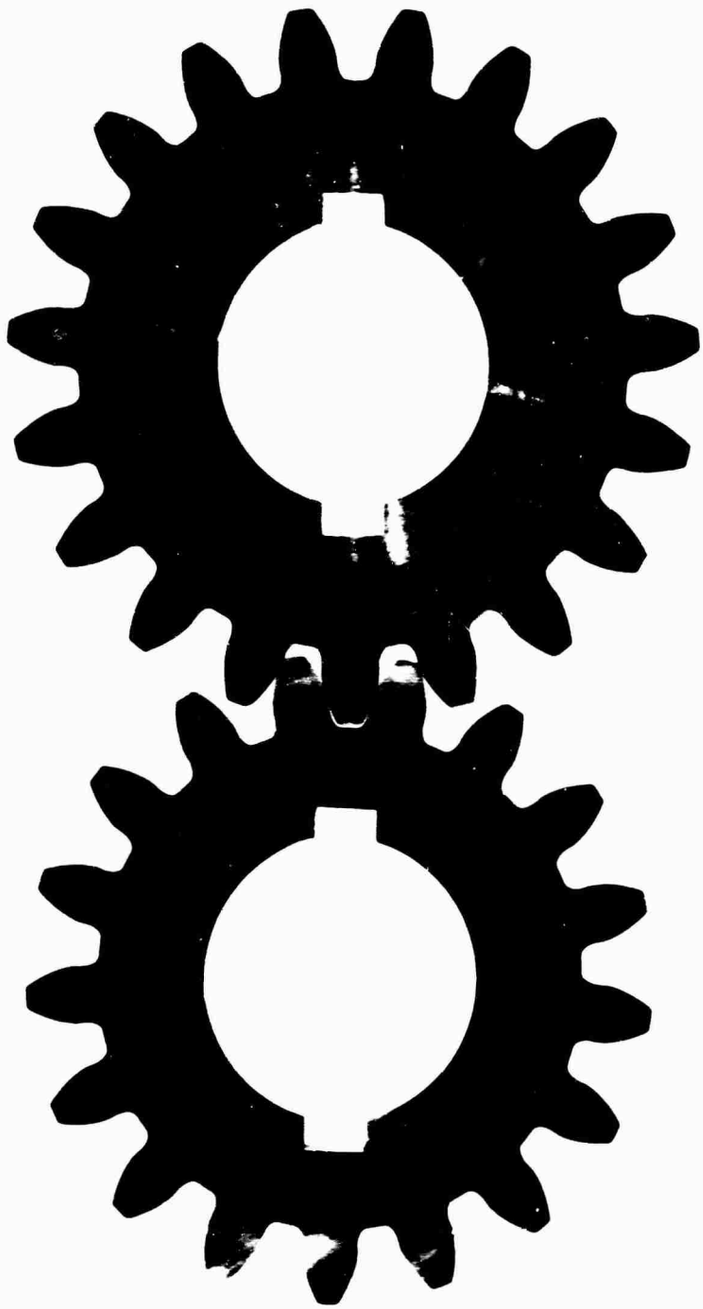

Figure 44. PAIR OF STANDARD TEST GEARS - SHOWN FULL SIZE

S-13926
59234-1

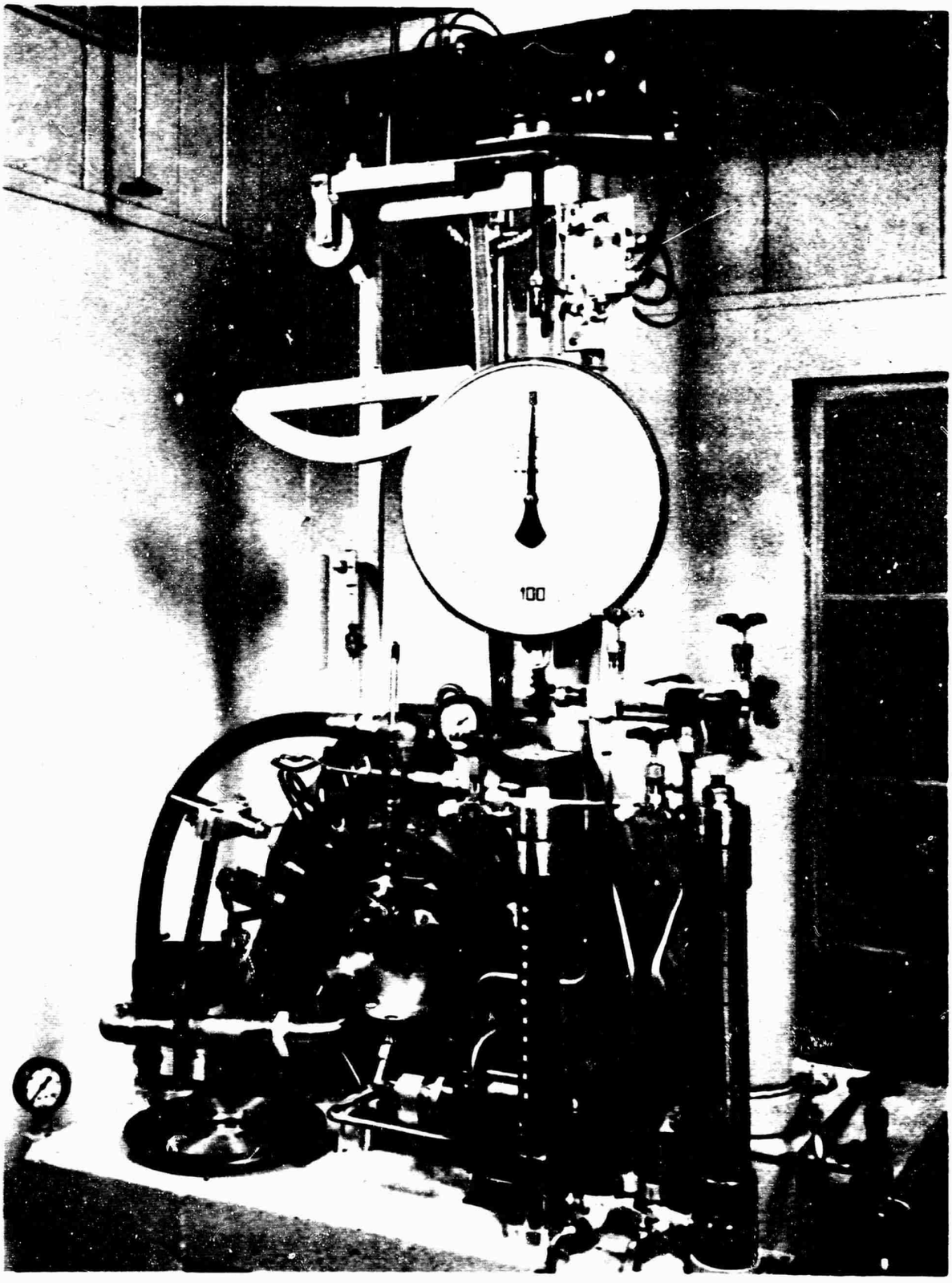

Figure 45. HIGH SPEED SPUR GEAR TEST MACHINE

S-13926
46730-A

S-13926
59926

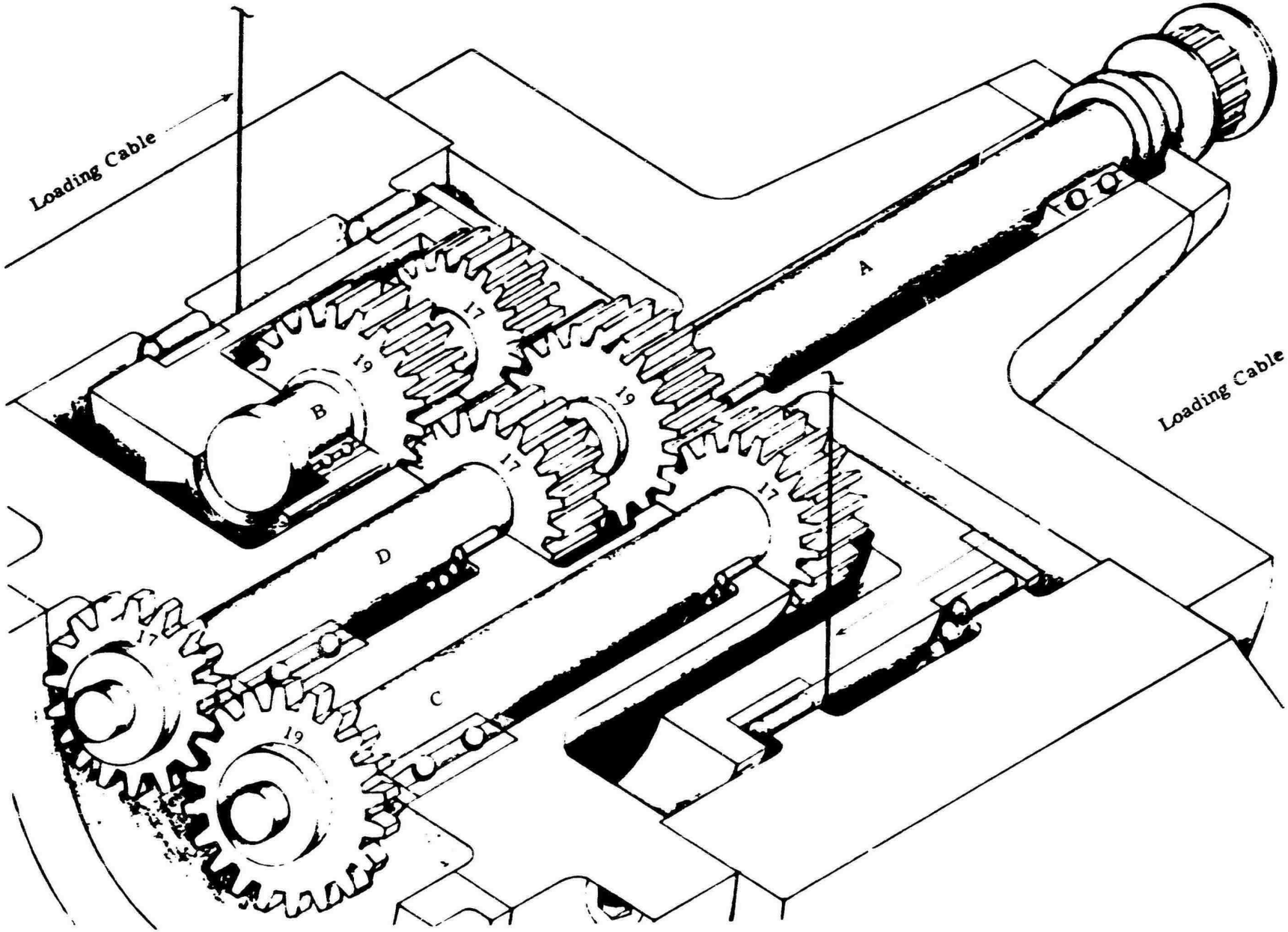

Figure 46. SECTION VIEW HIGH SPEED SPUR GEAR MACHINE

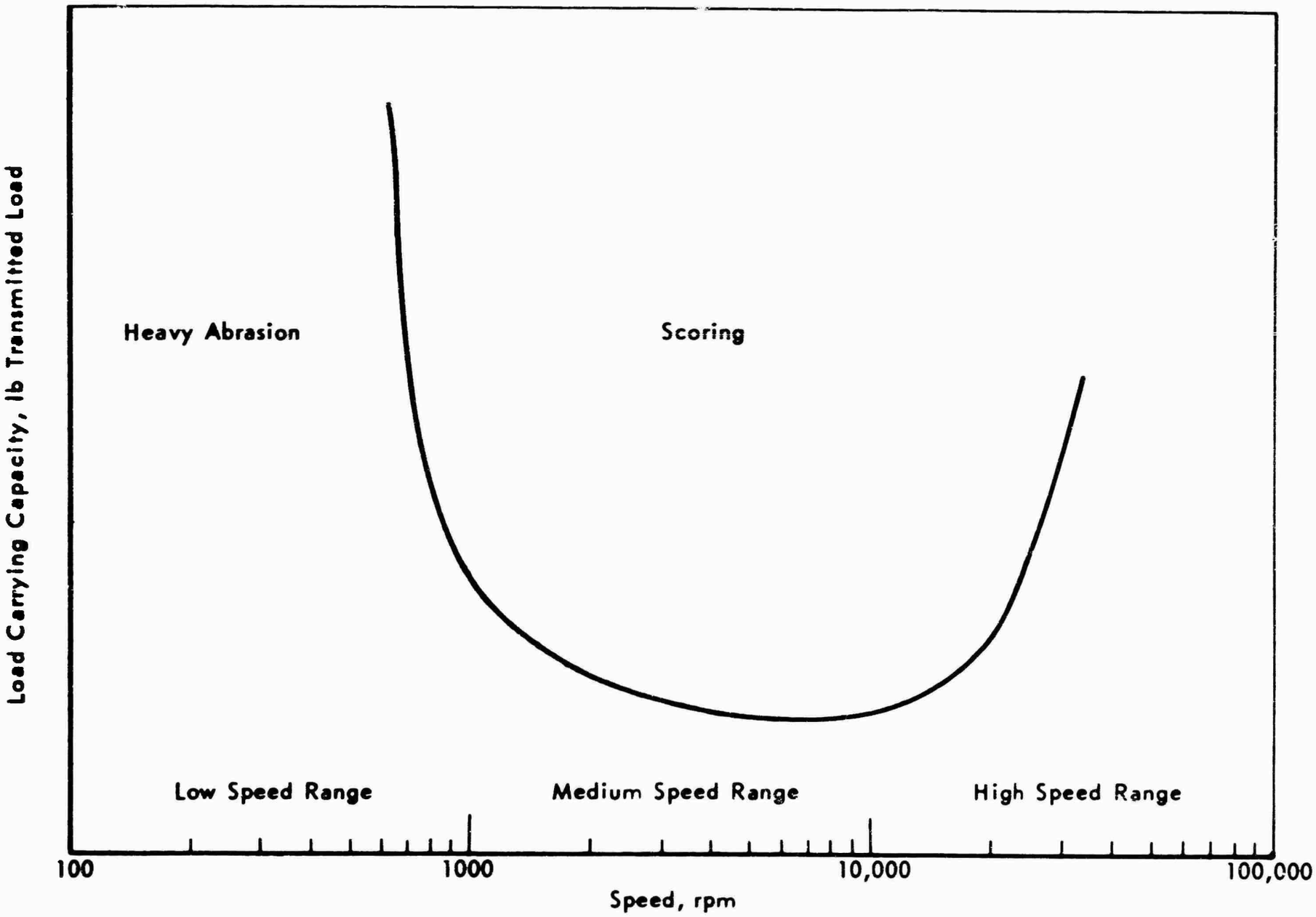

Figure 47. GENERAL LCC CURVE FOR MINERAL OIL

S-13926
59926

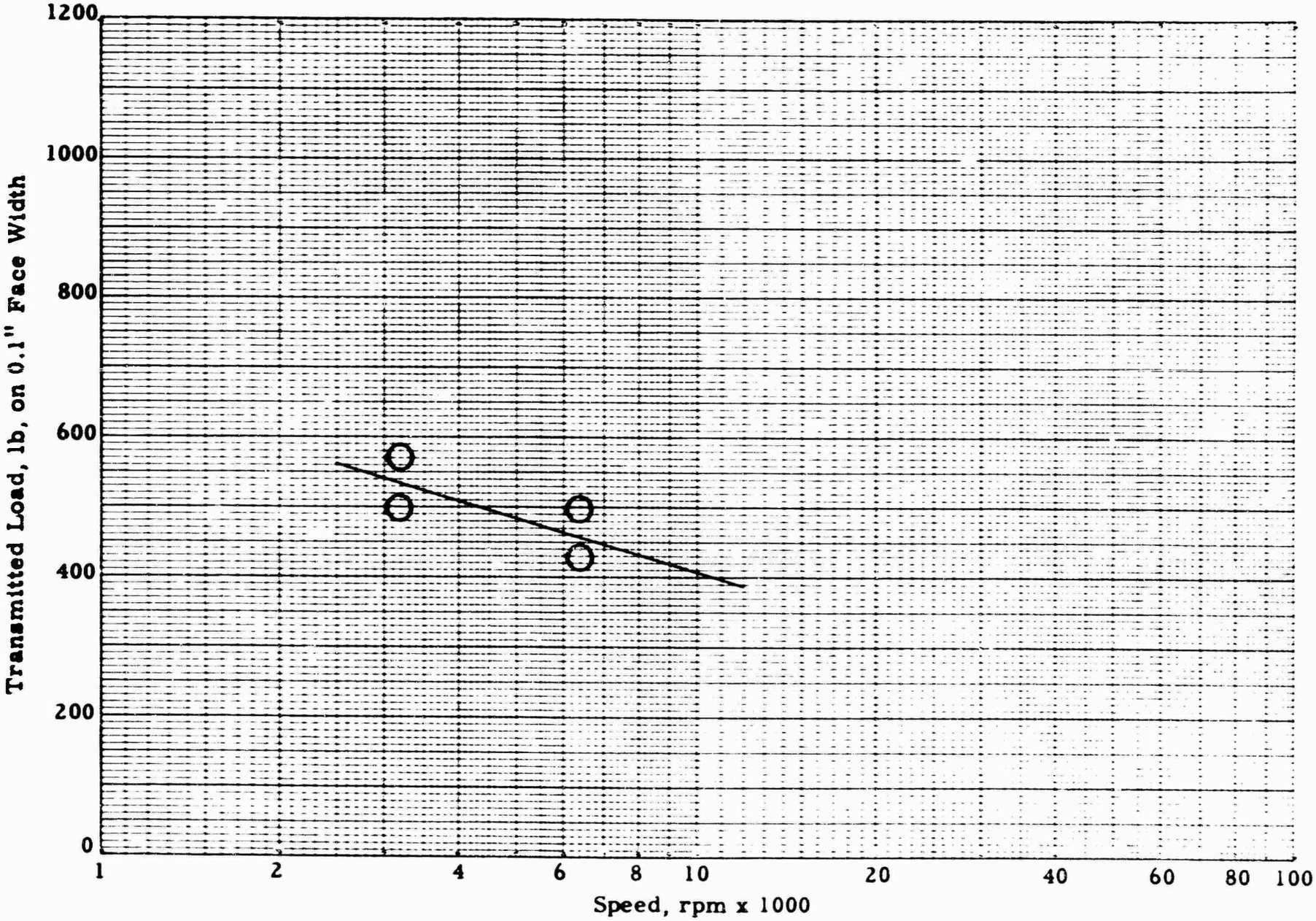

Figure 48. SPUR GEAR LOAD CARRYING CAPACITY FOR MIL-L-7808C OIL vs SPEED

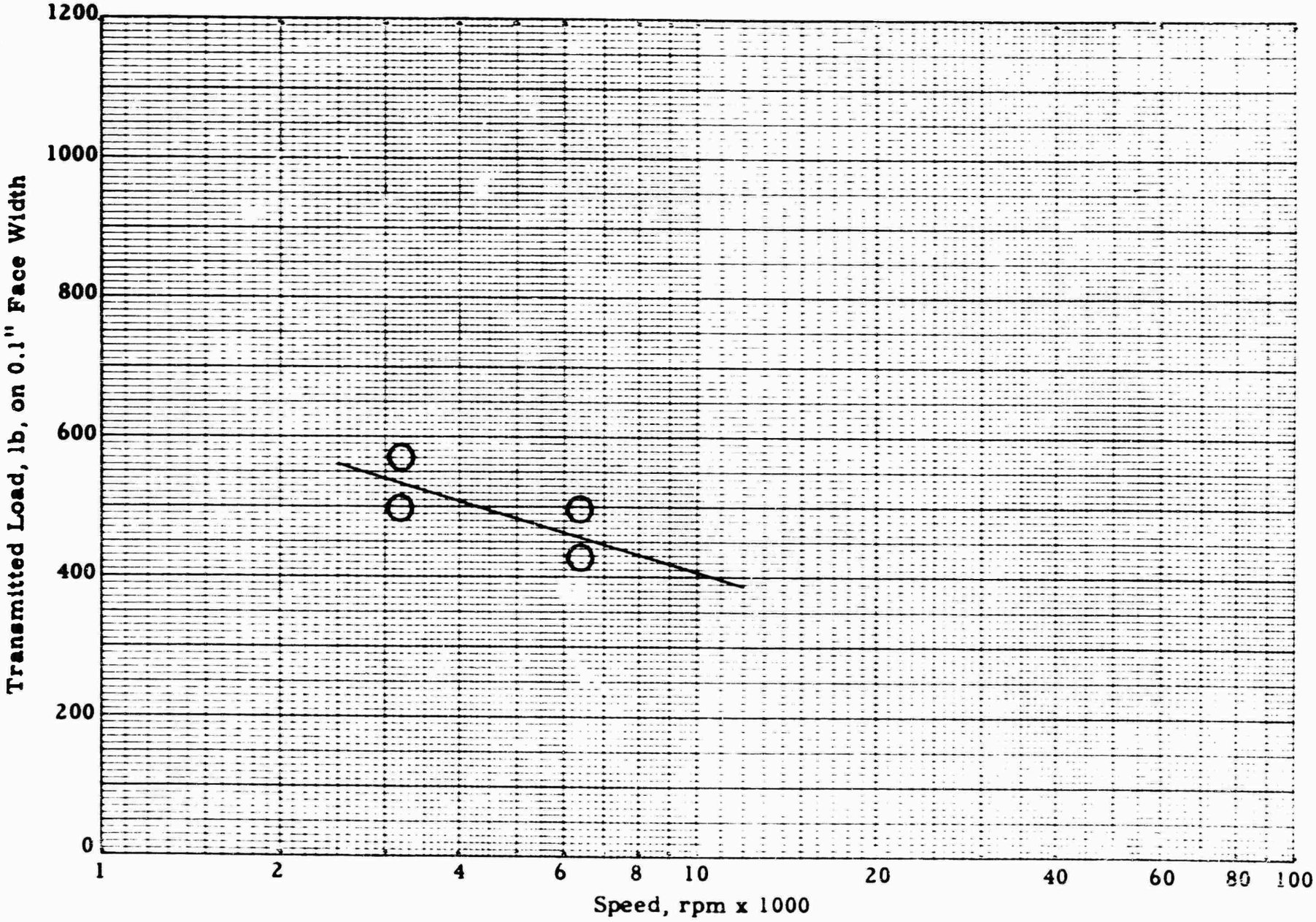

Figure 48. SPUR GEAR LOAD CARRYING CAPACITY FOR MIL-L-7808C OIL vs SPEED

S-13926
59926

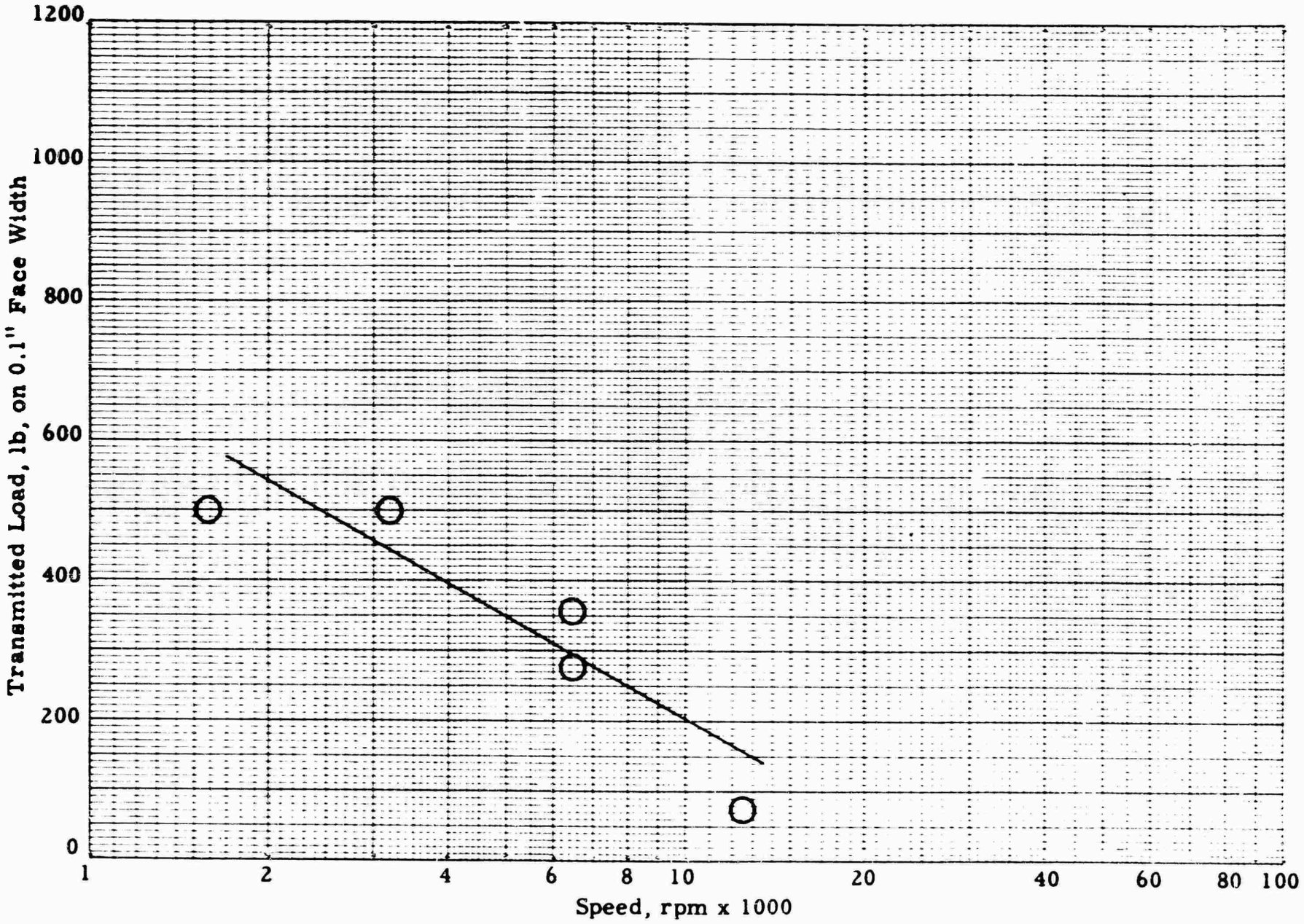

Figure 49. SPUR GEAR LOAD CARRYING CAPACITY FOR MIL-L-7808D OIL vs SPEED

S-13926
59926

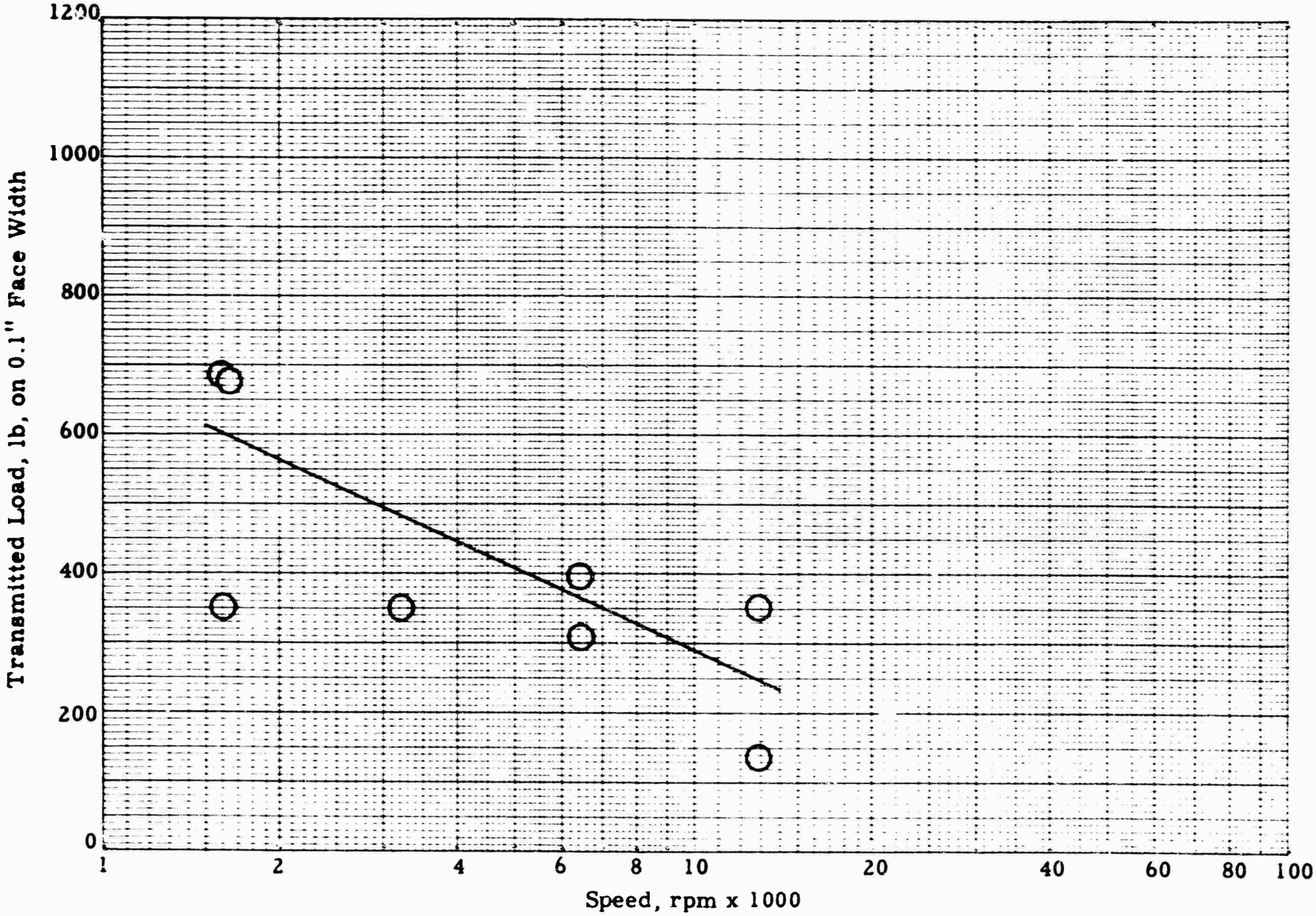

Figure 50. SPUR GEAR LOAD CARRYING CAPACITY FOR MIL-L-7808E OIL vs SPEED

S-13926
59926

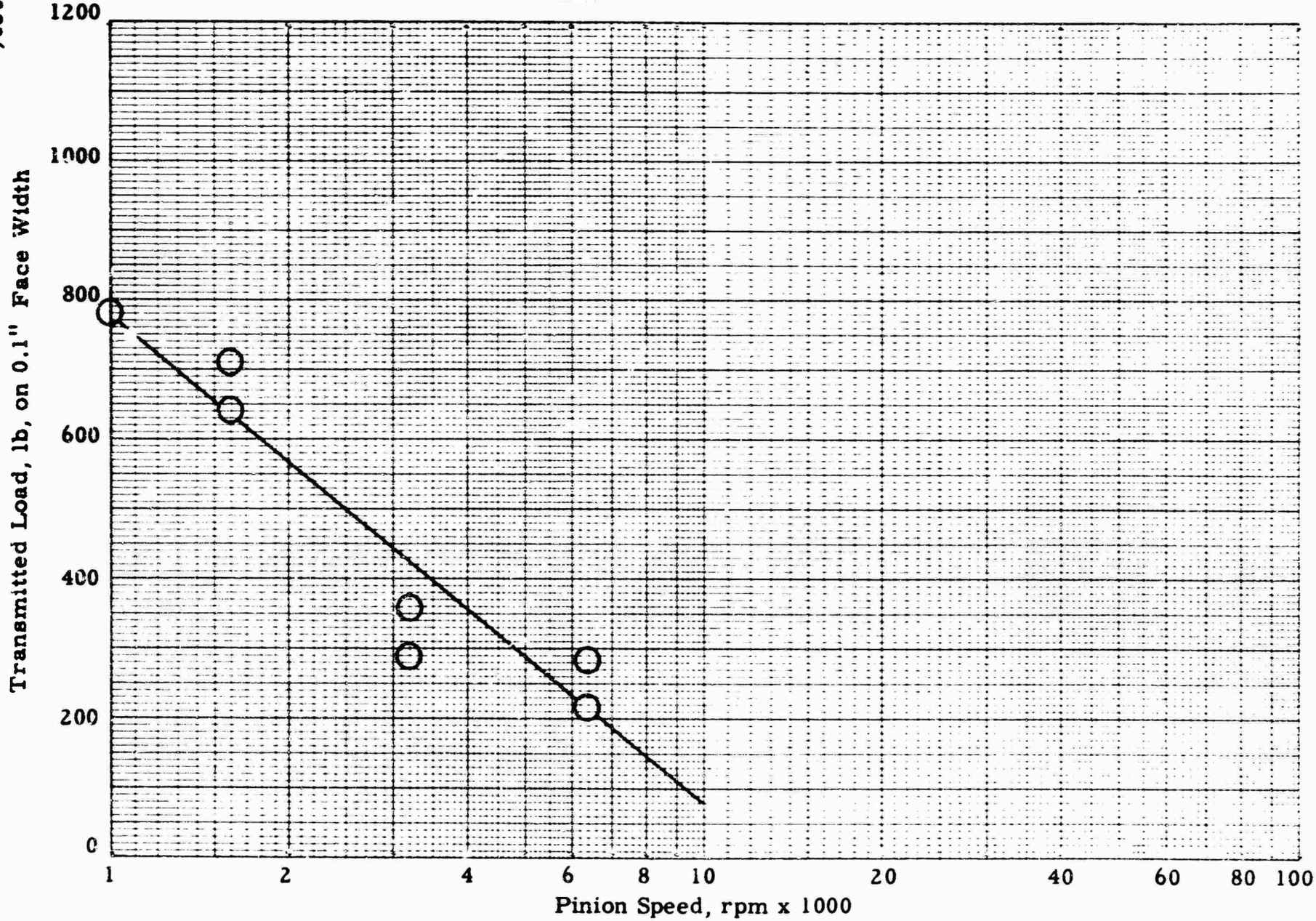

Figure 51. SPUR GEAR LOAD CARRYING CAPACITY FOR MIL-L-21260 (GRADE 2) vs SPEED

92665
S-13926

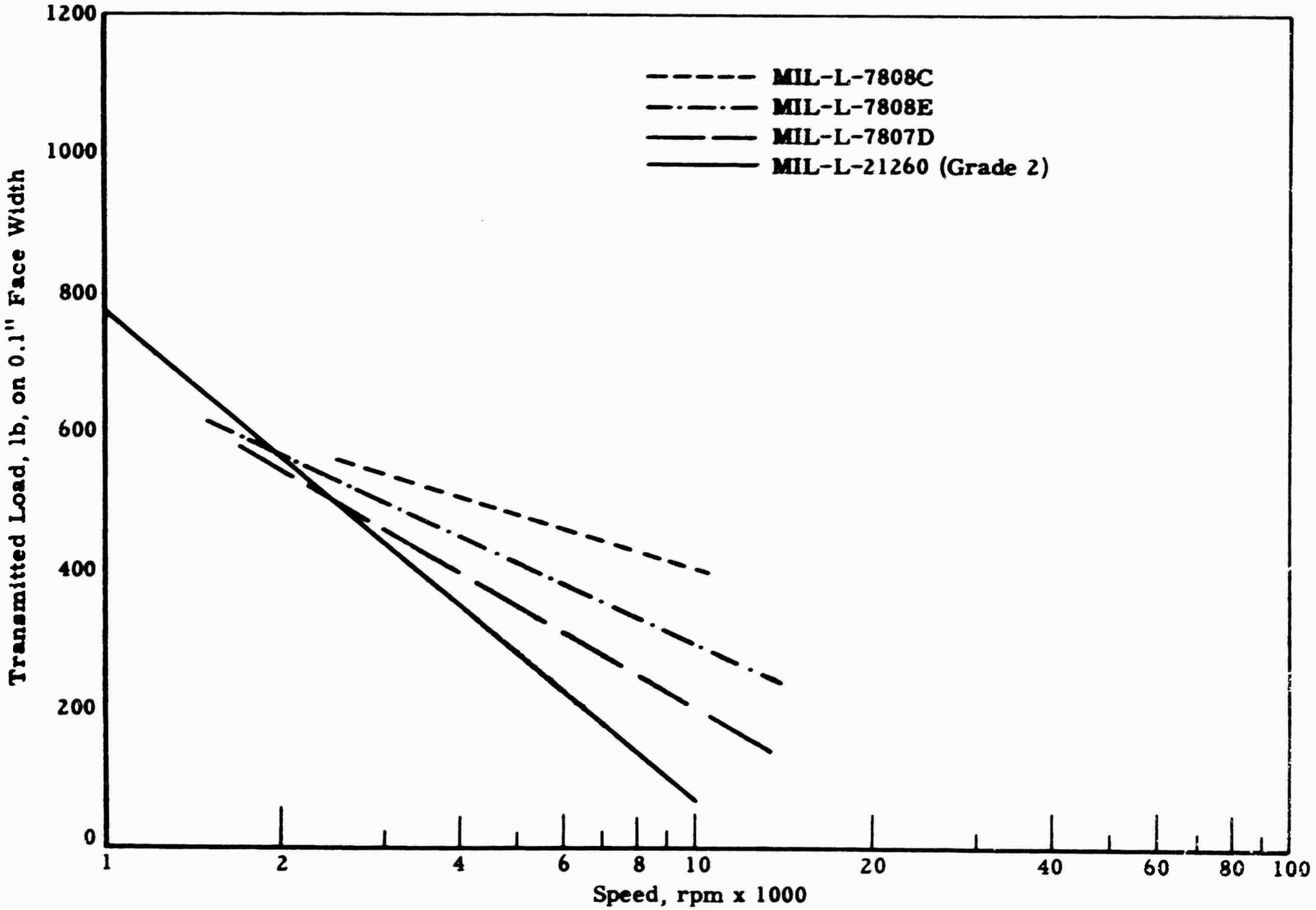

Figure 52. SPUR GEAR LOAD CARRYING CAPACITY OF FOUR MIL SPEC. OILS vs SPEED

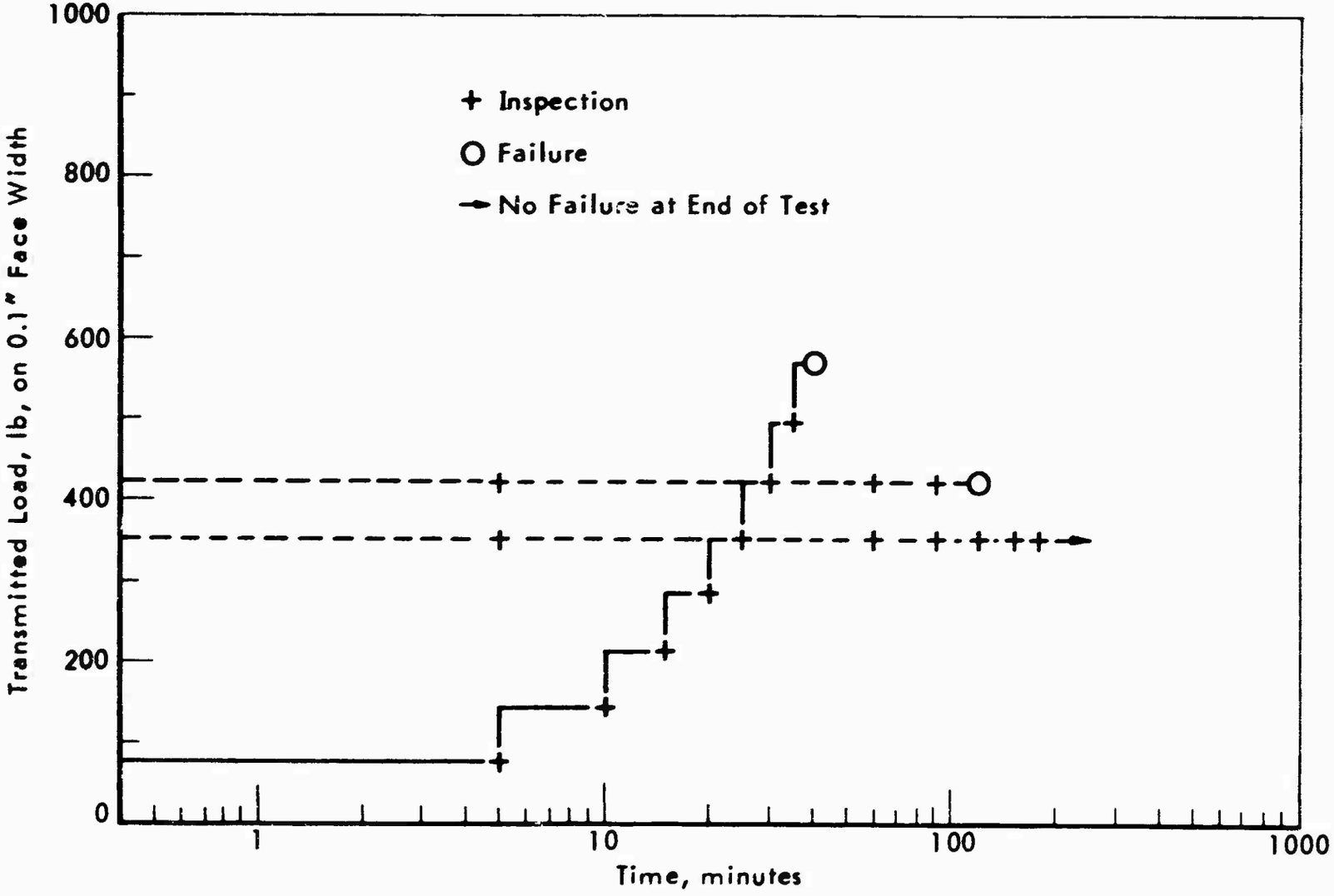

Figure 53. COMPARISON OF CONSTANT LOAD TEST SCHEDULE WITH LOAD CARRYING CAPACITY TEST SCHEDULE

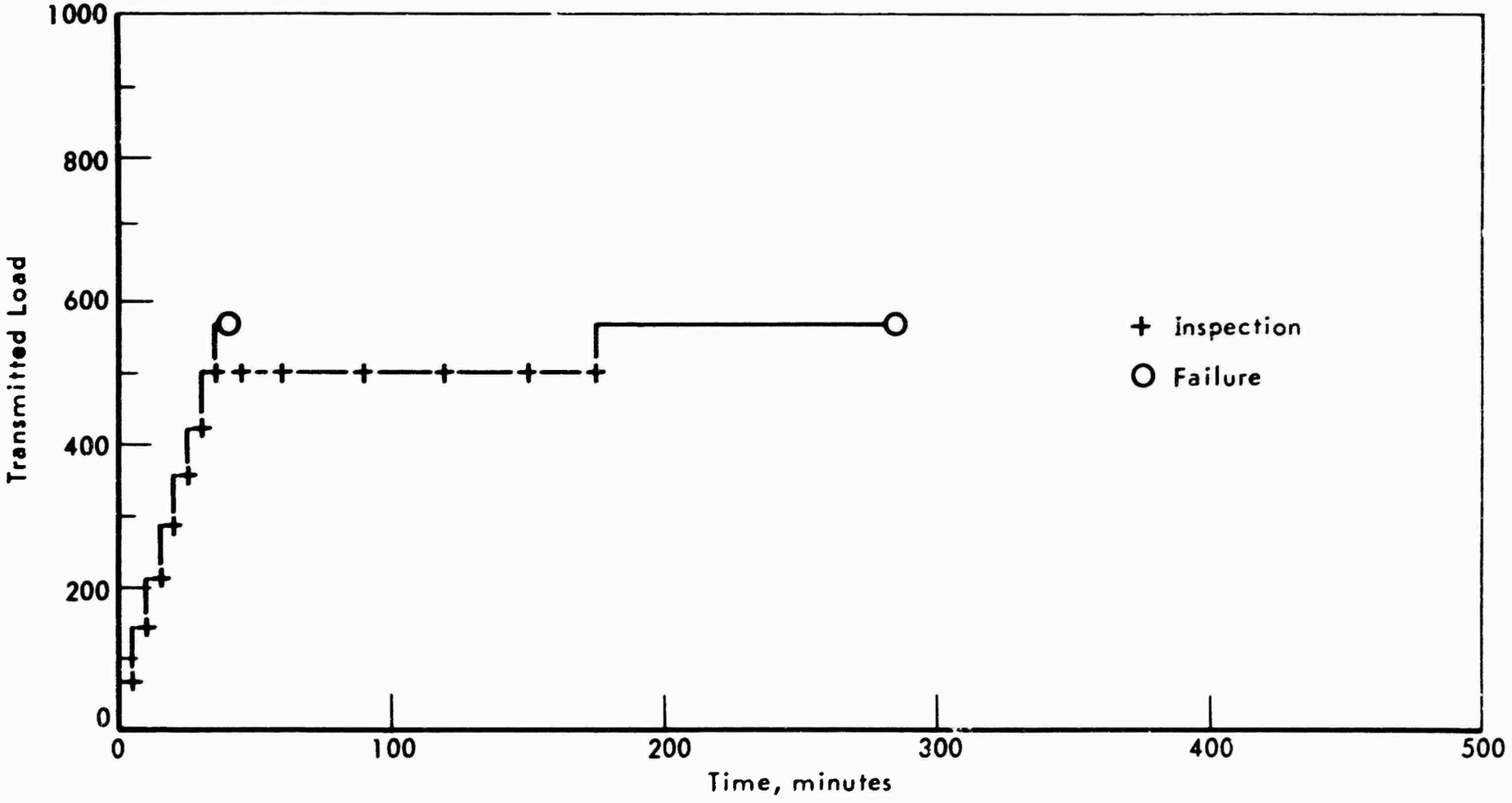

Figure 54. COMPARISON OF BREAK-IN TEST SCHEDULE WITH LOAD CARRYING CAPACITY TEST SCHEDULE

S-13926
59926

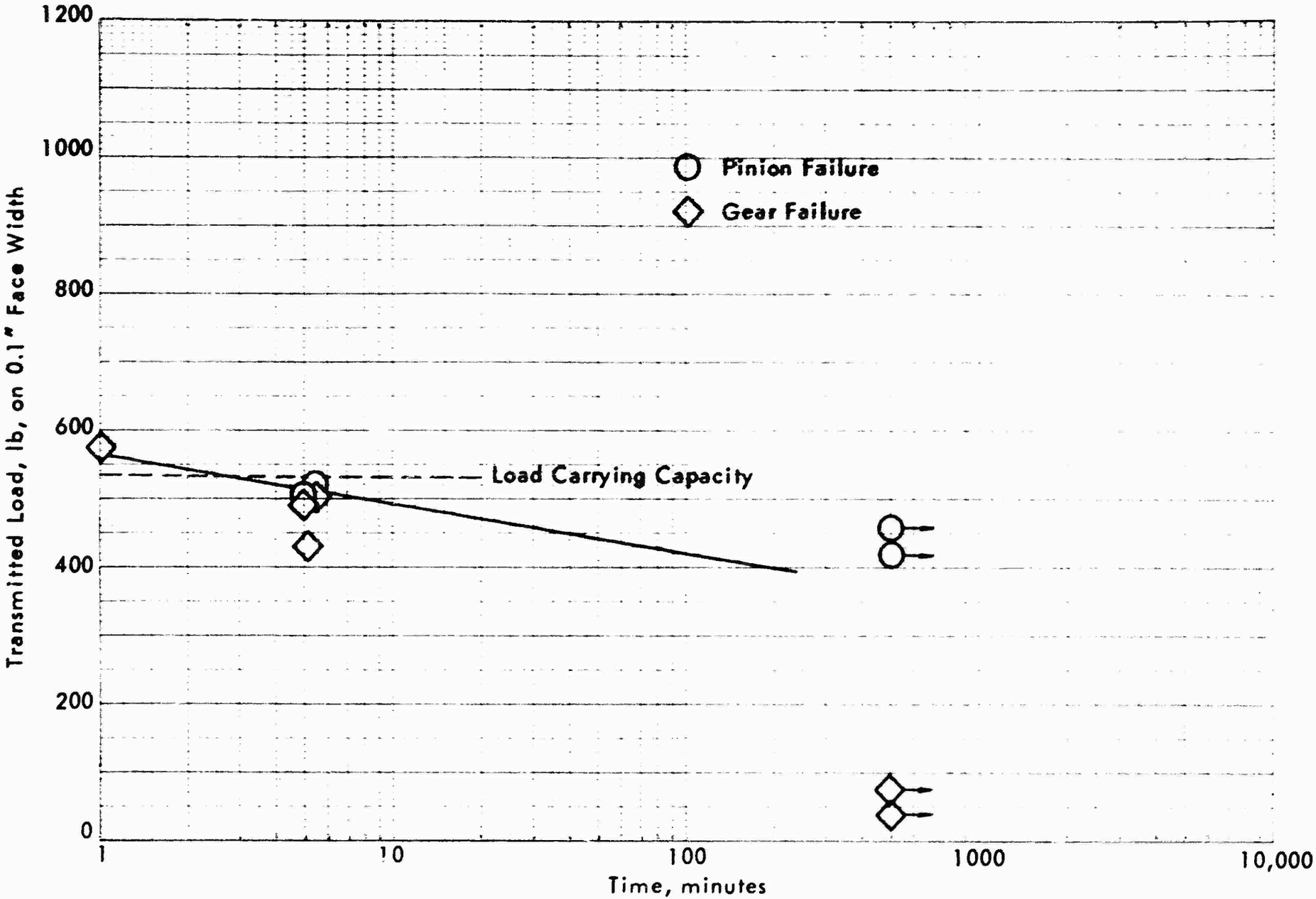

Figure 55. CONSTANT LOAD LIFE OF SPUR GEARS AT 3200 rpm LUBRICATED WITH MIL-L-7808C OIL

S-13926
59926

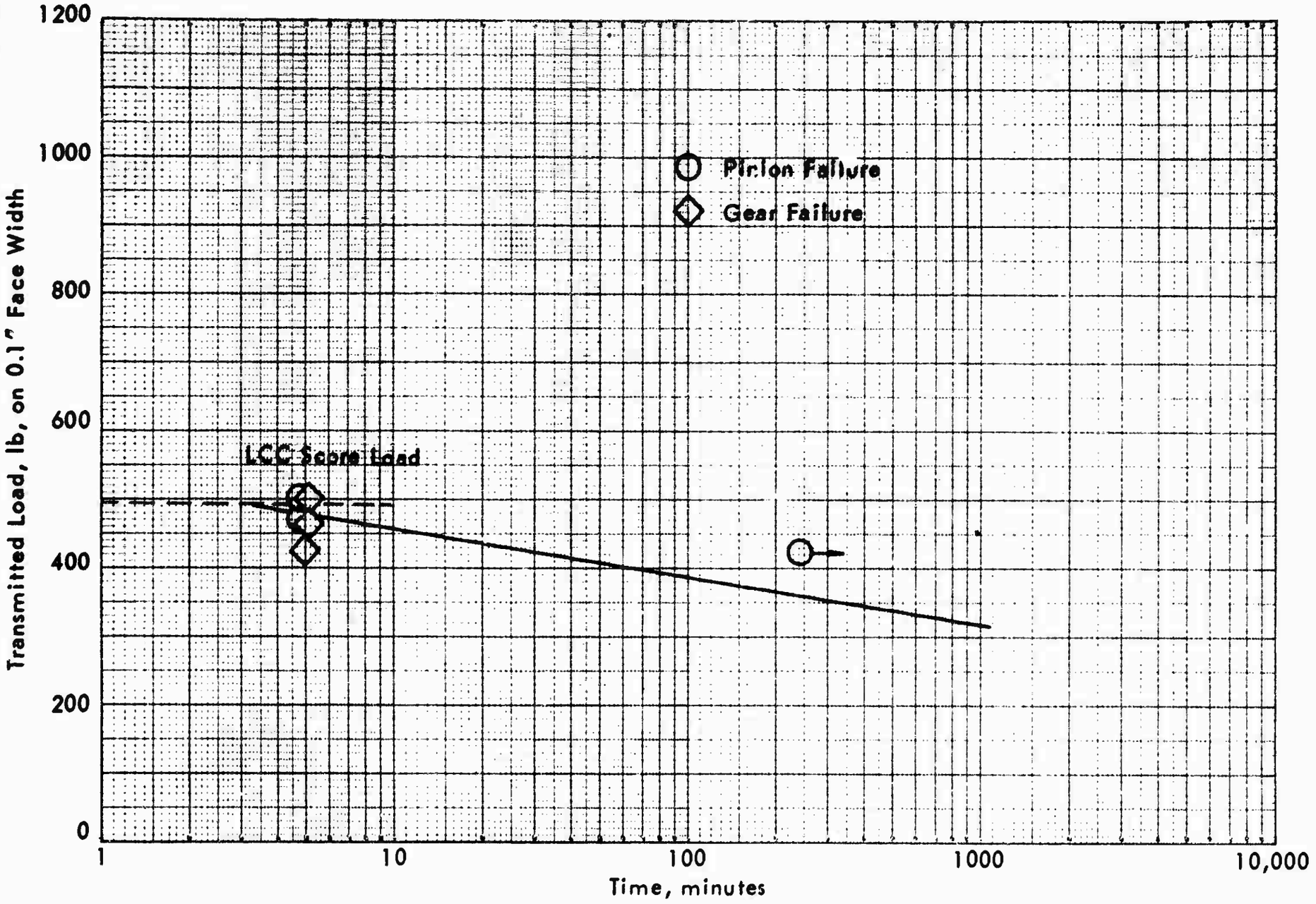

Figure 56. CONSTANT LOAD LIFE OF SPUR GEARS AT 1600 rpm LUBRICATED WITH MIL-L-7808D OIL

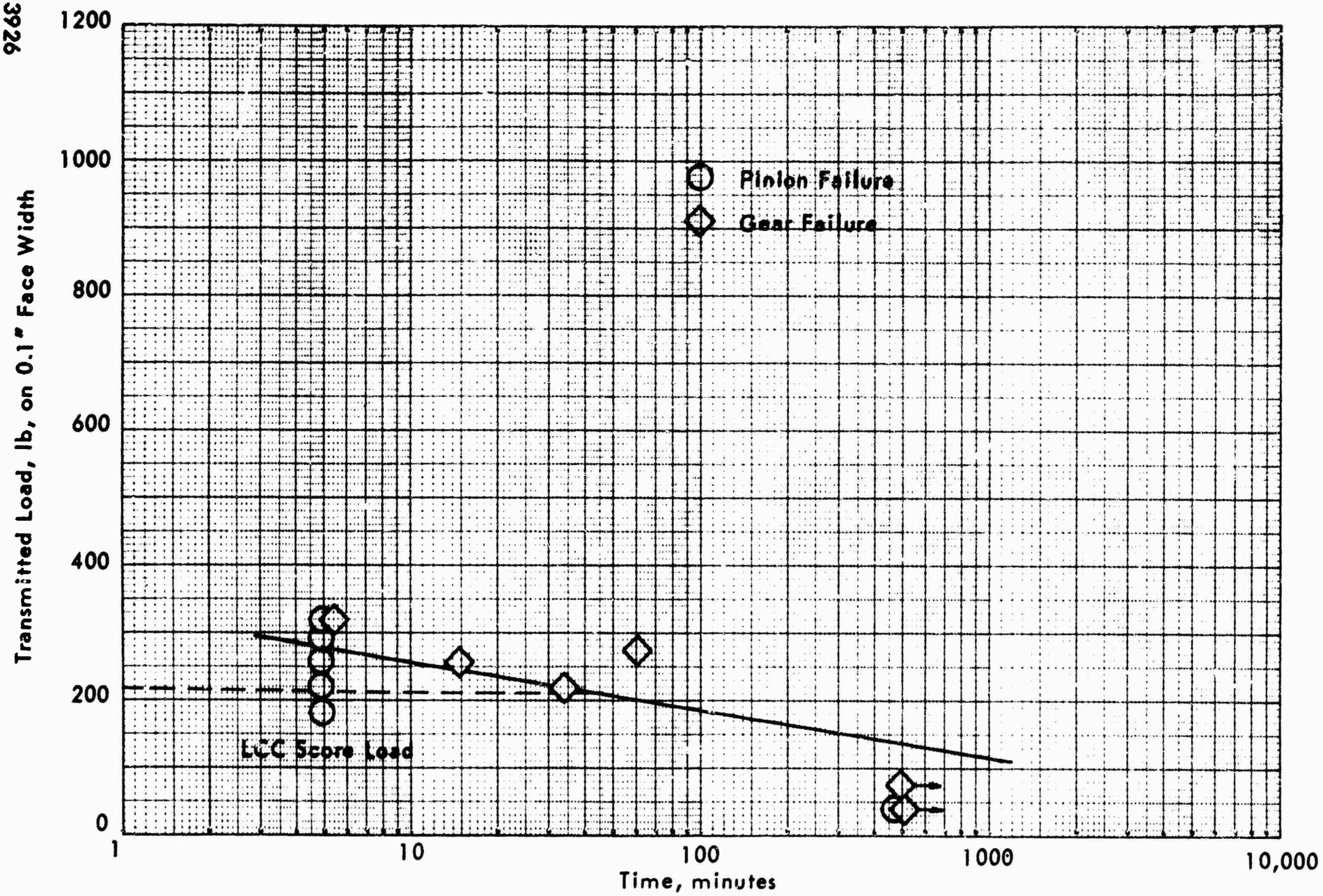

Figure 57. CONSTANT LOAD LIFE OF SPUR GEARS AT 6400 rpm LUBRICATED WITH MIL-L-7808D OIL

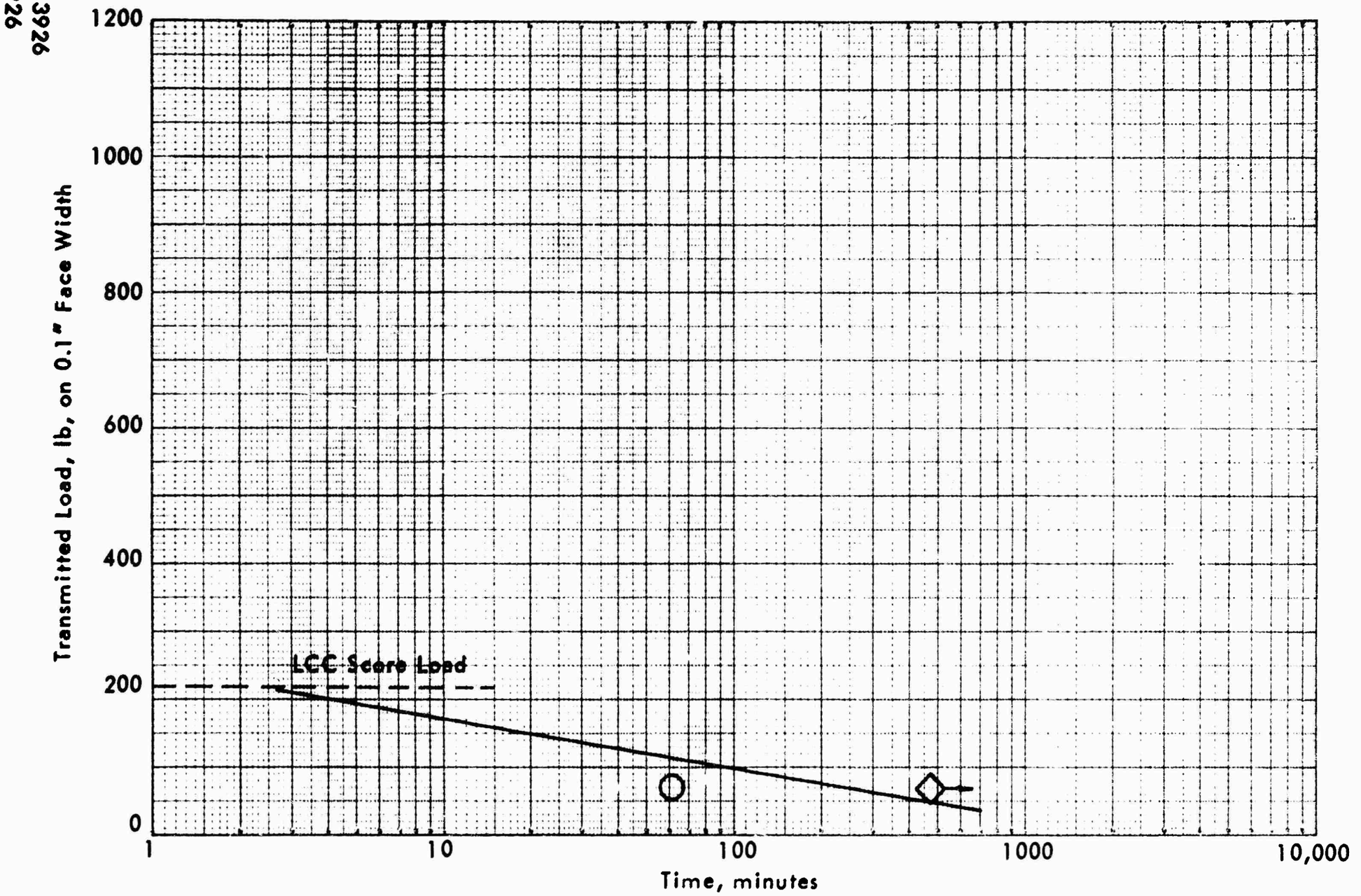

Figure 58. CONSTANT LOAD LIFE OF SPUR GEARS AT 12,800 rpm LUBRICATED WITH MIL-L-7808D OIL

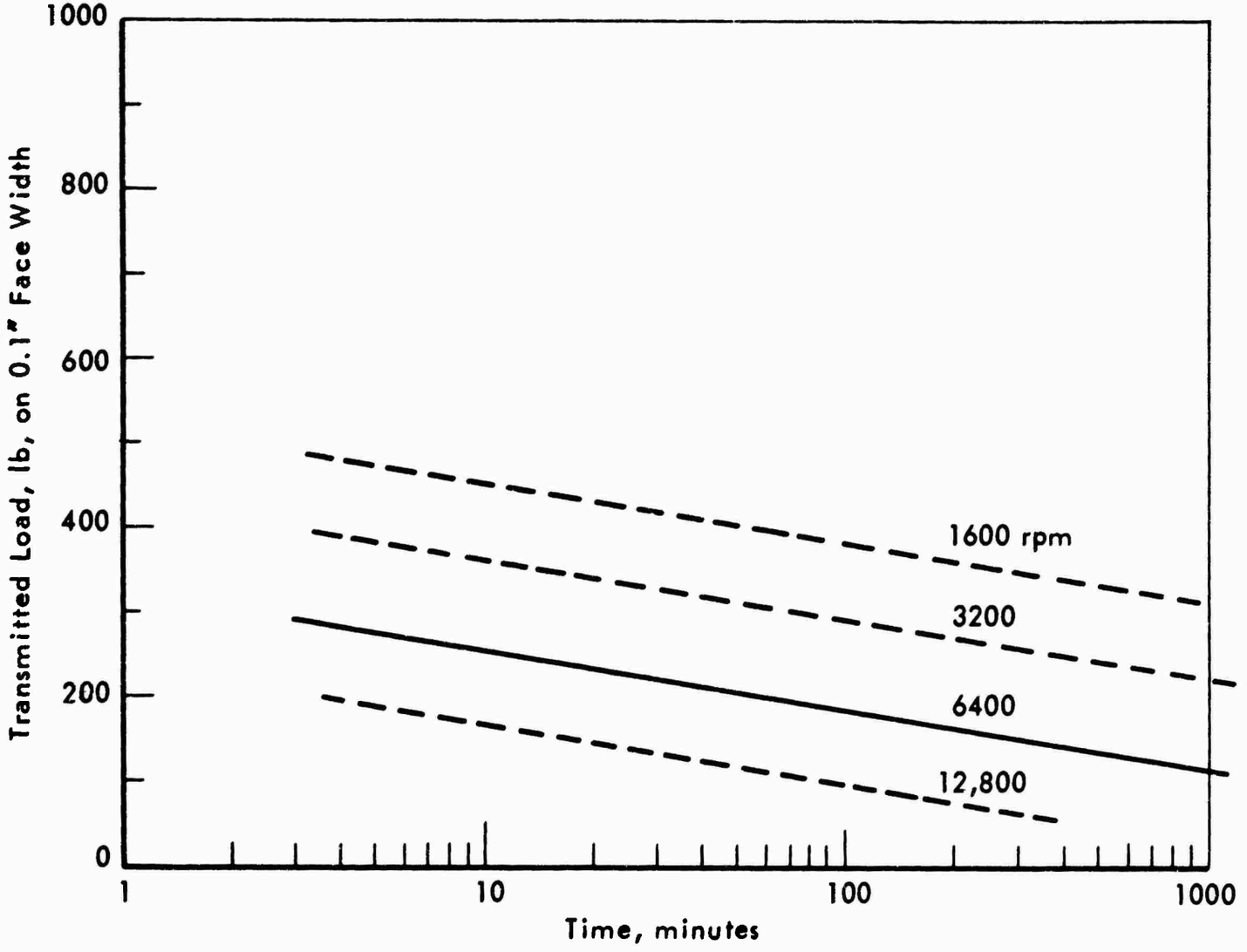

Figure 59. CONSTANT LOAD LIFE OF SPUR GEARS AT SEVERAL SPEEDS, LUBRICATED WITH MIL-L-7808D OIL

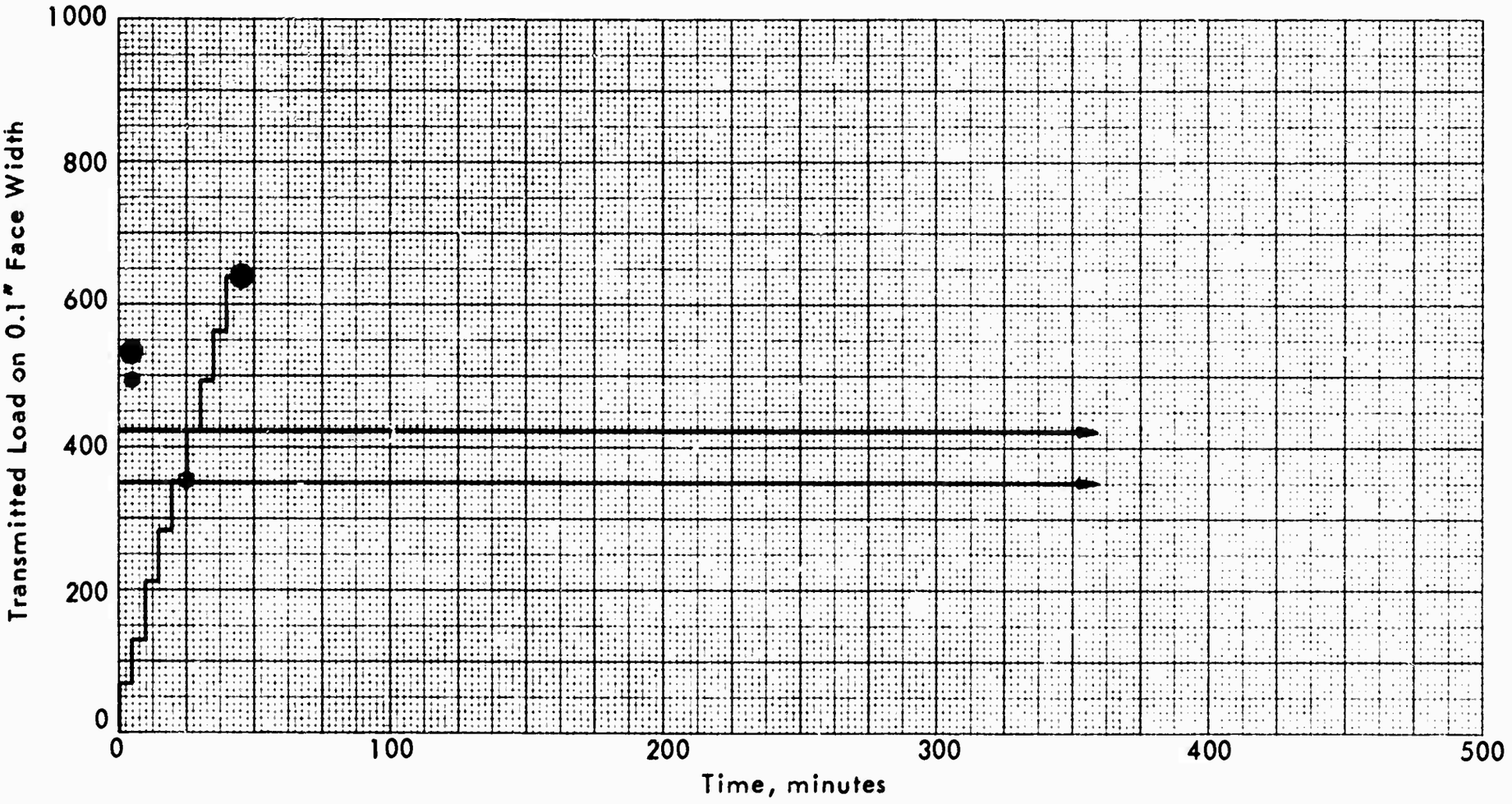

Figure 60. COMPARISON OF CONSTANT LOAD TESTS WITH LOAD CARRYING CAPACITY TESTS FOR MIL-L-7808E OIL AT 1600 rpm

S-13926
59926

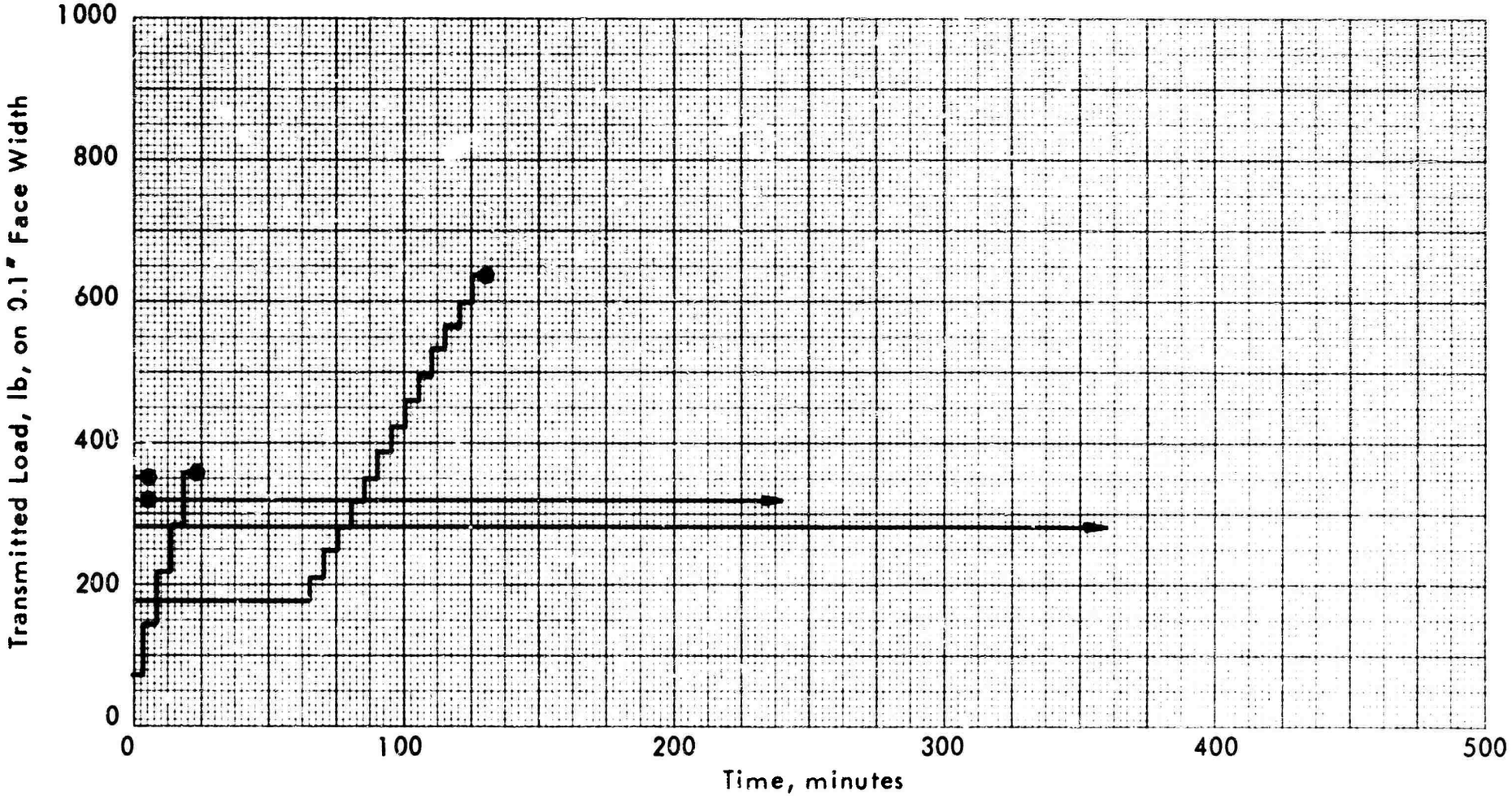

Figure 61. COMPARISON OF CONSTANT LOAD TESTS AND A BREAK-IN TEST WITH LOAD CARRYING CAPACITY TEST FOR MIL-L-7808E OIL AT 3200 rpm

S-13926
59926

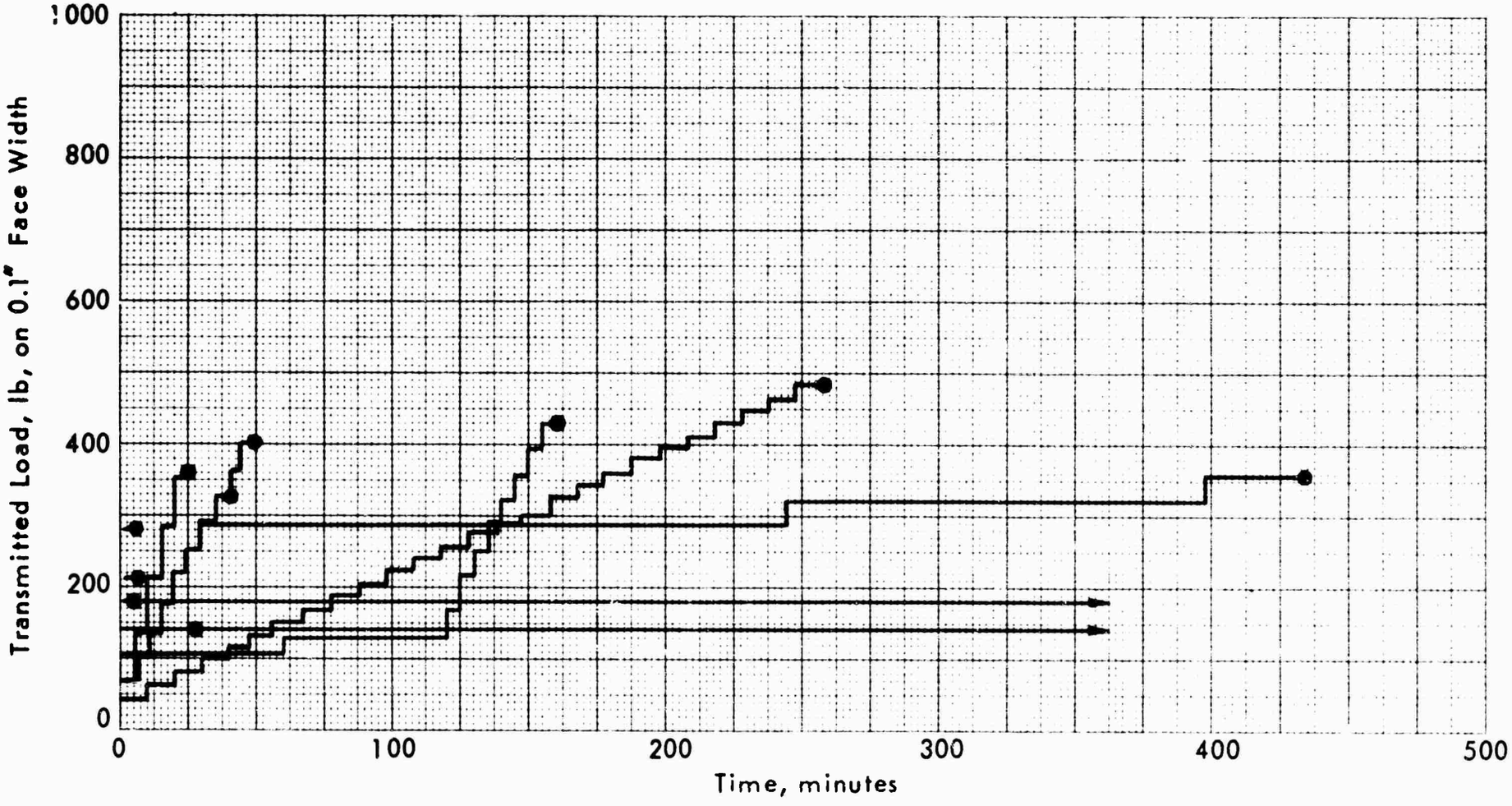

Figure 62. CONSTANT LOAD, BREAK-IN AND LOAD CARRYING CAPACITY TESTS FOR MIL-L-7808E OIL AT 6400 rpm

S-13926
59926

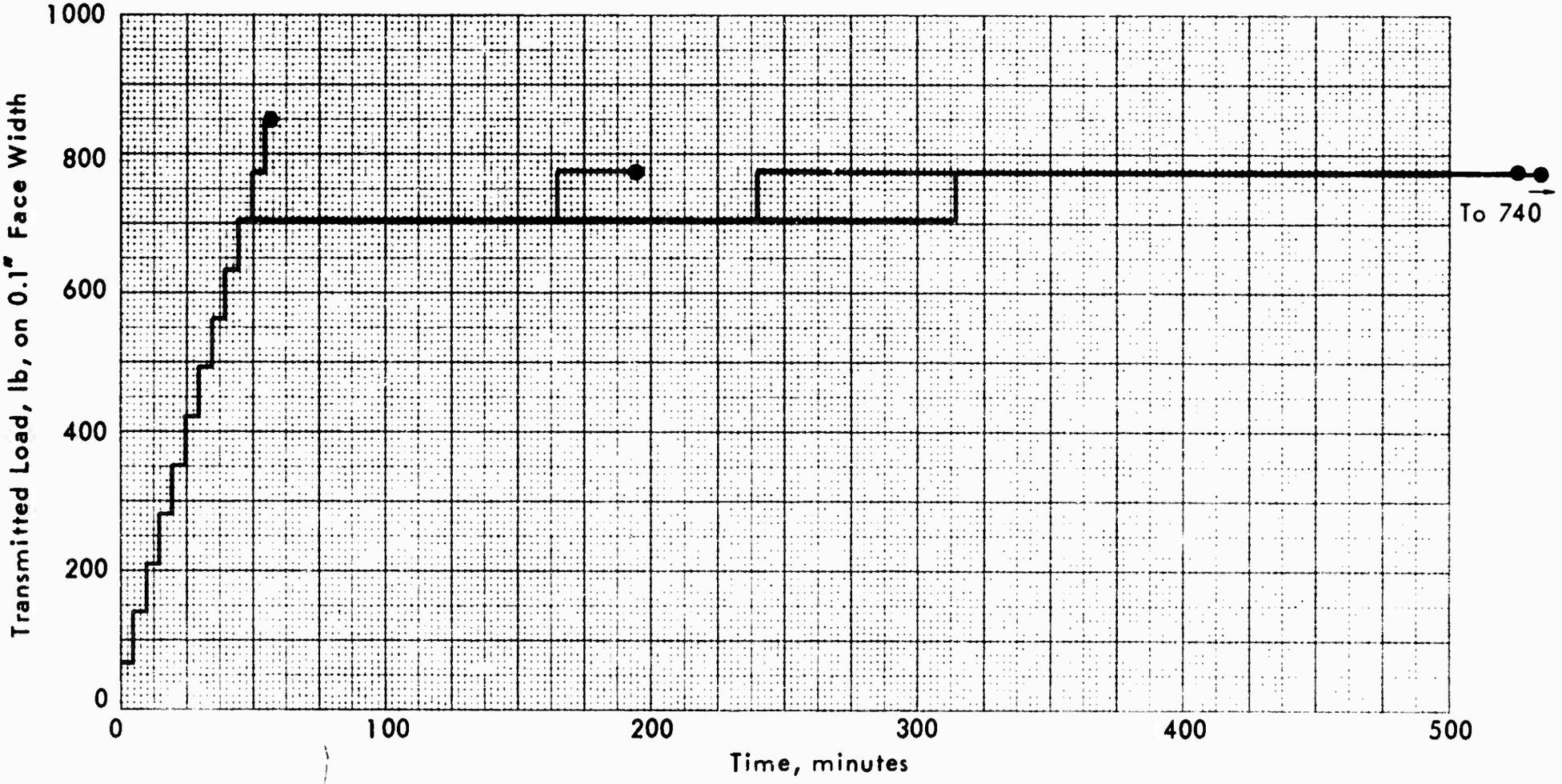

Figure 63. LOAD CARRYING CAPACITY AND BREAK-IN TESTS FOR MIL-L-21260 (GRADE 2) OIL AT 1000 rpm

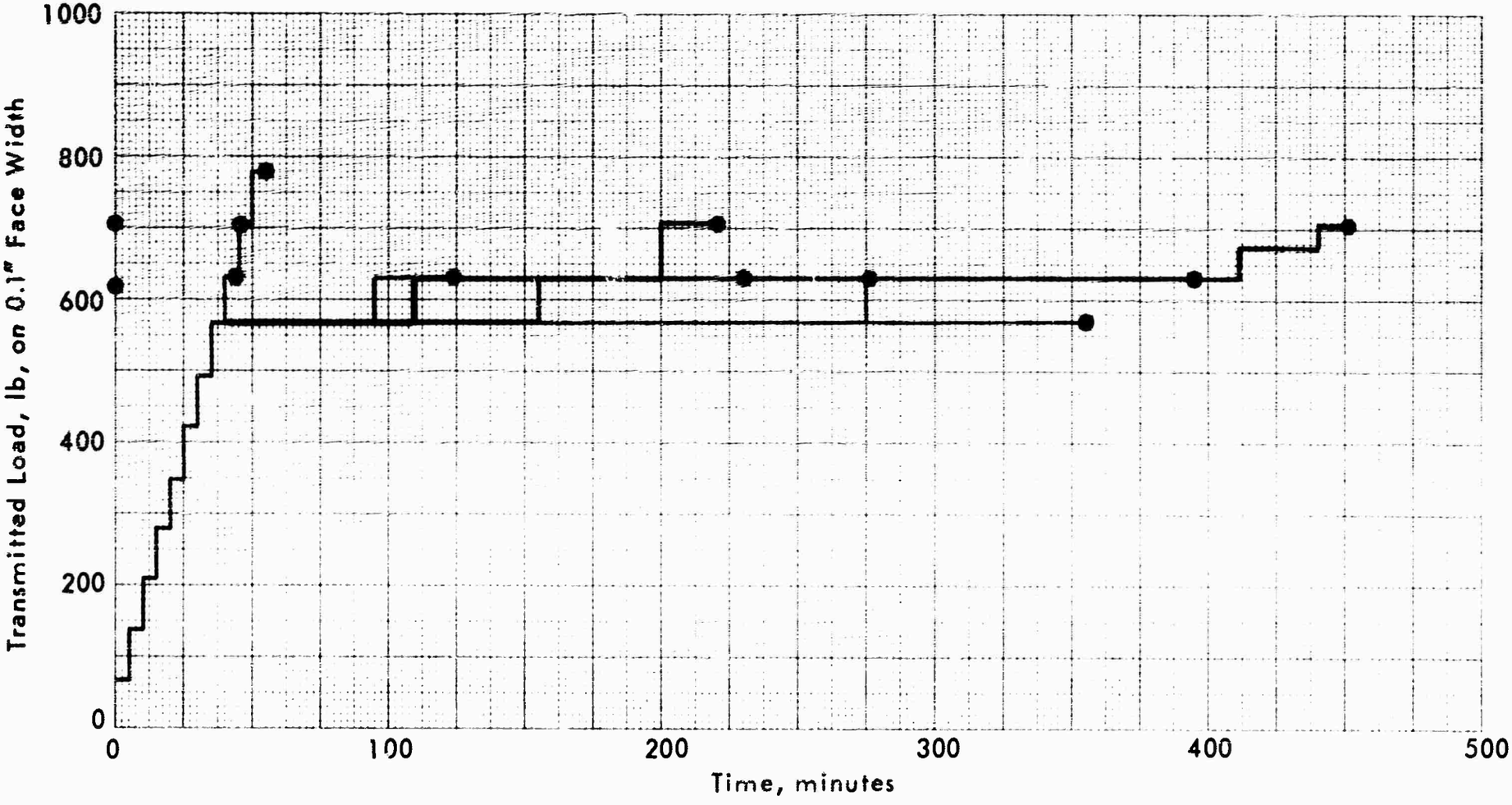

Figure 64. BREAK-IN AND LOAD CARRYING CAPACITY TESTS FOR MIL-L-21260 (GRADE 2) OIL AT 1600 rpm

S-13926
59926

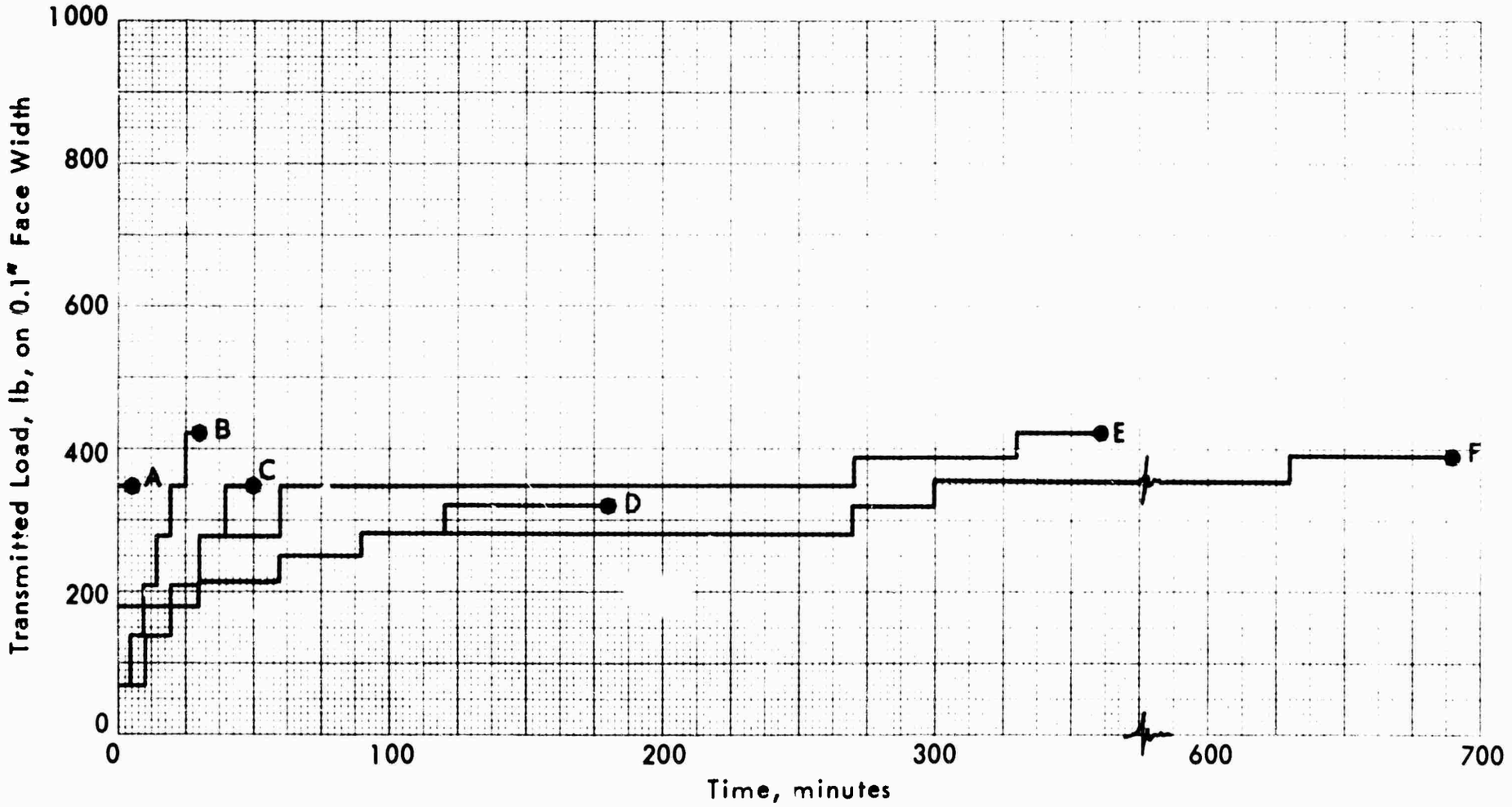

Figure 65. BREAK-IN AND LOAD CARRYING CAPACITY TESTS FOR MIL-L-21260 (GRADE 2) OIL AT 3200 rpm

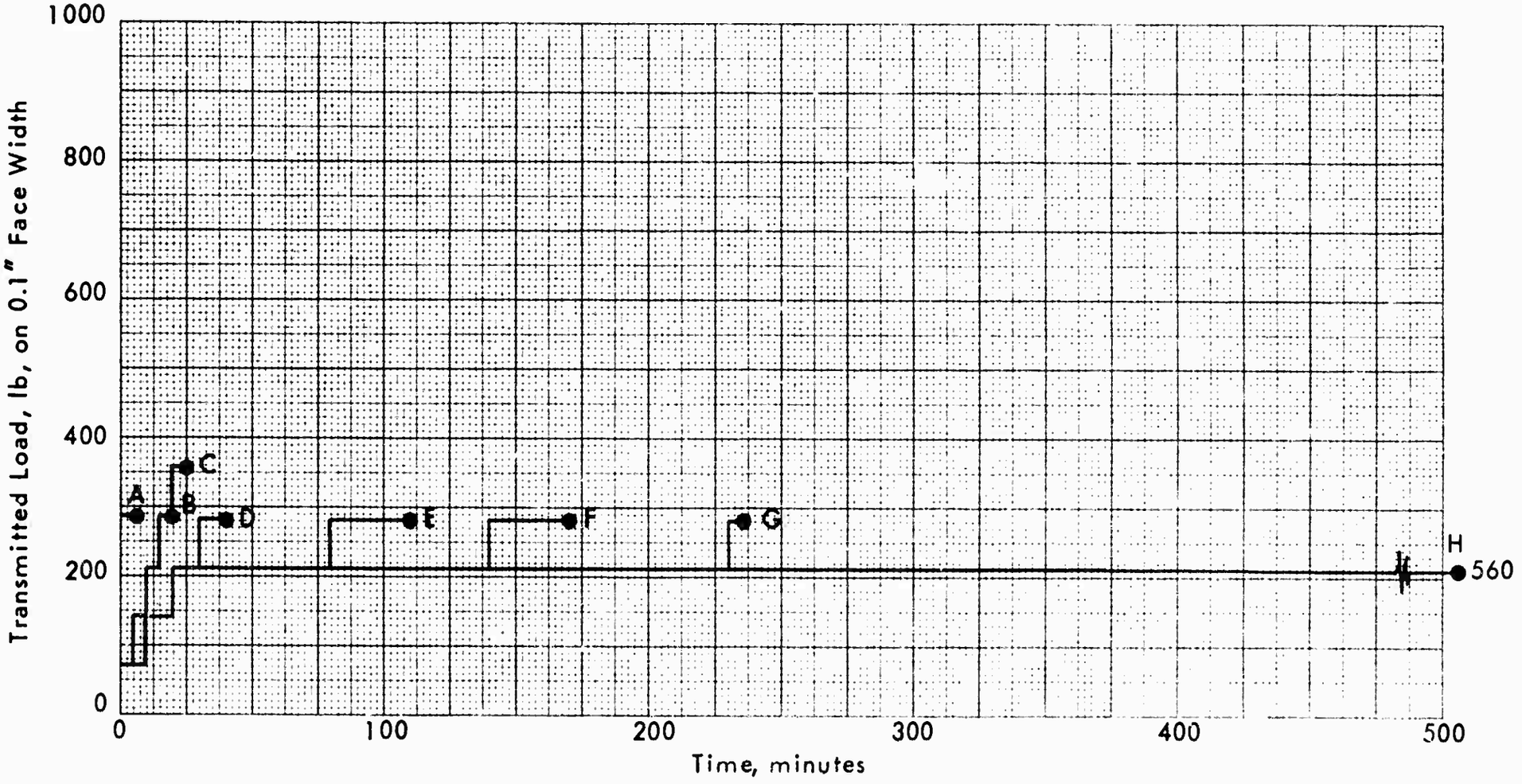

Figure 66. BREAK-IN AND LOAD CARRYING CAPACITY TESTS FOR MIL-L-21260 (GRADE 2) OIL AT 6400 rpm

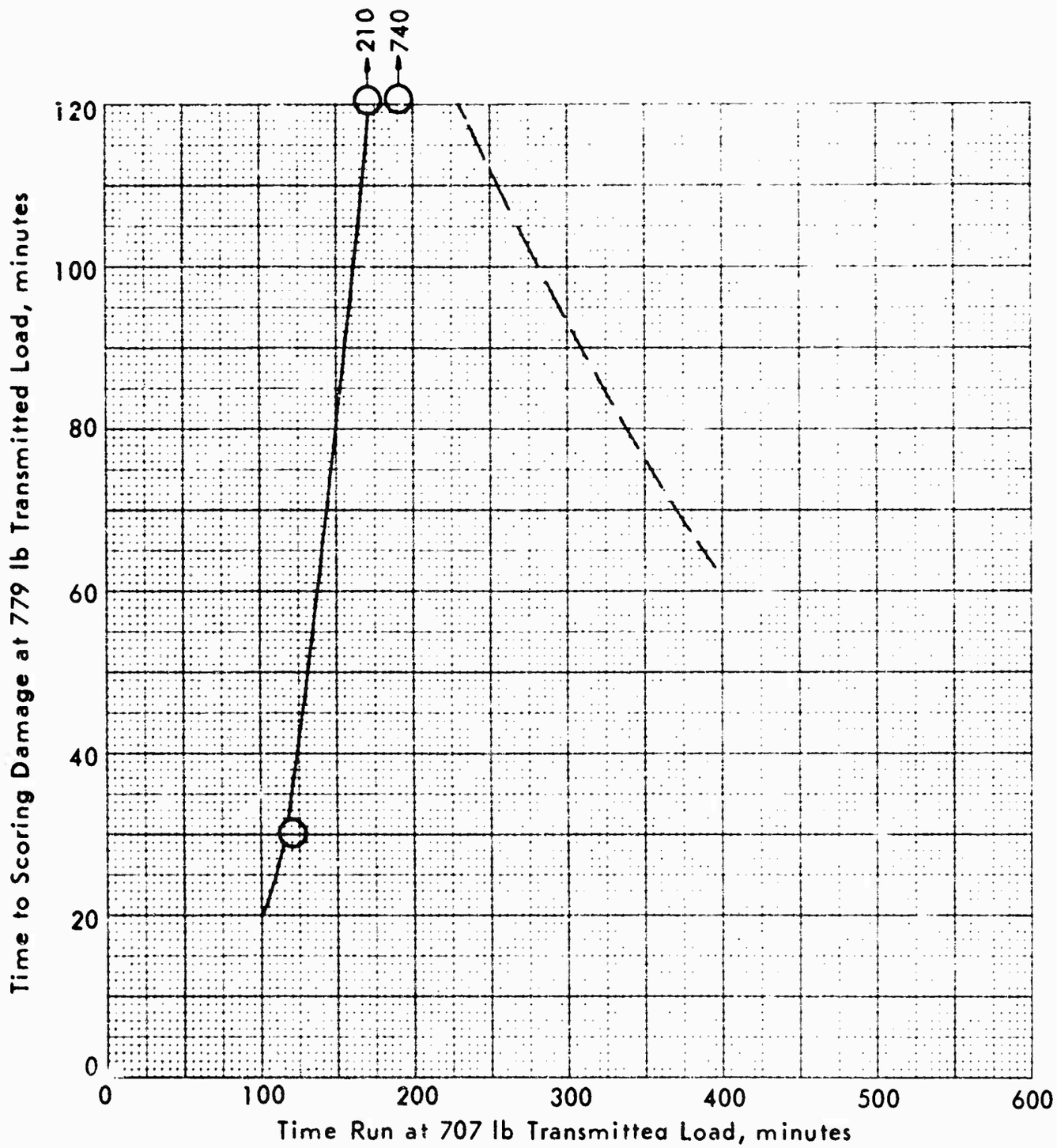

Figure 67. SPUR GEAR BREAK-IN DATA FOR MIL-L-21260 (GRADE 2) OIL AT 1000 rpm

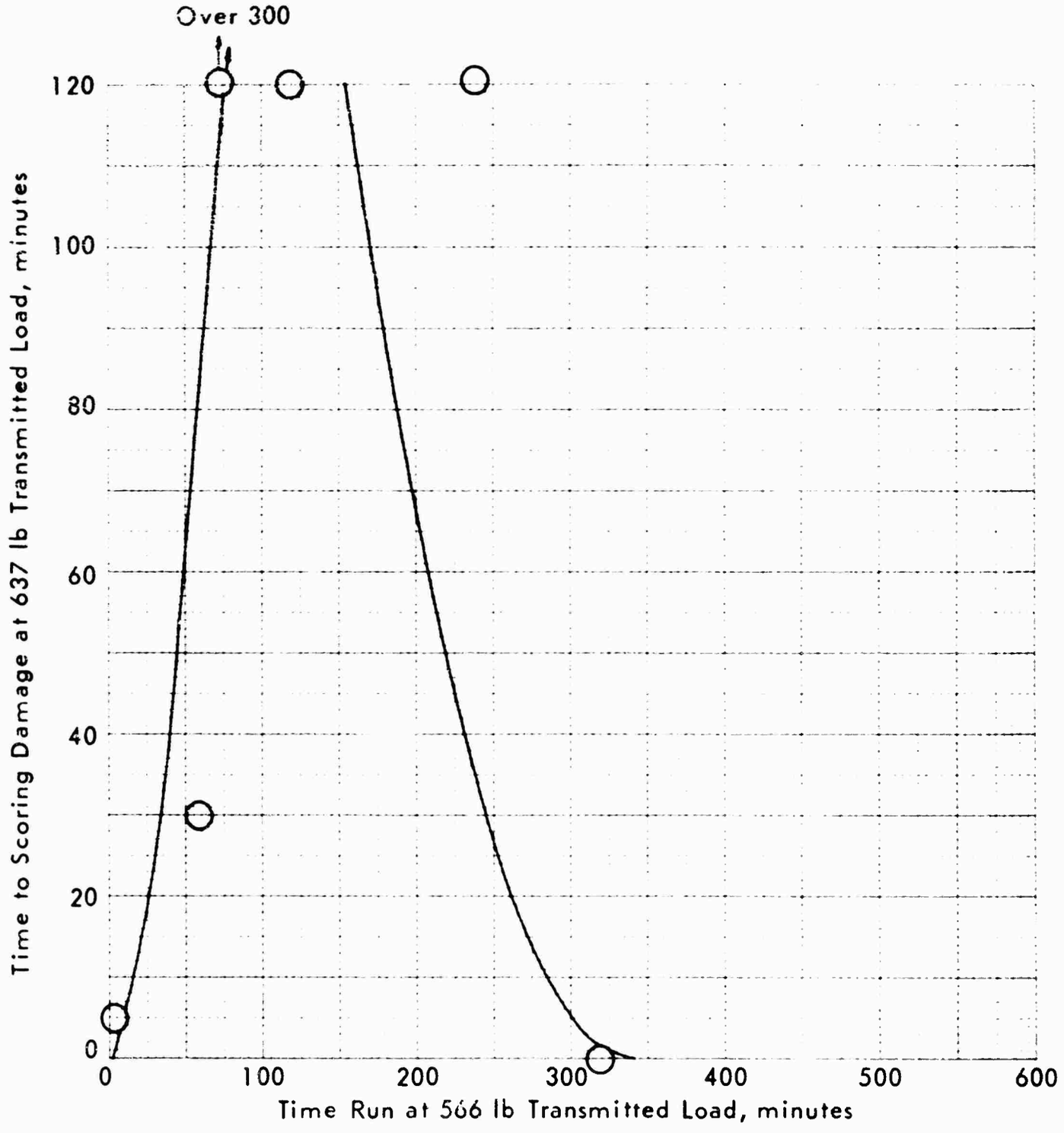

Figure 68. SPUR GEAR BREAK-IN DATA FOR MIL-L-21260 (GRADE 2) OIL AT 1600 rpm

S-13926
59926

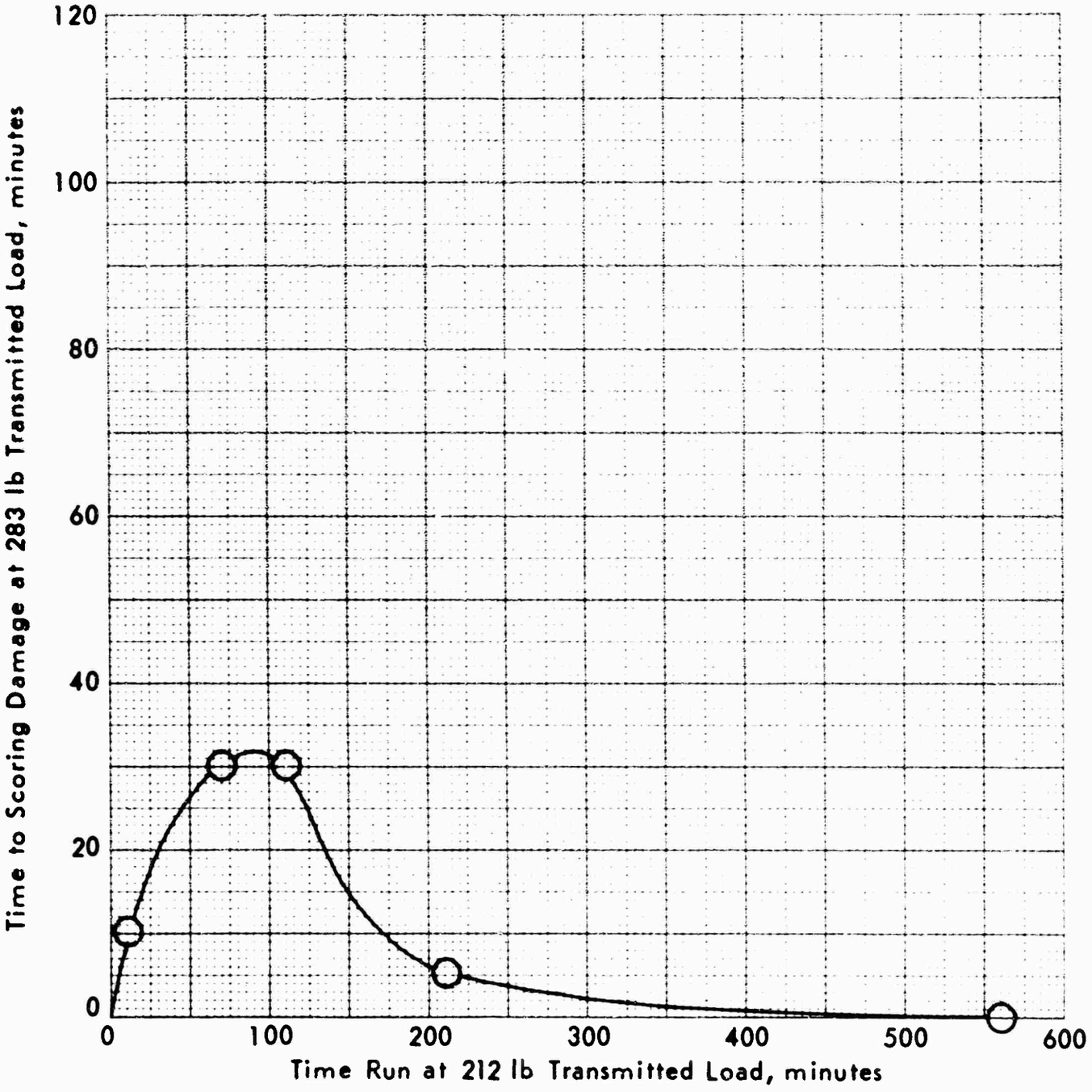

Figure 69. SPUR GEAR BREAK-IN DATA FOR MIL-L-21260 (GRADE 2) OIL AT 6400 rpm

S-13926
59926

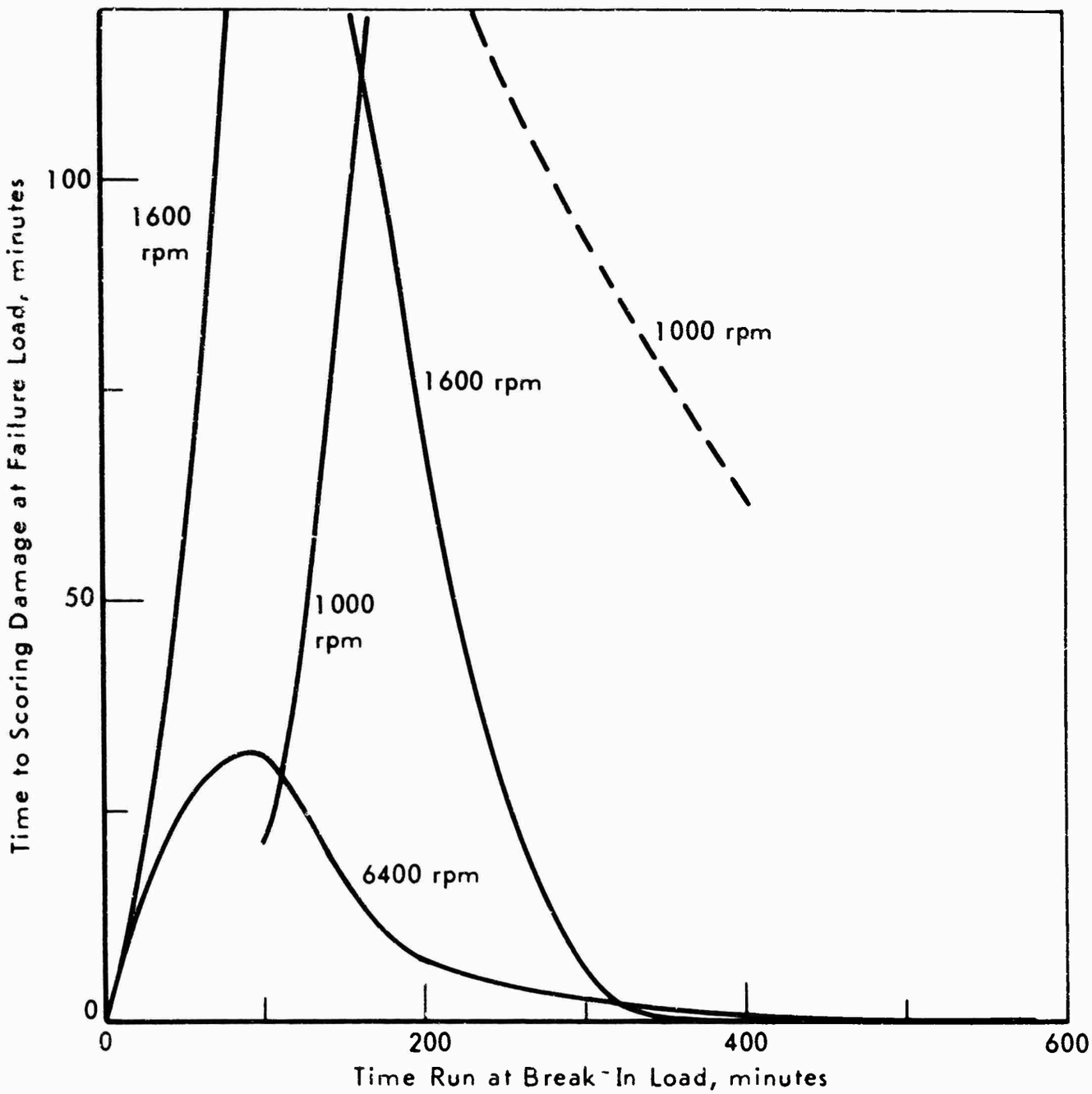

Figure 70. COMPARISON OF BREAK-IN DATA FOR MIL-L-21260 (GRADE 2) OIL AT THREE SPEEDS

S-13926
59926

S-13926
59926

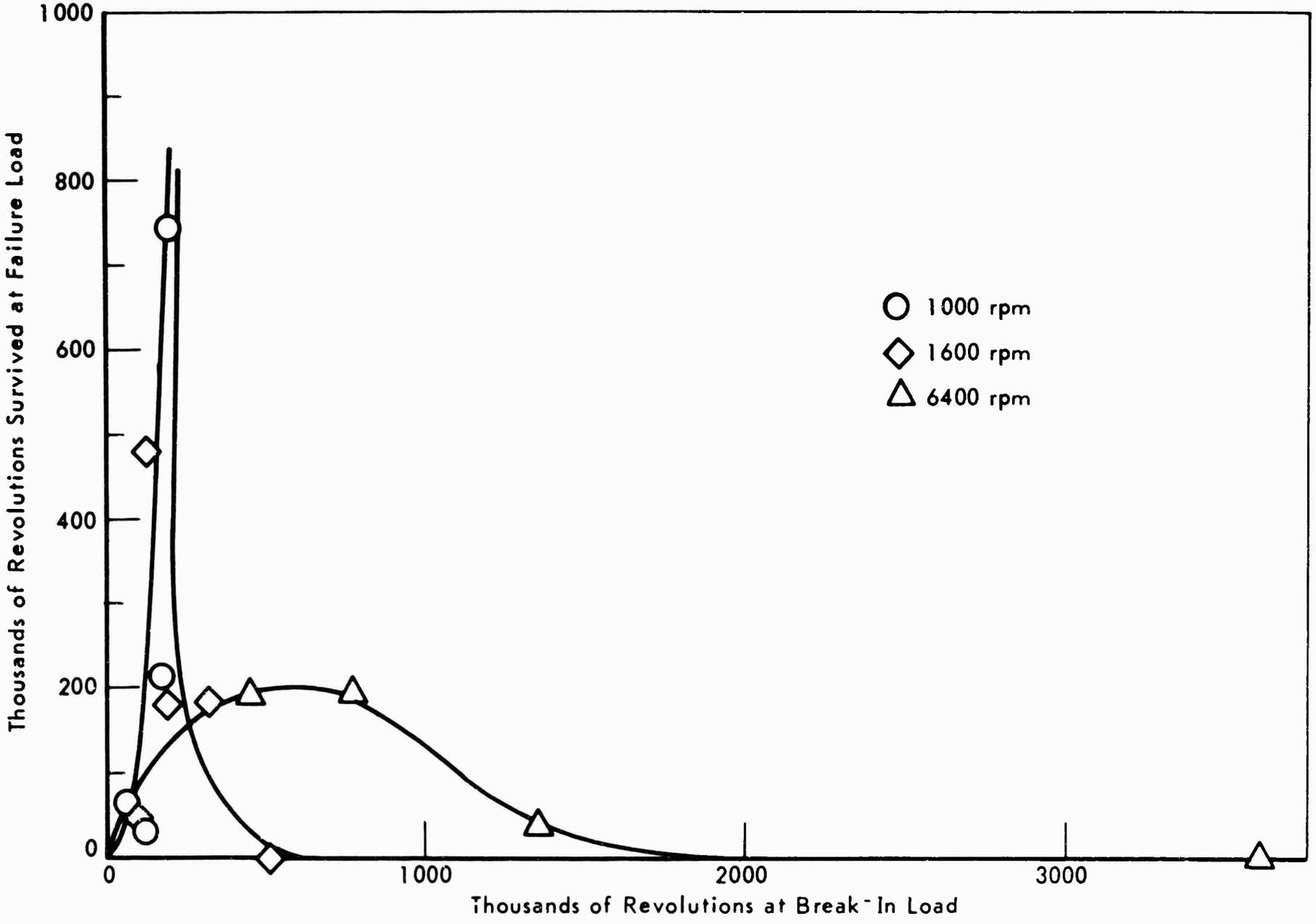

Figure 71. COMPARISON OF BREAK-IN DATA FOR MIL-L-21260 (GRADE 2) OIL AT THREE SPEEDS BASED ON NUMBER OF REVOLUTIONS

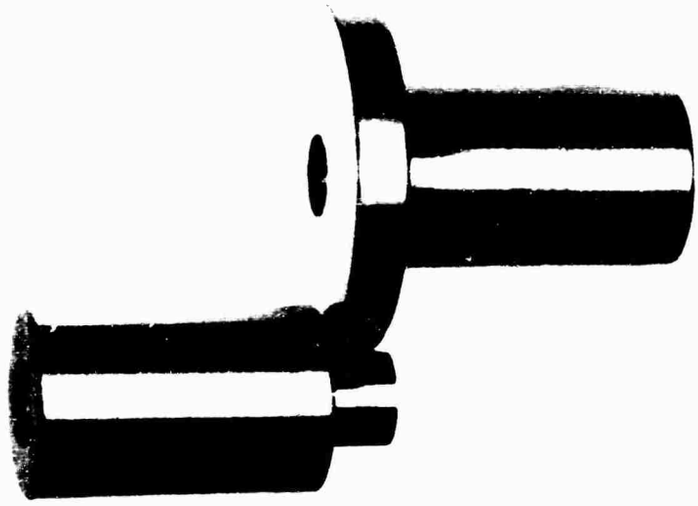

Figure 72. ROTARY CONTACT SIMULATOR SPECIMENS SHOWN FULL SIZE AND IN TEST POSITION

S-13926
59234-J

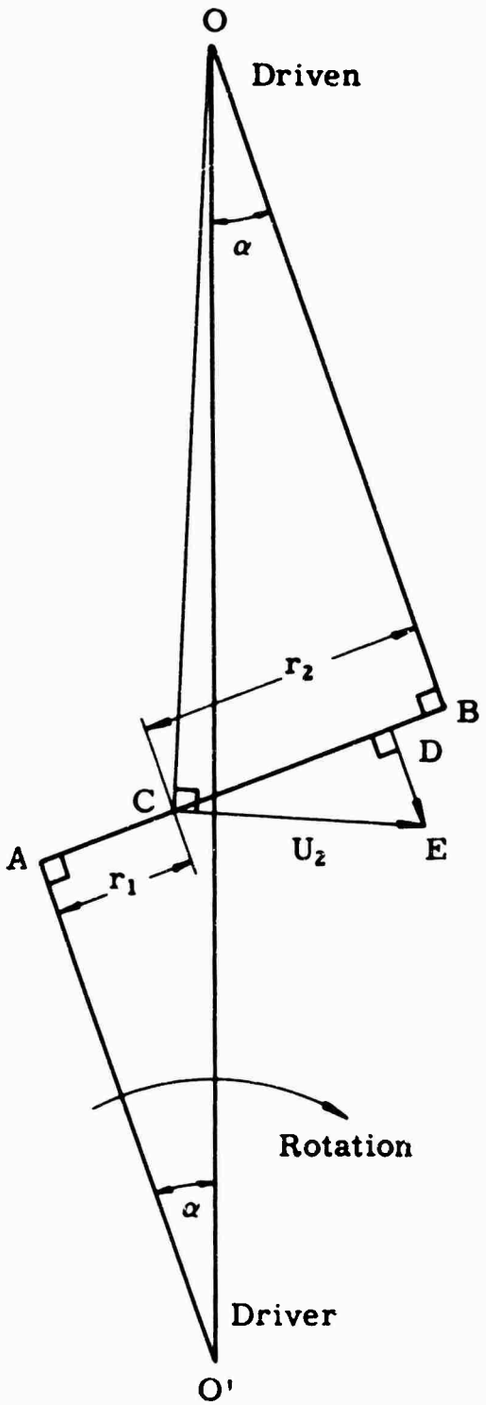

Figure 73. GEAR GEOMETRY DIAGRAM

Figure 74. GAGES FOR DETERMINING RADII OF CURVATURE OF GEAR AND PINION TEETH

S-13926
59059

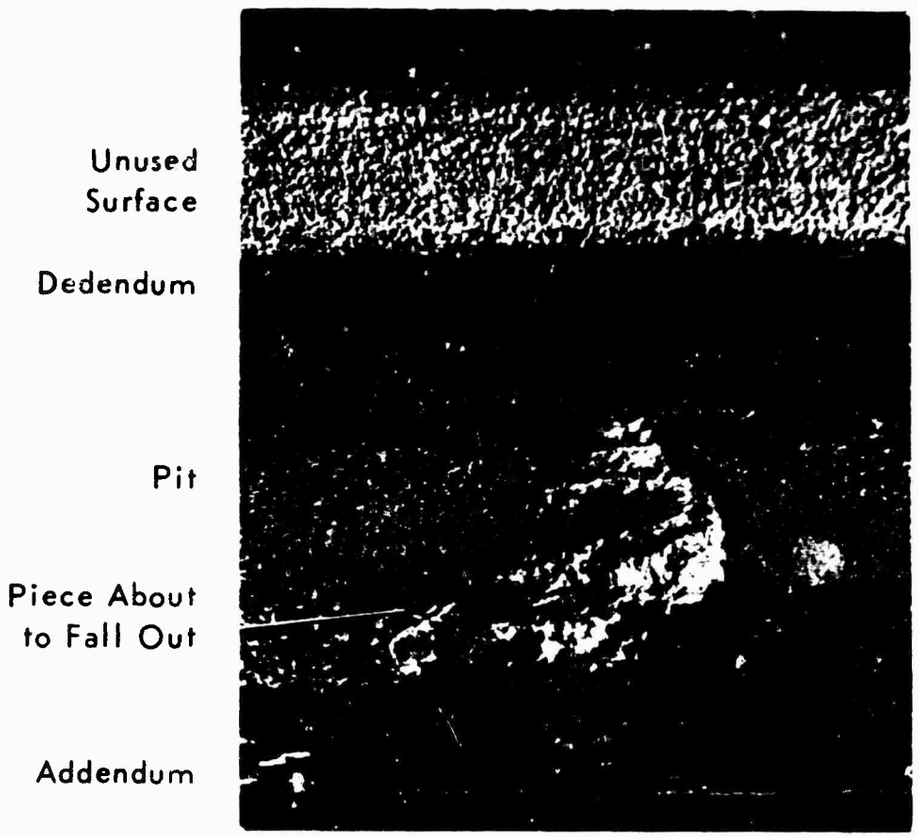

Figure 75. PITTED HELICOPTER GEAR TOOTH

S-13926
58970-A

Figure 76. PITTED PINION ADDENDUM
8X Magnification

S-13926
59068-1441-1

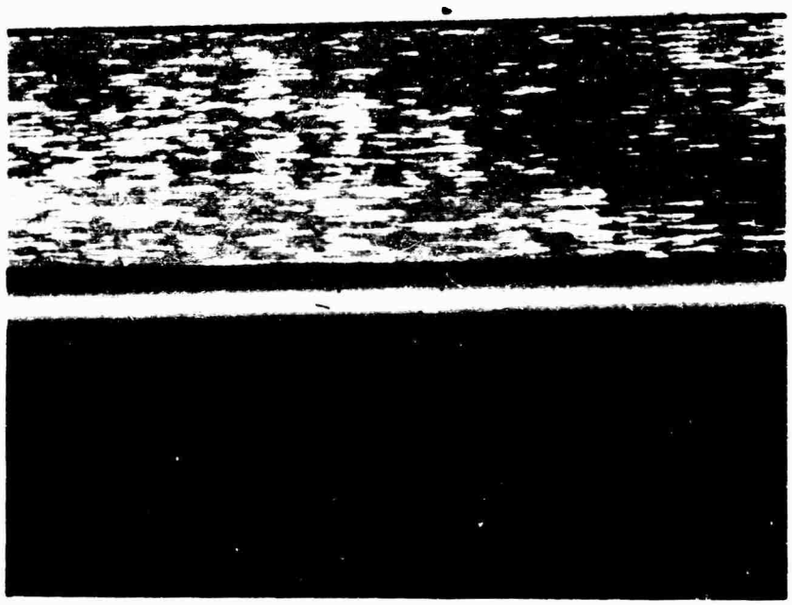

Figure 77. ROTARY CONTACT SIMULATOR TEST SPECIMEN SIMULATING PINION ADDENDUM
(Surface Unrolled by Special Photographic Technique)

S-13926
59234

Figure 78. WORN SURFACE OF ROTARY CONTACT SIMULATOR SPECIMEN SIMULATING GEAR DEDENDUM

S-13926
59234-H

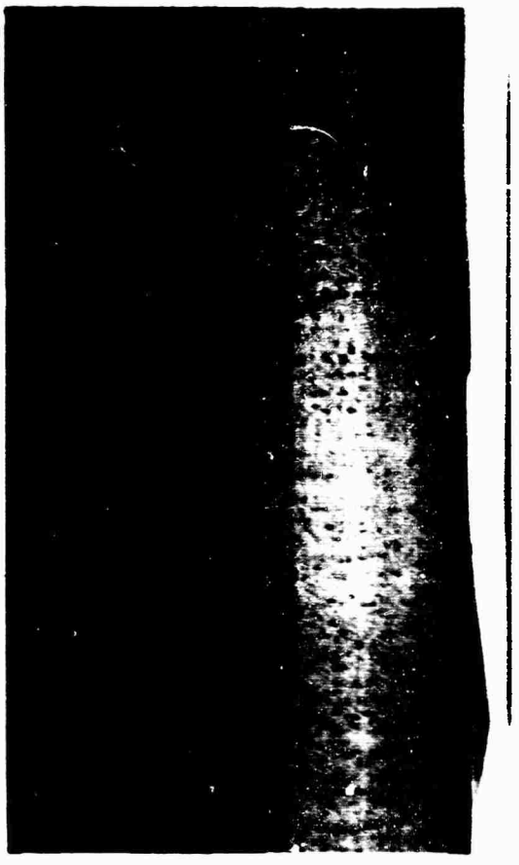

Figure 79. WORN SURFACE OF ROTARY CONTACT SIMULATOR SPECIMEN SIMULATING GEAR DEDENDUM
(Surface Unrolled by Special Photographic Technique)

S-13926
59234-E

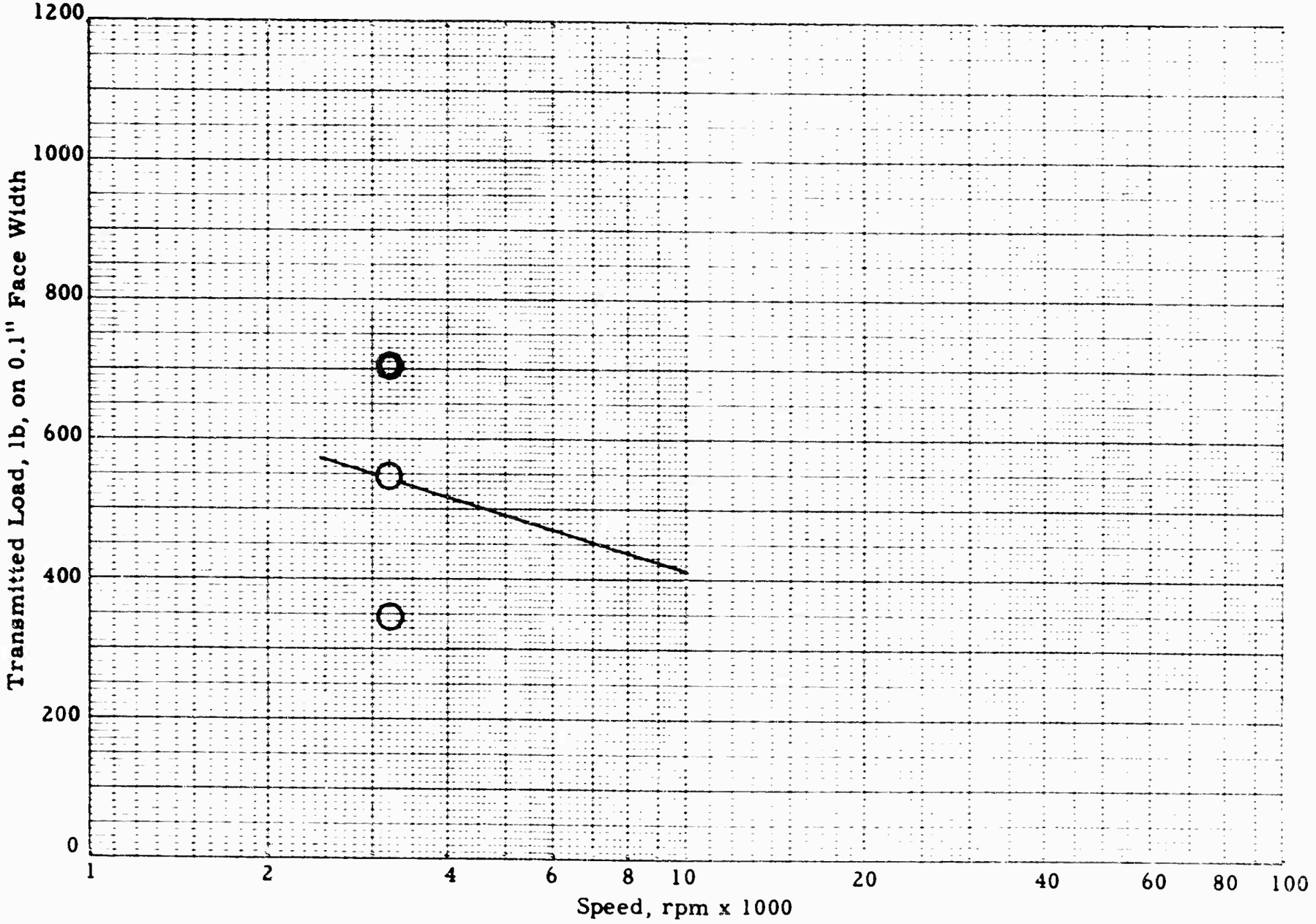

Figure 80. ROTARY CONTACT SIMULATOR SCORE LOAD DATA AT 3200 rpm COMPARED WITH SPUR GEAR SCORE LOAD CURVE FOR MIL-L-7808C OIL AT 3200 rpm

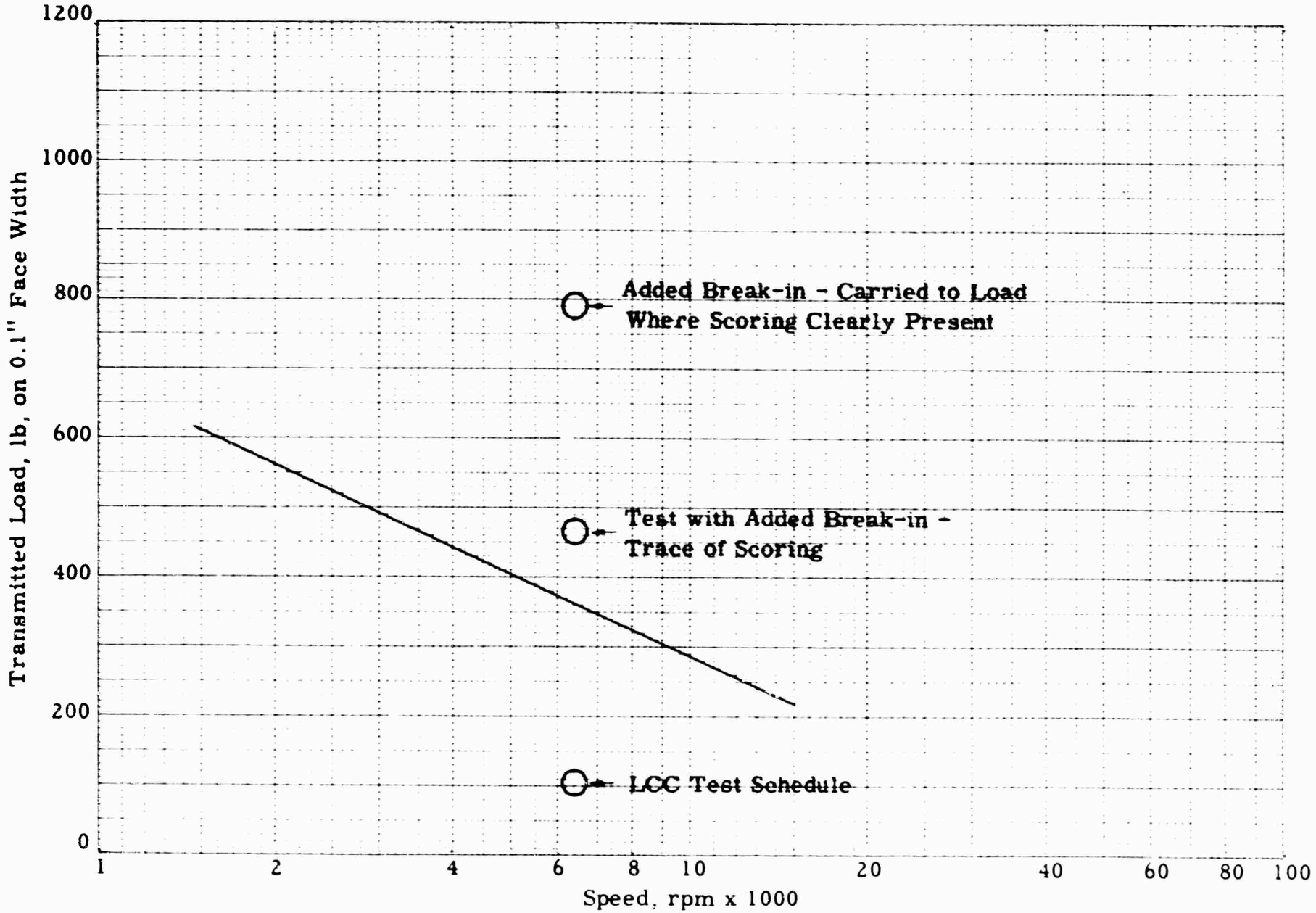

Figure 81. ROTARY CONTACT SIMULATOR SCORE LOAD DATA AT 6400 rpm COMPARED WITH SPUR GEAR SCORE LOAD CURVE FOR MIL-L-7808E OIL

S-13926
59926

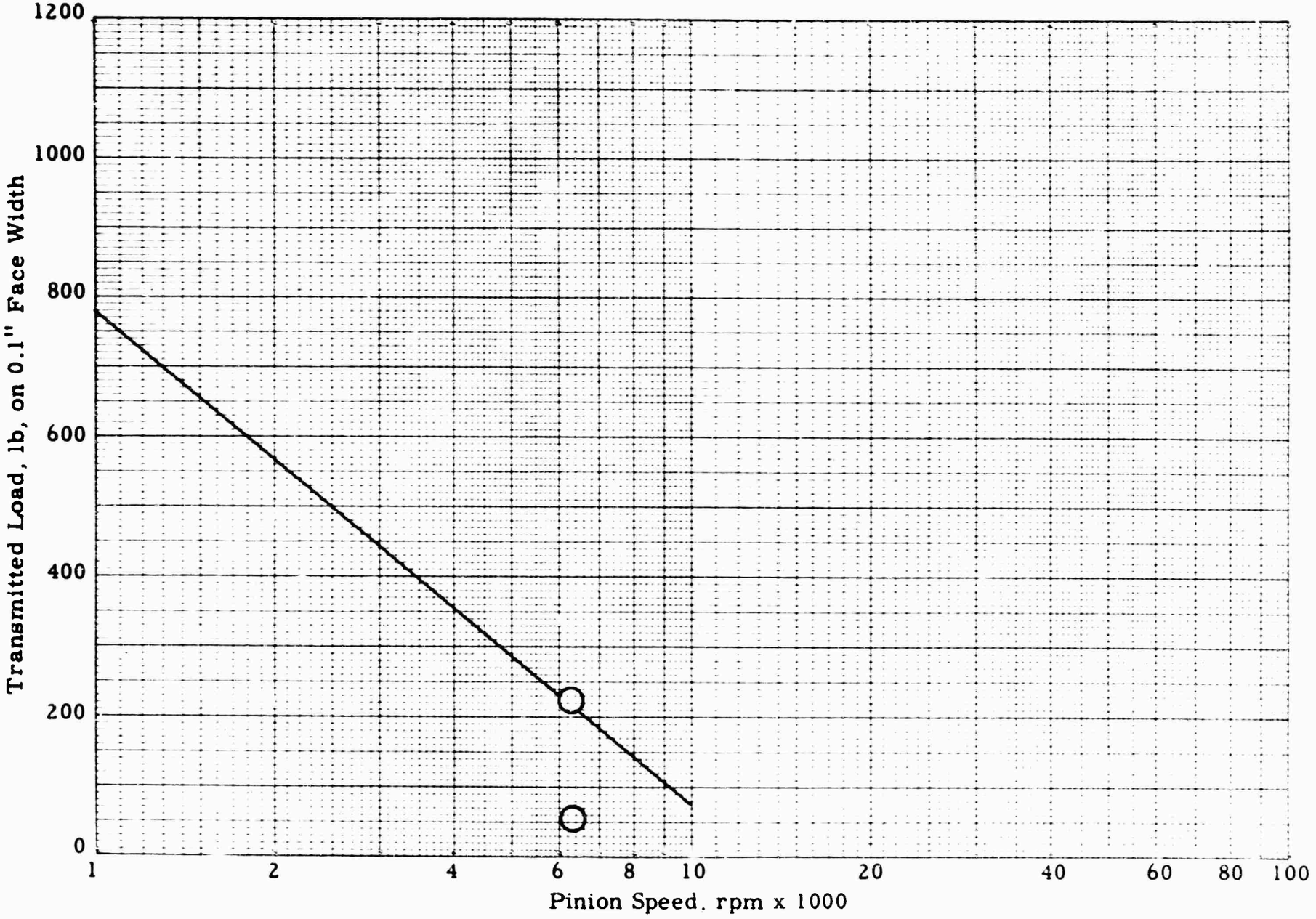

Figure 82. ROTORY CONTACT SIMULATOR SCORE LOAD DATA AT 6400 rpm COMPARED WITH SPUR GEAR SCORE LOAD CURVE FOR MIL-L-21260 (GRADE 2) OIL